Eur. Phys. J. C 50, 467–504 (2007)
DOI 10.1140/epjc/s10052-007-0258-y

THE EUROPEAN PHYSICAL JOURNAL C

Special Article – Tools for Experiment and Theory

A generalised manifestly gauge invariant exact renormalisation group for SU(N) Yang–Mills

S. Arnone[1], T.R. Morris[2], O.J. Rosten[2,a]

[1] Dipartimento di Fisica, Università degli Studi di Roma "La Sapienza", P.le Aldo Moro 2, 00185 Roma, Italy
[2] School of Physics and Astronomy, University of Southampton, Highfield, Southampton SO17 1BJ, UK

Received: 10 March 2006 /
Published online: 6 March 2007 –

Abstract. We take the manifestly gauge invariant exact renormalisation group previously used to compute the one-loop β function in SU(N) Yang–Mills without gauge fixing, and generalise it so that it can be renormalised straightforwardly at any loop order. The diagrammatic computational method is developed to cope with general group theory structures, and new methods are introduced to increase its power, so that much more can be done simply by manipulating diagrams. The new methods allow the standard two-loop β function coefficient for SU(N) Yang–Mills to be computed, for the first time without fixing the gauge or specifying the details of the regularisation scheme.

1 Introduction

In 1929, in pursuit of a manifestly relativistic quantum electrodynamics, Pauli and Heisenberg discovered the famous obstruction to its canonical quantisation, which in modern terms is the lack of an inverse for the gauge field two-point vertex [1].[1] Their solution in the same paper, effectively gauge fixing, is still followed to this day. Much later, Feynman's unitarity argument for Faddeev–Popov ghosts in non-Abelian gauge theory [2], and the elegance and power of the resulting BRST symmetries [3–6], strengthened the case for gauge fixing to such an extent that it is now often taken for granted that it is a necessary first step to make sense of a quantum gauge theory or, more extremely, that the original manifestly gauge invariant formulation is nothing but a sort of slight of hand, only the gauge fixed version having any real claim to existence (this despite the fact that lattice gauge theory simulations are routinely made without gauge fixing).

Nevertheless, in a series of works [7–23], we have been developing techniques that allow computations directly in the continuum, in particular perturbative computations in SU(N) Yang–Mills, to proceed without any gauge fixing. How can we avoid the well-known obstructions above? We do not compute contributions to the S matrix (where at the perturbative level, Feynman's arguments would necessarily apply [2]) but instead compute local objects: the vertices of a gauge invariant Wilsonian effective action.[2] The construction of a real gauge invariant cutoff Λ, using spontaneously broken SU($N|N$) gauge theory [12], allows this for the first time to be properly defined [10]. To compute the effective action without fixing the gauge, we use the fact that there are an infinity of possible exact renormalisation groups[3] (ERGs) that specify its flow as modes are integrated out [48, 49] (the continuum equivalent to the infinite number of ways of blocking on a lattice [13] – we expand on this in Sect. 2.1) and that out of these there are infinite number that *manifestly* preserve the gauge invariance, their weak coupling expansion at no stage requiring the introduction of an inverse for the gauge field two-point vertex [8, 9].

Although it took some time to clarify and develop the ideas in the initial works [7, 8] to a point where we had a coherent 'calculus' – with which the one-loop β function coefficient, β_1, was computed without gauge fixing – we knew that significant additional development would be required to apply these ideas further [19]. Indeed, although the analysis of [19] generalises the original $N = \infty$ calculation to one that holds at finite N, the Wilsonian effective action is restricted to single supertrace terms only. Removing this restriction is one of the key elements in generalising the formalism such that it is suitable for further computation. The period between [19] and the present publication is in part a measure of the scale of the difficulties we still had to overcome.

[a] e-mail: ojr@phys.soton.ac.uk

[1] Of course they followed Hamiltonian quantisation, where the problem manifests itself in the vanishing of π_0, the momentum conjugate to the time component of the gauge field.

[2] Correlators of gauge invariant operators can be computed by introducing appropriate sources [10]. To consider on-shell gluons, one can gauge fix after the computation [19].

[3] For alternative approaches which involve gauge fixing, see [24–42]; for those based on the Vilkovisky–DeWitt formalism [43–45], see [46, 47].

The incorporation of multiple supertrace terms is necessary for the complete renormalisation of the gauge invariant Wilsonian effective action at one-loop and beyond, as we discuss in Sect. 2. Importantly, this must be done in such a way as to respect the central term in the SU($N|N$) algebra, implemented via the so-called no-$\mathcal{A}^0$ symmetry [19]. This then allows us to properly distinguish the coupling $g(\Lambda)$ associated with the original SU(N) Yang–Mills from the coupling $g_2(\Lambda)$ associated with the unphysical copy, which arises due to the SU($N|N$) regulating structure [14].

Since the manifest preservation of gauge invariance ensures that the gauge fields have no wavefunction renormalisation [8], we can ensure that g and g_2 are the only quantities which run.[4] We can then expect to recover the standard two-loop β function coefficient, β_2, by taking the limit $g_2/g \to 0$, at the end of the calculation. As we will see in [50], subject only to very general conditions, this expectation is confirmed. For future convenience, we define

$$\alpha := \frac{g_2^2}{g^2}\,. \tag{1}$$

However, introducing multiple supertrace terms rapidly increases the number of Wilson-loop-like diagrams [8, 9, 19], even at one-loop. (Such diagrams simply correspond to drawing explicitly the [super]colour flow, in common with other diagrammatics inspired by t'Hooft's large N diagrams [51].)

The first step in bringing this complication under control, as we describe in Sect. 3.3, is to replace these diagrams by 'group theory blind' diagrams. Just as in Feynman diagrams, which they now very closely resemble, the result of combining the structure constants is then implicit at the diagrammatic level. This step is also the group theory analogue of leaving the momentum dependence in the higher-point vertices of the flow equation implicit, which underlies the diagrammatic computational methods developed in [15, 19, 20]. The result is a streamlined computation, allowing many diagrams of different group-theory structure to be processed in parallel.

Recall that, central to the diagrammatic methods of [19], is the introduction of an 'effective propagator'. Like ordinary propagators these are inverses of the classical two-point vertex. However, since no gauge fixing has been done they are inverses only in the transverse space. Equivalently we can say that they are inverses up to remainder terms. These were called 'gauge remainder' terms because they are forced by gauge invariance to be there; moreover, if a remainder strikes a vertex, then they can be processed via gauge invariance identities, which we recall in Sect. 2.1. In fact, the full spontaneously broken SU($N|N$) acts in this way [19].

In [19] we used integration by parts of $\Lambda\partial/\partial\Lambda$ (the generator of renormalisation group flow) and these effective propagator relations to iteratively simplify the expressions, purely by manipulating diagrams. We were left with terms which were algebraically completely determined, the gauge remainder terms described above and total Λ-derivative terms (which, in the formalism of this paper, become performed at constant α).

Whilst all these terms can be further manipulated algebraically to arrive at β_1, at two-loops this is no longer possible, at least not without algebraic computing facilities and even then this would be a major task. Instead, one of us was inspired to generalise these ideas [23, 52] so that all contributions to β_1 can be reduced to diagrammatic Λ-derivative terms, as we will see in Sect. 5. It is from these terms that the numerical value of β_1 can be straightforwardly extracted in a manifestly universal way.

The strategy at two-loops is essentially to repeat the same diagrammatic steps. There are, however, a number of complications. The first is that the procedure generates an almost prohibitively large number of diagrams (we return to this point, and its resolution [23, 53, 54], in the conclusion). Secondly, certain diagrammatic structures, which look to be different, turn out to be algebraically the same. Diagrams in which these structures are embedded as a subdiagram cannot be manipulated and so should be collected together. At two loops and beyond, all such terms cancel amongst themselves [23, 53, 54]. Thirdly, there is a subtlety associated with the Taylor expansions of a small number of diagrams, necessary for the β_2 diagrammatics. At the one-loop level, the Taylor expansions can be performed blindly; at the two-loop level, however, this process is not always trivial as it can generate IR divergences in individual terms. The key is to consider sets of terms together, whence these divergences cancel out. There is a particularly elegant way of thus organising the calculation – using 'subtraction techniques' [23] – the explanation of which we defer until [50].

Despite these complications, the two-loop and one-loop diagrammatics are very similar. Although a very large number of diagrams are generated at two-loops, the vast majority cancel out to leave behind a manageable set of Λ-derivative terms[5]. The extraction of the numerical coefficient from the Λ-derivative terms at two-loops is subtle, heavily involving the use of the subtraction techniques.

In this paper, we focus on the construction of the formalism and perform the β_1 diagrammatics. We emphasise that the purpose of this calculation is a comprehensive illustration of the raw diagrammatic techniques. As discussed further in the conclusion, refinement of the methodology [23, 52–54] reduces the complexity of the computation of β_1 to the level of a calculation using standard techniques; this paper provides a necessary bridge between these sophisticated ideas and the diagrammatic calculus of [19]. In the partner paper [50], we give the expression for β_2 in terms of Λ-derivatives, describe the subtraction techniques and extract the universal coefficient.

The paper is organised as follows. In the next section we explain why we need new terms in the flow equation to allow straightforward renormalisation at one-loop

[4] For technical reasons, a superscalar field is given zero mass dimension [19], and thus is associated by the usual dimensional reasoning with an infinite number of dimensionless couplings. These couplings do not require renormalisation, as we will see explicitly in [50].

[5] And a set of terms that vanish in the $\alpha \to 0$ limit.

and beyond. Having introduced these new terms we first appropriately adapt the 'old-style' diagrammatics of [19] in Sect. 3.2, before refining the diagrammatics in Sect. 3.3. The weak coupling flow equations are phrased in this new notation, and some of their properties are discussed in Sect. 3.4. The new diagrammatic techniques are described in Sect. 4. In Sect. 5, we use these techniques to redo the diagrammatics for β_1, setting the stage for the numerical evaluation of β_2, in [50]. We conclude in Sect. 6.

2 Gauge invariance and the ERG

We start with a quick review of the basic elements and then explain why it is desirable to further modify the flow equation for computations at arbitrary loop order. In all that follows, we work in D dimensional Euclidean space.

2.1 Review

Our starting point is the recognition that there are an infinity of unrelated ERGs corresponding to the infinite number of ways of blocking on the lattice [13, 48, 49]. It may help to make this observation more concrete. Thus consider a general Kadanoff blocking for the single, real scalar field φ, which in continuum notation takes the form $\varphi(x) = b_x[\varphi_0]$, φ being the blocked field and b_x the blocking function (a functional of the microscopic field φ_0). The blocking function could be linear $b_x[\varphi_0] = \int_y K(x-y)\varphi_0(y)$, for some kernel $K(z)$ which is steeply decaying once $z\Lambda > 1$, or even something non-linear.[6] In the standard way we define

$$\mathrm{e}^{-S[\varphi]} = \int \mathrm{d}\varphi_0 \delta\Big[\varphi - b[\varphi_0]\Big] \mathrm{e}^{-S_{\mathrm{bare}}[\varphi_0]}\,, \qquad (2)$$

so that equality of microscopic and blocked partition functions follows:

$$\mathcal{Z} = \int \mathrm{d}\varphi \mathrm{e}^{-S[\varphi]} = \int \mathrm{d}\varphi_0 \mathrm{e}^{-S_{\mathrm{bare}}[\varphi_0]}.$$

We get an ERG by computing the flow of (2). Defining

$$\Psi_x[\varphi] = \mathrm{e}^{S[\varphi]} \int \mathrm{d}\varphi_0\; \delta\Big[\varphi - b[\varphi_0]\Big] \Lambda \frac{\partial b_x}{\partial \Lambda} \mathrm{e}^{-S_{\mathrm{bare}}[\varphi_0]}\,,$$

we see that

$$\Lambda \frac{\partial}{\partial \Lambda} \mathrm{e}^{-S[\varphi]} = -\int_x \frac{\delta}{\delta \varphi(x)} \left(\Psi_x \mathrm{e}^{-S[\varphi]} \right)\,, \qquad (3)$$

which is the starting point in [8, 9, 48, 49], arrived at by different arguments.

[6] The particular blocking that yields the Legendre flow equation, a.k.a. effective average action approach, is given in [58]. This is directly related to Polchinski's version through a Legendre transformation [59].

For the single scalar field, φ, we can use [20]

$$\Psi_x = \frac{1}{2} \int_y \dot{\Delta}_{xy} \frac{\delta \Sigma_1}{\delta \varphi(y)}\,,$$

where $\dot{\Delta}$ is an ERG kernel. This choice yields:

$$\begin{aligned} \dot{S} \equiv -\Lambda \partial_\Lambda S &= a_0[S, \Sigma_1] - a_1[\Sigma_1] \\ &= \frac{1}{2} \frac{\delta S}{\delta \varphi} \cdot \dot{\Delta} \cdot \frac{\delta \Sigma_1}{\delta \varphi} - \frac{1}{2} \frac{\delta}{\delta \varphi} \cdot \dot{\Delta} \cdot \frac{\delta \Sigma_1}{\delta \varphi}\,, \end{aligned} \qquad (4)$$

which will be referred to as the scalar flow equation. S is the Wilsonian effective action and $\Sigma_1 = S - 2\hat{S}$, where $\hat{S}$ is the 'seed action' [15, 19, 20]. We define

$$f \cdot W \cdot g = \int_{x,y} f(x) W_{xy} g(y) = \int_x f(x) W(-\partial^2/\Lambda^2) g(x)\,,$$

which holds for any momentum space kernel $W(p^2/\Lambda^2)$ and functions of spacetime f, g, using

$$W_{xy} = W(-\partial^2/\Lambda^2)\delta(x-y) = \int \frac{d^D p}{(2\pi)^D} W(p^2/\Lambda^2) \mathrm{e}^{ip(x-y)}.$$

The seed action is a generally non-universal input functional which controls the flow and which satisfies the same symmetries as S. $\hat{S}$ must possess a kinetic term; in the case that $\hat{S}$ comprises just a kinetic term, (4) reduces to Polchinski's version [55] of Wilson's ERG [56], up to a discarded vacuum energy term. The seed action, like all other ingredients of the flow equation, must be infinitely differentiable in momenta. This property, referred to as quasilocality [57] guarantees that each RG step $\Lambda \to \Lambda - \delta\Lambda$ does not generate IR singularities [56].

For a particular choice of $\hat{S}$, which we will discuss shortly, the integrated ERG kernel, Δ, is the inverse of the classical two-point vertex. In recognition of this, we henceforth refer to Δ as an 'effective propagator' [19, 20]. We use the word effective advisably since its equivalence to a propagator even in scalar field theory is down to choice. Moreover, when we generalise to gauge theory, where we will not fix the gauge, we cannot even define a propagator in the usual sense. However, even in this case, Δ plays a diagrammatic rôle somewhat analogous to a real propagator, and we recognise this similarity.

Returning to (4), we refer to a_0 as the classical term of the flow equation, since this generates tree level diagrams, and a_1 as the quantum term, since this generates loop corrections. With this in mind, let us analyse the flow of the classical Wilsonian effective action two-point vertex, ${S_0}^{\varphi\varphi}$. We can consistently choose $\hat{S}_0{}^{\varphi\varphi} = {S_0}^{\varphi\varphi}$ and, doing so, we have:

$$\dot{S}_0^{\varphi\varphi} = -S_0^{\varphi\varphi} \dot{\Delta} S_0^{\varphi\varphi}\,. \qquad (5)$$

Integrating up and setting the integration constant to zero yields the effective propagator relation:

$${S_0}^{\varphi\varphi} \Delta = 1\,. \qquad (6)$$

It is easy to generalise this analysis to pure U(1) gauge theory [7]: we simply replace φ by A_μ in (4) to give

$$\dot{S} = \frac{1}{2}\frac{\delta S}{\delta A_\mu}\cdot\dot{\Delta}\cdot\frac{\delta \Sigma_1}{\delta A_\mu} - \frac{1}{2}\frac{\delta}{\delta A_\mu}\cdot\dot{\Delta}\cdot\frac{\delta \Sigma_1}{\delta A_\mu}\,. \tag{7}$$

Because the gauge field only transforms by a shift under a U(1) transformation $A_\mu \mapsto A_\mu + \partial_\mu \Omega$, the functional derivatives $\delta/\delta A_\mu$ are gauge *invariant*. Thus (7) is also gauge invariant. Once again, we choose the classical seed action two-point vertex equal to its Wilsonian effective action counterpart. Equation (5) becomes

$$\dot{S}_{0\mu\nu} = -S_{0\mu\alpha}\dot{\Delta}S_{0\alpha\nu}\,. \tag{8}$$

Gauge invariance forces $S_{0\alpha\nu}$ to be transverse. Utilising this and integrating up, we now find that the integration constant is constrained to be zero, if we demand that Δ is well behaved as $p \to \infty$. Equation (6) becomes

$$S_{0\mu\nu}\Delta = \delta_{\mu\nu} - \frac{p_\mu p_\nu}{p^2}\,. \tag{9}$$

Thus, the effective propagator is the inverse of the classical two-point vertex only in the transverse space. The object $p_\mu p_\nu/p^2$ is our first example of a gauge remainder.

Of course, pure U(1) gauge theory is not very interesting, but nevertheless the flow equation we have written down is *manifestly gauge invariant*. No gauge fixing is necessary to define it and no gauge fixing is needed to calculate with it, perturbatively or nonperturbatively [7].

The next step is to generalise our analysis to gauge theories with interesting interactions and clearly the most important, and challenging, direction is to generalise this to non-Abelian gauge theories. (However, for application to QED, see [22].) The first, obvious, difficulty is that if A_μ is a non-Abelian gauge field, equation (7) is no longer gauge invariant: the functional derivatives $\delta/\delta A_\mu$ now transform homogeneously in the adjoint representation of the gauge group. It is easy to overcome this problem: we simply choose

$$\Psi = \frac{1}{2}\{\dot{\Delta}\}\frac{\delta \Sigma_g}{\delta A_\mu}\,, \tag{10}$$

where $\{\dot{\Delta}\}$ is some covariantisation of the kernel. For example, we could replace $\dot{\Delta}(-\partial^2/\Lambda^2)$ by $\dot{\Delta}(-D^2/\Lambda^2)$, where $D_\mu = \partial - iA_\mu$ is the covariant derivative, but there are infinitely many other possible covariantisations [8, 9]. We have scaled g out of its normal place in the covariant derivative, which is why in (10) we have [8, 9]

$$\Sigma_g := g^2 S - 2\hat{S}\,. \tag{11}$$

Replacing φ by A_μ and substituting Ψ in (3), we get the manifestly gauge invariant flow equation

$$\dot{S} = \frac{1}{2}\frac{\delta S}{\delta A_\mu}\{\dot{\Delta}\}\frac{\delta \Sigma_g}{\delta A_\mu} - \frac{1}{2}\frac{\delta}{\delta A_\mu}\{\dot{\Delta}\}\frac{\delta \Sigma_g}{\delta A_\mu}\,. \tag{12}$$

Although this equation allows computations in non-Abelian Yang–Mills without gauge fixing, we run into a problem at one-loop because covariant higher-derivatives provide insufficient regularisation [9, 60, 61]. The essentially unique solution [8] to this problem is to embed the theory inside a spontaneously broken supergauge theory [14].

Hence we regularise SU(N) Yang–Mills theory by instead working with SU($N|N$) Yang–Mills. The gauge field is valued in the Lie superalgebra and thus takes the form of a Hermitian supertraceless supermatrix:

$$\mathcal{A}_\mu = \begin{pmatrix} A^1_\mu & B_\mu \\ \bar{B}_\mu & A^2_\mu \end{pmatrix} + \mathcal{A}^0_\mu \mathbb{1}\,. \tag{13}$$

Here, $A^1_\mu(x) \equiv A^1_{a\mu}\tau^a_1$ is the physical SU(N) gauge field, τ^a_1 being the SU(N) generators orthonormalised to $\mathrm{tr}(\tau^a_1\tau^b_1) = \delta^{ab}/2$, while $A^2_\mu(x) \equiv A^2_{a\mu}\tau^a_2$ is an unphysical SU(N) gauge field. The B fields are fermionic gauge fields which will gain a mass of order Λ from the spontaneous breaking; they play the rôle of gauge invariant Pauli–Villars (PV) fields, furnishing the necessary extra regularisation to supplement the covariant higher derivatives.

To unambiguously define contributions which are finite only by virtue of the PV regularisation, a preregulator must be used in $D = 4$ [14]. This amounts to a prescription for discarding otherwise non-vanishing surface terms which can be generated by shifting loop momenta. Hence, we work in $D = 4 - 2\epsilon$, so that such contributions are automatically discarded. There are, however, very strong indications [23, 53, 54] that an entirely diagrammatic prescription can instead be adopted, which one might hope would be applicable to phenomena for which one must work strictly in $D = 4$.

$\mathcal{A}^0$ is the gauge field for the centre of the SU($N|N$) Lie superalgebra. Equivalently, one can write

$$\mathcal{A}_\mu = \mathcal{A}^0_\mu \mathbb{1} + \mathcal{A}^A_\mu T_A\,, \tag{14}$$

where the T_A are a complete set of traceless and supertraceless generators normalised as in [14].

The theory is subject to the local invariance:

$$\delta\mathcal{A}_\mu = [\nabla_\mu, \Omega(x)] + \lambda_\mu(x)\mathbb{1}\,, \tag{15}$$

where the first term generates supergauge transformations, $\nabla_\mu = \partial_\mu - i\mathcal{A}_\mu$ being the covariant derivative, and the second divides out by the centre of the algebra. Indeed this 'no-$\mathcal{A}^0$ shift symmetry' ensures that nothing depends on $\mathcal{A}^0$ and that $\mathcal{A}^0$ has no degrees of freedom [19]. The spontaneous breaking is carried by a superscalar field

$$\mathcal{C} = \begin{pmatrix} C^1 & D \\ \bar{D} & C^2 \end{pmatrix}\,, \tag{16}$$

which transforms covariantly:

$$\delta\mathcal{C} = -i[\mathcal{C}, \Omega]\,. \tag{17}$$

It can be shown that, at the classical level, the spontaneous breaking scale (effectively the mass of B) tracks the covariant higher derivative effective cutoff scale Λ, if $\mathcal{C}$ is

made dimensionless (by using powers of Λ) and $\hat{S}$ has the minimum of its effective potential at:

$$\langle \mathcal{C} \rangle = \sigma \equiv \begin{pmatrix} \mathbb{1} & 0 \\ 0 & -\mathbb{1} \end{pmatrix} . \tag{18}$$

In this case the classical action S_0 also has a minimum at (18). At the quantum level this can be imposed as a constraint on S, which can be satisfied by a suitable choice of $\hat{S}$ [19, 23]. When we shift to the broken phase, D becomes a super-Goldstone mode (eaten by B in unitary gauge) whilst the C^i are Higgs bosons and can be given a running mass of order Λ [8, 14, 19]. Working in our manifestly gauge invariant formalism, B and D gauge transform into each other; in recognition of this, we define the composite fields[7]

$$F_R = (B_\mu, D) , \quad \bar{F}_R = (\bar{B}_\mu, -\bar{D}) . \tag{19}$$

It will be useful to define the projectors $\sigma_+ = \frac{1}{2}(\mathbb{1}+\sigma)$ and $\sigma_- = \frac{1}{2}(\mathbb{1}-\sigma)$. With a slight abuse of notation we can then write the components of the superfields in terms of full supermatrices: $\tilde{A}^1_\mu = \sigma_+ \mathcal{A}_\mu \sigma_+$, $\tilde{A}^2_\mu = \sigma_- \mathcal{A}_\mu \sigma_-$, $B_\mu = \sigma_+ \mathcal{A}_\mu \sigma_-$, $\bar{B}_\mu = \sigma_- \mathcal{A}_\mu \sigma_+$, and similarly for C^i, D and $\bar{D}$. (Note that these $\tilde{A}^i$ thus contain $\mathcal{A}^0 \sigma_i$. We will see in Sects. 3.2.5 and 4.1 how we can effectively remove $\mathcal{A}^0$ from our considerations, using it to map us into a particular diagrammatic picture.) As will become clear later, in general this is a more useful notation in the broken phase than the one employed in [19] where we split the superfields only into full block (off)diagonal components such as $A_\mu = \tilde{A}^1_\mu + \tilde{A}^2_\mu$.

We generalise (12) by first working out a form for the classical two-point vertices in the broken phase, in particular consistent with spontaneously broken SU($N|N$) invariance [19]. Generalisations of (8) then determine the kernels $\dot{\Delta}$, providing there are sufficiently many different terms in the flow equation to furnish different kernels for each different two-point vertex. This, together with respect for (15) and (17), are the main constraints on the choice of Ψ. The solution given in [19] amounts to:

$$\dot{S} = a_0[S, \Sigma_g] - a_1[\Sigma_g] , \tag{20}$$

where

$$a_0[S, \Sigma_g] = \frac{1}{2} \frac{\delta S}{\delta \mathcal{A}_\mu} \{ \dot{\Delta}^{\mathcal{A}\mathcal{A}} \} \frac{\delta \Sigma_g}{\delta \mathcal{A}_\mu} + \frac{1}{2} \frac{\delta S}{\delta \mathcal{C}} \{ \dot{\Delta}^{\mathcal{C}\mathcal{C}} \} \frac{\delta \Sigma_g}{\delta \mathcal{C}} , \tag{21}$$

and

$$a_1[\Sigma_g] = \frac{1}{2} \frac{\delta}{\delta \mathcal{A}_\mu} \{ \dot{\Delta}^{\mathcal{A}\mathcal{A}} \} \frac{\delta \Sigma_g}{\delta \mathcal{A}_\mu} + \frac{1}{2} \frac{\delta}{\delta \mathcal{C}} \{ \dot{\Delta}^{\mathcal{C}\mathcal{C}} \} \frac{\delta \Sigma_g}{\delta \mathcal{C}} , \tag{22}$$

where the natural definitions of functional derivatives of SU($N|N$) matrices are used [10, 14, 19]:

$$\frac{\delta}{\delta \mathcal{C}} := \begin{pmatrix} \delta/\delta C^1 & -\delta/\delta \bar{D} \\ \delta/\delta D & -\delta/\delta C^2 \end{pmatrix} , \tag{23}$$

and from (14) [14, 19]:

$$\frac{\delta}{\delta \mathcal{A}_\mu} := 2T_A \frac{\delta}{\delta \mathcal{A}_{A\mu}} + \frac{\sigma}{2N} \frac{\delta}{\delta \mathcal{A}^0_\mu} . \tag{24}$$

The crucial freedom we need to generalise (9) is hidden in the definition of what we now mean by a covariantised kernel. For both $W = \dot{\Delta}^{\mathcal{A}\mathcal{A}}$ and $W = \dot{\Delta}^{\mathcal{C}\mathcal{C}}$ we set $\{W\} = \{W\}_{\mathcal{A}\mathcal{C}}$, where

$$u \{W\}_{\mathcal{A}\mathcal{C}} v = u \{W\}_{\mathcal{A}} v - \frac{1}{4} [\mathcal{C}, u] \{W_m\}_{\mathcal{A}} [\mathcal{C}, v] , \tag{25}$$

and $\{W\}_{\mathcal{A}}$ is a supercovariantisation, extending that introduced in (10) and which is defined precisely below, and the $\mathcal{C}$ commutator terms are introduced to allow a difference between B and A kernels, and C and D kernels, in the broken phase. They do this because at the level of two-point flow equations, $\mathcal{C}$ is replaced by σ in (25), and σ (anti)commutes with the (fermionic) bosonic elements of the algebra. Thus, extracting the broken-phase two-point classical flow equations from (21), we find that the A^i kernels are given by $\dot{\Delta}^{\mathcal{A}\mathcal{A}}$, the C^i kernels by $\dot{\Delta}^{\mathcal{C}\mathcal{C}}$, but the B kernel is $\dot{\Delta}^{\mathcal{A}\mathcal{A}} + \dot{\Delta}^{\mathcal{A}\mathcal{A}}_m$ and the D kernel is $\dot{\Delta}^{\mathcal{C}\mathcal{C}} + \dot{\Delta}^{\mathcal{C}\mathcal{C}}_m$ [19]. The B and D kernels can be combined:

$$\dot{\Delta}^{F\bar{F}}_{MN}(p) = \begin{pmatrix} \dot{\Delta}^{B\bar{B}}_p \delta_{\mu\nu} & 0 \\ 0 & -\dot{\Delta}^{D\bar{D}}_p \end{pmatrix} . \tag{26}$$

Notice in (25) that we use $\{W\}_{\mathcal{A}\mathcal{C}}$ to label a covariantisation of two kernels, W and W_m.

The other main constraint is invariance under (15) and (17). The general covariantisation encodes the invariance by insisting that

$$\begin{aligned} u\{W\}_{\mathcal{A}} v = & \sum_{m,n=0}^{\infty} \int_{x_1,\cdots,x_n;y_1,\cdots,y_m;x,y} \\ & \times W_{\mu_1\cdots\mu_n,\nu_1\cdots\nu_m}(x_1, \ldots, x_n; y_1, \ldots, y_m; x, y) \\ & \times \mathrm{str}\ [u(x)\mathcal{A}_{\mu_1}(x_1)\cdots\mathcal{A}_{\mu_n}(x_n) v(y) \mathcal{A}_{\nu_1}(y_1)\cdots\mathcal{A}_{\nu_m}(y_m)] . \end{aligned} \tag{27}$$

a is invariant under (15), where u and v are supermatrix representations transforming homogeneously as in (17) and where, without loss of generality, we may insist that $\{W\}_{\mathcal{A}}$ satisfies $u \{W\}_{\mathcal{A}} v \equiv v \{W\}_{\mathcal{A}} u$. For simplicity's sake, we have chosen (27) to contain only a single supertrace. The $m = n = 0$ term is just the original kernel, i.e.

$$W_{,}(;;x,y) \equiv W_{xy} . \tag{28}$$

The requirement that (27) is supergauge invariant enforces a set of Ward identities on the vertices $W_{\mu_1\cdots\mu_n,\nu_1\cdots\nu_m}$ which we describe later. Note that, for the sake of brevity, we will often loosely refer to vertices of the covariantised kernels simply as kernels. The no-$\mathcal{A}^0$ symmetry is obeyed by requiring the coincident line identities [9]. These identities are equivalent to the requirement that the gauge fields all act by commutation [10], thus trivially the $\mathcal{A}^0$ parts of (13) disappear, ensuring that the no-$\mathcal{A}^0$ part of (15) is satisfied. A consequence of the coincident line identities,

[7] These definitions are consistent with those in [23] but differ, for convenience, from those in [19] by signs in the fifth component.

which also trivially follows from the representation of (27) in terms of commutators, is that if $v(y) = \mathbb{1}g(y)$ for all y, i.e. is in the scalar representation of the gauge group, then the covariantisation collapses to

$$u\,\{W\}_{\mathcal{A}}\,v = (\mathrm{str}\ u)\cdot W\cdot g\,. \tag{29}$$

Note that the same identity therefore holds for the extended version (25).

Under (17), the $\mathcal{C}$ functional derivative transforms homogeneously:

$$\delta\left(\frac{\delta}{\delta\mathcal{C}}\right) = -i\left[\frac{\delta}{\delta\mathcal{C}}, \Omega\right], \tag{30}$$

and thus by (25) and (27), the corresponding terms in (21) and (22) are invariant. The $\mathcal{A}$ functional derivative, however, transforms as [19]:

$$\delta\left(\frac{\delta}{\delta\mathcal{A}_\mu}\right) = -i\left[\frac{\delta}{\delta\mathcal{A}_\mu}, \Omega\right] + \frac{i\mathbb{1}}{2N}\mathrm{tr}\left[\frac{\delta}{\delta\mathcal{A}_\mu}, \Omega\right]. \tag{31}$$

The correction is there because (24) is traceless, which in turn is a consequence of the supertracelessness of (13). The fact that $\delta/\delta\mathcal{A}$ does not transform homogeneously means that supergauge invariance is destroyed unless the correction term vanishes for other reasons.

Here, no-$\mathcal{A}^0$ symmetry comes to the rescue. Using the invariance of (25) for homogeneously transforming u and v, and the invariance of S and $\hat{S}$, we have by (31) and (29), that the $\mathcal{A}$ term in (21) transforms to

$$\delta\left(\frac{\delta S}{\delta\mathcal{A}_\mu}\{\dot{\Delta}^{\mathcal{A}\mathcal{A}}\}\frac{\delta\Sigma_g}{\delta\mathcal{A}_\mu}\right) = \frac{i}{2N}\mathrm{tr}\left[\frac{\delta S}{\delta\mathcal{A}_\mu}, \Omega\right]\cdot\dot{\Delta}^{\mathcal{A}\mathcal{A}}\cdot \mathrm{str}\,\frac{\delta\Sigma_g}{\delta\mathcal{A}_\mu} + (S \leftrightarrow \Sigma_g), \tag{32}$$

a where $S \leftrightarrow \Sigma_g$ stands for the same term with S and Σ_g interchanged. But by (24) and no-$\mathcal{A}^0$ symmetry,

$$\mathrm{str}\,\frac{\delta\Sigma_g}{\delta\mathcal{A}_\mu} = \frac{\delta\Sigma_g}{\delta\mathcal{A}^0_\mu} = 0\,,$$

similarly for S, and thus the tree level terms are invariant under (15) and (17). Likewise, the quantum terms in (22) are invariant, since

$$\delta\left(\frac{\delta}{\delta\mathcal{A}_\mu}\{\dot{\Delta}^{\mathcal{A}\mathcal{A}}\}\frac{\delta}{\delta\mathcal{A}_\mu}\Sigma_g\right) = \frac{i}{N}\mathrm{tr}\left[\frac{\delta}{\delta\mathcal{A}_\mu}, \Omega\right]\cdot\dot{\Delta}^{\mathcal{A}\mathcal{A}}\cdot \mathrm{str}\,\frac{\delta\Sigma_g}{\delta\mathcal{A}_\mu} = 0\,. \tag{33}$$

This completes the proof that the ERG (20) is both supergauge and no-$\mathcal{A}^0$ invariant.

To state the Ward identities we first modify the definition of the vertices of the kernels to reflect the structure of the ERG equation:

$$\begin{aligned}\frac{\delta}{\delta Z_1^c}\left\{W^{Z_1Z_2}\right\}\frac{\delta}{\delta Z_2^c} = \sum_{m,n=0}^{\infty}\int_{x_1,\cdots,x_n;y_1,\cdots,y_m;x,y} &\times W^{X_1\cdots X_n,Y_1\cdots Y_m,Z_1Z_2}_{a_1\cdots a_n,b_1\cdots b_m}(x_1,\ldots,x_n;y_1,\ldots,y_m;x,y)\\ &\times \mathrm{str}\left[\frac{\delta}{\delta Z_1^c(x)}X_1^{a_1}(x_1)\cdots X_n^{a_n}(x_n)\right.\\ &\left.\times\frac{\delta}{\delta Z_2^c(y)}Y_1^{b_1}(y_1)\cdots Y_m^{b_m}(y_m)\right],\end{aligned} \tag{34}$$

where the X_i, Y_i and Z_i are any of the broken phase fields (up to certain restrictions to be discussed) and the indices a_i, b_i and c are Lorentz indices or null, as appropriate. The definition (25) restricts the appearances of the C^i, and the structure of the flow equation insists that the Z_i must be components of either $\mathcal{A}$ or $\mathcal{C}$. The combined X_i, Y_i and Z_i must be net-bosonic but note, in particular, that the there is no reason for the Z_i not to be net fermionic e.g. W^{F,A^1B}. Finally, we assign a value of zero to vertices which imply an illegal supertrace structure e.g. a vertex in which an A^1 directly follows an A^2.

Now we define the (broken phase) Wilsonian effective action/seed action vertices. Using the former as a template, this is simple: supergauge invariance demands that this expansion be in terms of supertraces and products of supertraces [19]:

$$\begin{aligned}S = \sum_{n=1}^{\infty}\frac{1}{s_n}\int_{x_1,\cdots,x_n} &S^{X_1\cdots X_n}_{a_1\cdots a_n}(x_1,\cdots,x_n)\\ &\times \mathrm{str}\,X_1^{a_1}(x_1)\cdots X_n^{a_n}(x_n)\\ &+\frac{1}{2!}\sum_{m,n=0}^{\infty}\frac{1}{s_ns_m}\int_{x_1,\cdots,x_n;y_1,\cdots,y_m}\\ &\times S^{X_1\cdots X_n,Y_1\cdots Y_m}_{a_1\cdots a_n,b_1\cdots b_m}(x_1,\cdots,x_n;y_1\cdots y_m)\\ &\times \mathrm{str}\,X_1^{a_1}(x_1)\cdots X_n^{a_n}(x_n)\mathrm{str}\,Y_1^{b_1}(y_1)\cdots Y_m^{b_m}(y_m)\\ &+\ldots,\end{aligned} \tag{35}$$

a where the labels and indices are as before and the vacuum energy is ignored. Due to the invariance of the supertrace under cyclic permutations of its arguments, we take only one cyclic ordering for the lists $X_1\cdots X_n$, $Y_1\cdots Y_m$ in the sums over n, m. Furthermore, if either list is invariant under some nontrivial cyclic permutations, then s_n (s_m) is the order of the cyclic subgroup, otherwise $s_n = 1$ ($s_m = 1$). Charge conjugation invariance, under which $\mathcal{A} \to -\mathcal{A}^T$ and $\mathcal{C} \to \mathcal{C}^T$ [9, 19] provides relationships between various vertices, which will be exploited throughout this paper.

We write the momentum space vertices as

$$S^{X_1\cdots X_n}_{a_1\cdots a_n}(p_1,\cdots,p_n)\,(2\pi)^D\,\delta\left(\sum_{i=1}^{n}p_i\right) = \int \mathrm{d}^Dx_1\cdots\mathrm{d}^Dx_n\,\mathrm{e}^{-i\sum_i x_i\cdot p_i}S^{X_1\cdots X_n}_{a_1\cdots a_n}(x_1,\cdots,x_n)\,,$$

where all momenta are taken to point into the vertex, and similarly for the multiple supertrace vertices. We will em-

ploy the shorthand

$$S^{X_1X_2}_{a_1a_2}(p) \equiv S^{X_1X_2}_{a_1a_2}(p,-p)\,.$$

The Ward identities, which follow from applying (15), (17), (30) and (31) to the flow equations (20)–(22) can now be expressed in terms of the vertices of (34) and (35). From the unbroken bosonic gauge transformations follows [9, 19]

$$\begin{aligned} &q_\nu U^{\cdots XA^{1,2}Y\cdots}_{\cdots a\nu b\cdots}(\dots,p,q,r,\dots)\\ &= U^{\cdots XY\cdots}_{\cdots ab\,\cdots}(\dots,p,q+r,\dots) - U^{\cdots XY\cdots}_{\cdots ab\cdots}(\dots,p+q,r,\dots), \end{aligned} \tag{36}$$

a where U can be a vertex from either action or any of the kernels. The field X and/or Y can, unlike $A^{1,2}_\nu$, represent the end of a vertex of a covariantised kernel; in which case they are to be identified with the Z_1 and/or Z_2 of equation (34), as appropriate. There is an appealing geometrical picture of (36): we can view the momentum of the field $A^{1,2}_\nu$ as being pushed forward on to the next field with a plus and pulled back on to the previous field with a minus [8, 9, 19].

The second Ward identity follows from the (broken) fermionic gauge transformations and is most neatly written in terms of the composite fields F and $\bar{F}$. To this end, we define a five-momentum [19][8]

$$q_M = (q_\mu, 2)\,. \tag{37}$$

The Ward identity corresponding to the broken, fermionic gauge transformations can now be written in the following compact form (there is an identical equation involving $\bar{F}_N$):

$$\begin{aligned} &q_N U^{\cdots XFY\cdots}_{\cdots aNb\cdots}(\dots,p,q,r,\dots)\\ &= U^{\cdots X\overrightarrow{Y}\cdots}_{\cdots a\,b\cdots}(\dots,p,q+r,\dots) - U^{\cdots\overleftarrow{X}Y\cdots}_{\cdots ab\cdots}(\dots,p+q,r,\dots), \end{aligned} \tag{38}$$

a where the $\overrightarrow{X}$ etc. should be interpreted according to Table 1 and the index N is summed over, such that each product of components is weighted with unity. The null entries are those for which the required ordering of fields does not exist.

Apart from the general constraints already discussed, some weak constraints necessary for regularisation as reviewed below, and of course charge conjugation invariance and Poincaré invariance, the covariantisation (27) and seed action $\hat{S}$ in the flow equation (20) can be left unspecified [19]: the calculational methods (reviewed and extended in Sects. 3.2 and 4.2) are designed to turn this freedom to our advantage, by acting as a guide to the most efficient method of computation. In addition, this provides an automatic check on the universality of the terms we are computing.

The ERG (20) is properly ultraviolet regularised by virtue of the manifest spontaneously broken SU($N|N$) invariance and covariant higher derivative regularisation.

[8] Again, this definition is different from [9], where the two comes with a minus sign.

Table 1. The flavour changing effect of pushing forward and/or pulling back the momentum of the fermionic field, U on to the field V

U	V	$\overrightarrow{V}$	$\overleftarrow{V}$
$\bar{F}$	(A^1, C^1)	$(\bar{B}, \bar{D})$	–
	(A^2, C^2)	–	$(\bar{B}, \bar{D})$
	F	$(\tilde{A}^2, C^2)$	$(\tilde{A}^1, C^1)$
F	(A^2, C^2)	F	–
	(A^1, C^1)	–	F
	$\bar{F}$	$(\tilde{A}^1, -C^1)$	$(\tilde{A}^2, -C^2)$

This latter is determined by the functions in the general form of the two-point vertices [19], and corresponds to the introduction of cutoff functions. For a specific choice of bare action and power-law cutoff functions, the weak constraints that these powers have to satisfy were determined in [14]. They are not necessarily, however, the correct inequalities to ensure that the flow (20) itself is regularised, for a specific choice of seed action and covariantisation (27), nor is it necessary to restrict to only power law cutoff functions. Undoubtedly it is possible to work out some very general constraints on $\hat{S}$, the covariantisation (27) and the cutoff functions, which ensure that all quantities are properly ultraviolet regularised at all stages of calculation. However since all these details drop out of the calculation at the end, this effort would be largely wasted. Instead we follow [19], and simply assume that these constraints are satisfied.

Finally, we will require that the covariantisation satisfies

$$\frac{\delta}{\delta \mathcal{A}_\mu}\{W\}_{\mathcal{A}} = 0\,, \tag{39}$$

(where the functional derivative acts on all terms inside $\{W\}_{\mathcal{A}}$ but not on the unspecified right hand attachment) i.e. that there are no diagrams in which the kernel bites its own tail [8–10]. In general, certain such diagrams do appear to be improperly regularised, and this is why we apply this restriction; we will give an example in Sect. 3.2.4, after we have introduced the necessary diagrammatics. For general solutions to this constraint see [8, 19]. Equation (39) leads to identities for the W vertices which again we do not need in practice.

2.2 The need for a new flow equation

The running coupling $g(\Lambda)$ in (20), entering via (11), is identified with the original SU(N) coupling via the renormalisation condition

$$S[\mathcal{A}=A^1, \mathcal{C}=\sigma] = \frac{1}{2g^2}\mathrm{str}\int \mathrm{d}^D x \left(F^1_{\mu\nu}\right)^2 + \cdots\,, \tag{40}$$

where the ellipsis stands for higher dimension operators and the ignored vacuum energy. (No wavefunction renormalisation is required because exact preservation of gauge

invariance forbids it once the coupling is scaled out of the covariant derivative [8, 9].) This means that the coefficient for the two-point vertex with structure str $A^1_\mu(p)A^1_\nu(-p)$ must have the form

$$S^{11}_{\mu\nu}(p) = \frac{2}{g^2}\Box_{\mu\nu}(p) + \mathcal{O}(p^4)\,, \tag{41}$$

where $\Box_{\mu\nu}(p) = p^2\delta_{\mu\nu} - p_\mu p_\nu$. In order to go beyond one-loop computations of purely A^1 vertices (for example in computing the two-loop beta function [23, 50]) we will need to take into account the running coupling $g_2(\Lambda)$ associated with A^2. We define it via the renormalisation condition

$$S[\mathcal{A} = A^2, \mathcal{C} = \sigma] = \frac{1}{2g_2^2}\mathrm{str}\int \mathrm{d}^D x \left(F^2_{\mu\nu}\right)^2 + \cdots\,, \tag{42}$$

where the ellipsis has the same meaning as in (40). Note in particular the unphysical wrong sign for g_2^2, forced by the supertrace. (In turn this is a necessary consequence of global invariance under the supergroup in the unbroken phase. Indeed here the lowest dimension gauge field operator is proportional to str $\mathcal{F}^2_{\mu\nu}$, $\mathcal{F}_{\mu\nu} = i[\nabla_\mu, \nabla_\nu]$ being the superfieldstrength. The wrong sign in the A^2 sector leads to unitarity violation which decouples in the continuum limit [14, 19].) Equation (42) implies that the two-point vertex with the structure str $A^2_\mu(p)A^2_\nu(-p)$ must have the form

$$S^{22}_{\mu\nu}(p) = \frac{2}{g_2^2}\Box_{\mu\nu}(p) + \mathcal{O}(p^4)\,. \tag{43}$$

In [19] we restricted the classical effective action to a single supertrace. Since str $\sigma A_\mu A_\nu$ is not no-$\mathcal{A}^0$ invariant, this requires that the classical two-point A vertices have the structure:

$$\mathrm{str}\; A_\mu A_\nu = \mathrm{str}\; A^1_\mu A^1_\nu + \mathrm{str}\; A^2_\mu A^2_\nu\,,$$

which in turn enforces $g_2 = g$ at the classical level (in common with the unbroken phase).

However we also showed that the A two-point vertex (41) flows at one-loop into [19]

$$\frac{22}{3(4\pi)^2}\,\Box_{\mu\nu}(p)\;\mathrm{str}\;\sigma\mathrm{str}\;\sigma A_\mu A_\nu + \mathcal{O}(p^4)\,, \tag{44}$$

where the $\Box_{\mu\nu}$ factor follows from manifest gauge invariance. Utilising str $\sigma = 2N$, we recognise that the numerical coefficient of (44) is just equal to $-4\beta_1$, where β_1 is the famous one-loop SU(N) Yang–Mills β function coefficient. Since

$$\mathrm{str}\;\sigma A_\mu A_\nu = \mathrm{str}\; A^1_\mu A^1_\nu - \mathrm{str}\; A^2_\mu A^2_\nu\,,$$

this gives the expected flow of (41) and the expected wrong-sign β function for (43).

Now an obvious question arises: how can (44) be consistent with no-$\mathcal{A}^0$ invariance? In fact it is straightforward to repeat the computation of [19] for the case where a gauge field appears in each supertrace and thus show that the one-loop term

$$-\frac{22}{3(4\pi)^2}\,\Box_{\mu\nu}(p)\mathrm{str}\;\sigma A_\mu\;\mathrm{str}\;\sigma A_\nu \tag{45}$$

is also generated. Note that, from (13) or (14), this contains only $\mathcal{A}^0$s, and it cancels the $\mathcal{A}^0$ terms in (44). Therefore, together these terms form a combination invariant under the no-$\mathcal{A}^0$ symmetry of (15).

We thus confirm that (15) is operating as expected, but we see clearly that we have to abandon the single supertrace form for S in order to renormalise g and g_2 differently, already at one loop.

3 The new flow equation

3.1 Modifying the flow equation

The need to allow $g_2 \neq g$ implies that the classical two-point vertices $S^{11}_{0\mu\nu}$ and $S^{22}_{0\mu\nu}$ must also be free to differ. If we are to maintain the advantages of setting two-point vertices in S_0 and $\hat{S}$ equal, we must generalise the flow equation so that the kernels for A^1 and A^2 can also differ (cf. the arguments above (20) and surrounding (25)).

We therefore need to add new terms to the definition of the covariantised kernel in (25) for the case where this is used to connect two functional $\mathcal{A}$ derivatives. (We do not need it for the kernels connecting two functional $\mathcal{C}$ derivatives because we do not need to allow the C^i kernels to differ. This is because there are no terms that require renormalising in the $\mathcal{C}$ sector, as we will explicitly demonstrate in [50].) Clearly we need an insertion of $\mathcal{C}$, since in the broken phase this gives σ, the only algebraic object available for distinguishing A^1 from A^2. However it cannot be a commutator as in (25) since $[\sigma, \delta/\delta A^i] = 0$. From the above discussion of no-$\mathcal{A}^0$ invariance and the discussion of (31) (where also the need is to cancel terms proportional to $\mathbb{1}$) it is clear that we need to entertain multiple supertrace terms in order to preserve (15) and (17). The simplest solution is to define in (21) and (22),

$$\begin{aligned} u\{\dot{\Delta}^{\mathcal{A}\mathcal{A}}\}v &:= u\,\{\dot{\Delta}^{\mathcal{A}\mathcal{A}}\}_{\mathcal{A}\mathcal{C}}\,v \\ &+ u\,\{\dot{\Delta}^{\mathcal{A}\mathcal{A}}_\sigma\}_{\mathcal{A}}\mathcal{P}(v) + \mathcal{P}(u)\,\{\dot{\Delta}^{\mathcal{A}\mathcal{A}}_\sigma\}_{\mathcal{A}}\,v\,, \end{aligned} \tag{46}$$

a where

$$8N\mathcal{P}(X) = \{\mathcal{C}, X\}\mathrm{str}\;\mathcal{C} - 2\mathcal{C}\mathrm{str}\;\mathcal{C}X\,. \tag{47}$$

Note that $\mathcal{P}(X)$ has the following special properties: str $\mathcal{P}(X) = 0$ and $\mathcal{P}(\mathbb{1}) = 0$. Using (29), it is easy to see these ensure that the extra terms in (46) are supergauge invariant despite the inhomogeneous part of (31). The anticommutator structure in (47) arises without loss of generality from charge conjugation invariance of (21) and (22). $\mathcal{P}$ is added symmetrically in (46) to maintain the symmetry $u\{\dot{\Delta}^{\mathcal{A}\mathcal{A}}\}v = v\{\dot{\Delta}^{\mathcal{A}\mathcal{A}}\}u$ purely for convenience in the diagrammatic formalism to follow. Likewise the factor of $8N$ in (47) is purely for convenience. Finally note that the

redefinition (46) does not disturb the fact that (20) can be written in the form (3) (with φ replaced by a sum over $\mathcal{A}$ and $\mathcal{C}$ fields). Thus (20) still corresponds to a valid ERG.

3.2 The old-style diagrammatics

We introduce the diagrammatics of [19], adapted to the new flow equation, in the symmetric phase, as this allows us to describe the necessary elements whilst minimising new notation.

3.2.1 Diagrammatics for the action

The diagrammatic representation of the action is given in Fig. 1.

Each circle stands for a single supertrace containing any number of fields. The S is to remind us that this is an expansion of the action, since the seed action, $\hat{S}$, has a similar expansion. The dotted line reminds us that the two supertraces in the double supertrace term are part of the same vertex. The arrows indicate the cyclic sense in which fields should be read off; henceforth, this will always be done in the counterclockwise sense and so these arrows will generally be dropped.[9] In turn, each of these supertraces can now be expanded in terms of a sum over all explicit, cyclically independent combinations of fields, as in Fig. 2, where closed circles represent $\mathcal{A}$s and open circles represent $\mathcal{C}$s.

In this case, we have chosen not to indicate whether the supertraces we are considering come from the Wilsonian effective action, the seed action, or some linear combination of the two. Explicit instances of fields are referred to as decorations. Note that there are no supertraces containing a single $\mathcal{A}$, since str $\mathcal{A} = 0$. The str $\mathcal{AC}$ vertex vanishes by charge conjugation invariance.

As it stands, Figs. 1 and 2 provide representations of the action (35). However, as we will see shortly, it is often useful to interpret the explicitly decorated terms as just the vertex coefficient functions $S^{X_1\cdots X_n}_{a_1\cdots a_n}(p_1,\cdots,p_n)$ etc., the accompanying supertrace(s) and cyclic symmetry factors having been stripped off.

3.2.2 Diagrammatics for the kernels

The kernels have a very similar diagrammatic expansion [10, 19] to the action, as shown in Fig. 3.

The ellipsis represents terms with any number of fields distributed in all possible ways between the two sides of the kernel. We should note that Fig. 3 is not strictly a representation of (the symmetric phase version of) equation (34). Equation (34) involves not only the kernel vertices and the associated decorative fields, but also two functional derivatives which sit at the ends of the kernel. Moreover, according to (46), the kernels can now attach via $\mathcal{P}$.

[9] Arrows can always be dropped in complete diagrams formed by the flow equation. However, if we look at the diagrammatic representation of a kernel, in isolation, then it will be necessary to keep these arrows.

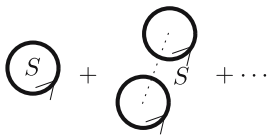

Fig. 1. Diagrammatic representation of the action

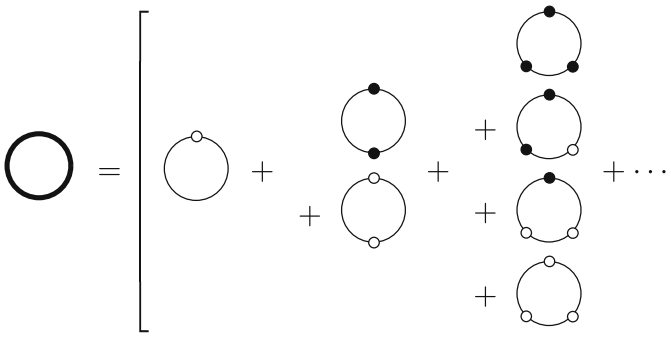

Fig. 2. Expansion of a single supertrace in powers of $\mathcal{A}$ and $\mathcal{C}$

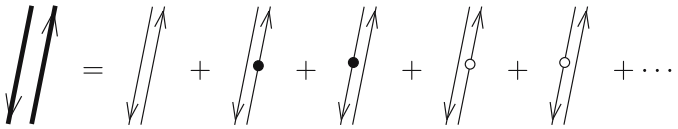

Fig. 3. Diagrammatic representation of the kernels

We can directly include both the functional derivatives and instances of $\mathcal{P}$ in our diagrammatics, as shown in Fig. 4; notice that, in combination, they unambiguously label the different kernels in the flow equation.

In the first diagram, the grey circles can be either both $\mathcal{A}$s or both $\mathcal{C}$s; since they sit at the end of the kernel they represent functional derivatives and label the kernel. The double circle notation, explicitly defined in Fig. 5, represents $\mathcal{P}$. Note that the presence of the double circles tells us that the associated kernel is of type $\dot{\Delta}^{\mathcal{AA}}_{\sigma}$.

In both diagrams, the dotted line is a 'false' kernel in the sense that, if joining two fields with position arguments x and y, it is just $\delta(x-y)$. Thus, in the first diagram on the right-hand side, the $\mathcal{C}$ embedded at the end of the kernel is attached, via a false kernel, to a separate str $\mathcal{C}$. In the sec-

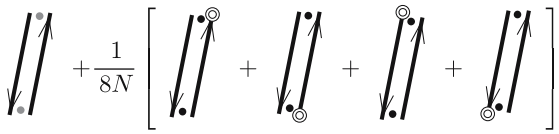

Fig. 4. Diagrammatic representation of the kernels, which recognises the structure of the flow equation

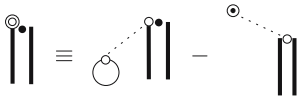

Fig. 5. Interpretation of the double circle notation

ond diagram, the operator ◎ tells us to replace an $\mathcal{A}$ with a $\mathcal{C}$. As for the kernel, it is 'plugged' by a $\mathcal{C}$, rather than ending in a functional derivative; the functional derivative being linked to this $\mathcal{C}$ via a false kernel. Note that one of the $\mathcal{A}$s which labels the kernel may now be linked to the end of the kernel by a false kernel.

3.2.3 The symmetric phase flow equation

To go from the diagrammatic representations of the actions and kernels to the diagrammatic flow equation, we require some properties of the functional derivative with respect to $\mathcal{A}$ and $\mathcal{C}$. Following [10, 19] we introduce the constant supermatrices X and Y and, neglecting the irrelevant spatial dependence, schematically represent first supersowing, whereby two supertraces are sown together:

$$\frac{\partial}{\partial\mathcal{C}}\mathrm{str}\,\mathcal{C}Y = Y \implies \mathrm{str}\,X\frac{\partial}{\partial\mathcal{C}}\mathrm{str}\,\mathcal{C}Y = \mathrm{str}\,XY\,, \tag{48}$$

and secondly supersplitting, whereby a single supertrace is split into two supertraces:

$$\mathrm{str}\,\frac{\partial}{\partial\mathcal{C}}X\mathcal{C}Y = \mathrm{str}\,X\,\mathrm{str}\,Y\,. \tag{49}$$

In the $\mathcal{A}$-sector, the analogue of these relationships, which can be deduced from the completeness relation for the T_A [14], receive corrections, since $\mathcal{A}$ is constrained to be supertraceless:

$$\mathrm{str}\,X\frac{\partial}{\partial\mathcal{A}}\mathrm{str}\,\mathcal{A}Y = \mathrm{str}\,XY - \frac{1}{2N}\mathrm{str}\,X\mathrm{tr}Y \tag{50}$$

$$\mathrm{str}\,\frac{\partial}{\partial\mathcal{A}}X\mathcal{A}Y = \mathrm{str}\,X\,\mathrm{str}\,Y - \frac{1}{2N}\mathrm{tr}XY\,. \tag{51}$$

These corrections, containing $\mathrm{tr}\cdots \equiv \mathrm{str}\,\sigma\cdots$, generically violate SU($N|N$) invariance and, as proved in [19], effectively vanish as a consequence of the SU($N|N$) invariance of the flow equation (the modification of the flow equation according to (46) does nothing to change this conclusion). Thus, the supersplitting and supersowing rules are essentially exact for both fields, enabling us to straightforwardly incorporate the gauge algebra into the diagrammatics, even at finite N [19].

Figure 6 shows the diagrammatic representation of the flow equation; the ellipses represent terms with additional supertraces. The 'dumbbell' terms of the top row are formed by a_0 (which sews two supertraces together) whereas the 'padlock' terms of the bottom row are formed by a_1 (which splits a single supertrace apart).

There are a number of important points to make about the diagrams of Fig. 6. First is that we have discarded all diagrams in which the kernels bite their tails (see Sects. 2.1 and 3.2.4). Secondly, the diagrammatic flow equation is naturally phrased (as with all good Feynman diagrammatics) in terms of *coefficient functions only*: all explicit supertraces and symmetry factors have been stripped off. Thus, the interpretation of the diagrammatic elements in Fig. 6, is not the same as in Figs. 1–5, where both the explicit supertraces and symmetry factors are still present.

However, we can think of each diagram as having an *implied* supertrace structure, and this must of course match between the diagrams on the right-hand side and the term on the left-hand side of the flow equation. The supertrace structure on the left-hand side is obvious, just being that naturally associated with the vertex coefficient function whose flow we are computing. To ensure that the diagrams on the right-hand side are consistent with this, we must understand how to read off the supertrace structure from our diagrams. The rules are simple and follow from exact supersowing/supersplitting. Having expanded out the double circles, each closed circuit represents a supertrace, the fields on the circuit representing the argument of the supertrace. For each circuit, we should sum over all independent cyclic permutations of the fields. If a circuit is empty, it corresponds to str $\mathbb{1}$, which vanishes. There is a single correction to this picture, which can be traced back to (51) [19]: if both ends of an undecorated $\dot{\Delta}^{\mathcal{A}\mathcal{A}}$ kernel attach to the same str $\mathcal{A}\mathcal{A}$ factor, then we supplement the usual grou p theory factor with an additional -2.

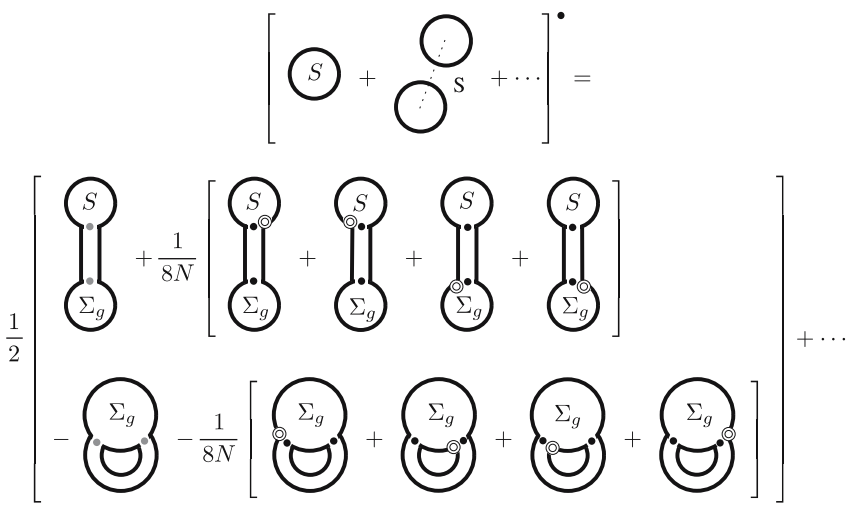

Fig. 6. The diagrammatic flow equation

In the unbroken phase, this actually causes a class of diagram which would naïvely vanish, to survive. These diagrams can possess any number of supertraces; the case in which a double supertrace is split into three supertraces is shown in Fig. 7.

Now, the expected group theory factor associated with this diagram arises from the two empty circuits in the padlock structure. These yield $(\mathrm{str}\ \mathbb{1})^2 = 0$. However, according to the above prescription, the group theory factor of this diagram is supplemented by -2, causing it to survive.

3.2.4 Kernels which bite their tails

As promised at the end of Sect. 2.1 we give, in Fig. 8, an explicit example of a portion of a diagram, potentially generated by the flow equation, which is not properly UV regularised; such diagrams, in which the kernel bites its tail are, as discussed already, to be discarded.

We take the explicitly shown fields, including the differentiated ones, to be components of supergauge fields, and the loop momentum to be k, as shown. The problem is that in the special case exemplified by Fig. 8, the integrand behaves at best as $1/k^3$ for large k, independent of the way the uncovariantised kernel decays with large momenta (and with a typically non-polynomial coefficient); this all follows from the Ward identities, cf. Appendix A of [9]. Although Lorentz invariance will then ensure that such a loop integral is only logarithmically divergent in $D = 4$ dimensions, the only escape from this divergence is by imposing (39) or by cancellation from some other contribution. In the latter case, however, whenever the inner and outer supertraces are decorated with specific flavours, the SU($N|N$) group theory properties are insufficient to enforce a cancellation. (For example we can take the inner supertrace to trap two A^1 fields, and assume the outer supertrace is fixed to be in the A^1 sector by decorations at the base of the kernel or on the vertex itself – where as a result these extra decorations do not dampen the large k behaviour.)

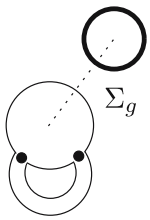

Fig. 7. A term which survives, despite naïvely vanishing by group theory considerations

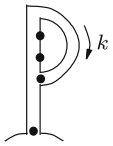

Fig. 8. An improperly UV regularised diagram

3.2.5 The broken phase flow equation

To work in the broken phase we now decorate our diagrams with the dynamical broken phase fields and σ, rather than $\mathcal{A}$ and $\mathcal{C}$ [19]. Functional derivatives are performed with respect to these dynamical fields, leading to corrections. These are easily computed by noting that (with a slight abuse of notation) e.g.

$$\frac{\delta}{\delta \tilde{A}^1} = \sigma_+ \frac{\delta}{\delta \mathcal{A}} \sigma_+ \,.$$

The effect of differentiating with respect to partial, rather than full, supermatrices is, therefore, simply insertions of $\sigma_\pm$. On a circuit containing other fields, these insertions have no effect, as they correspond to inserting unity in the appropriate subspace. On a circuit devoid of any fields, though, they have a profound effect: whereas, in the unbroken phase, such a circuit yields (up to the correction discussed earlier) $\mathrm{str}\ \mathbb{1} = 0$ now, however, such a circuit can produce $\mathrm{str}\ \sigma_\pm = \pm N$. (Note that the correction to exact supersplitting discussed earlier now manifests itself wherever there is an attachment of an undecorated $\dot{\Delta}^{AA}$ kernel to a separate str AA.)

Let us illustrate the use of the diagrammatic flow equation by considering the flow of the $S^{11}_{\mu\nu}(p)$ vertex. In Fig. 9 we focus on the classical part of the flow equation. Filled circles represent As and, if they are tagged with a '1', then they are restricted to the A^1 sector. The symbol $*$ represents insertions of σ and the symbol $\bullet$ tells us that an A has been differentiated and replaced with a σ. We have suppressed the Lorentz indices of the decorative fields. Note also that we have attached our false kernel to instances of σ, which do not carry a position argument. If the σ has replaced an A, then the position argument of the A is the information carried by the appropriate end of the false kernel. However, the other end may attach to a σ with no associated field to provide a position argument. In this case, the false kernel does not carry a position space δ-function, but just serves to remind us how the diagrams of which they comprise a part were formed. The ellipsis represents the un-drawn diagrams spawned by the quantum term.

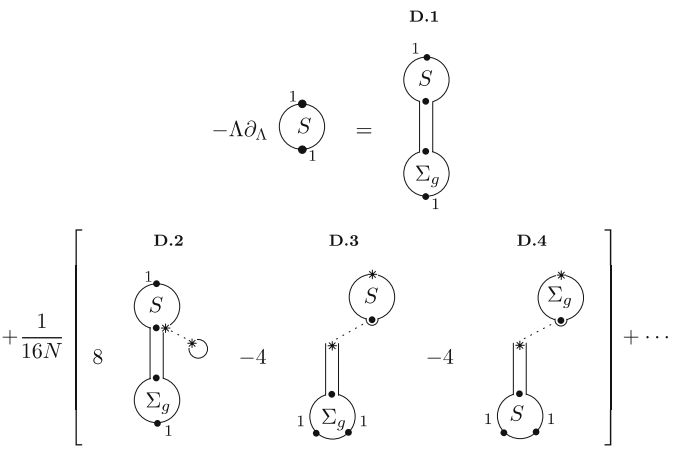

Fig. 9. Classical part of the flow of a vertex decorated by two A^1s

There are a number of important points to make about the diagrams of Fig. 9. Diagram D.1 is the only explicitly drawn diagram for which the kernel attaches to both vertices directly, as opposed to via $\mathcal{P}$. The factor of $1/2$ associated with the original a_0 terms has been killed by the factor of two coming from summing over the two possible locations of the fields which decorate the dumbbell. Notice that the differentiated fields are in the A-sector only. Generically, the differentiated fields can also be Fs and Cs. However, both of these are forbidden in this case by our choice of external fields: in the former case because S^{AF} vertices do not exist and, in the latter case, because the S^{AC} vertex vanishes by charge conjugation invariance.

Whilst we are free to choose the external fields to be A^1s, as opposed to $\tilde{A}^1$s, the internal fields necessarily possess an $\mathcal{A}^0$ component. Indeed, for internal fields to properly label the $\dot{\Delta}^{AA}$ kernel, we should take them to be full As, though noting that they are effectively reduced to $\tilde{A}^1$s by the choice of external fields. This feels somewhat unnatural and we will shortly adopt a more pleasing prescription. First, though, we will analyse the remaining diagrams of Fig. 9.

Diagram D.2 is a combination of four diagrams produced by the contributions to the flow equation involving $\mathcal{P}$, corresponding to the four ends of the kernel on which the σ can sit. Since these diagrams are equivalent, we can add them. Summing over the two locations of the decorative fields gives an overall relative factor of eight, as shown. The kernel is $\dot{\Delta}^{AA}_{\sigma}$. That it must be this, and not $\dot{\Delta}^{AA}$, can be deduced by the presence of components of ◎ at one of its ends. The final point to note about this diagram is that the extra supertrace, attached to the kernel via a false kernel, is just str $\sigma = 2N$. Thus we see that this diagram has the same overall factor as the first diagram.

Diagrams D.3 and D.4 both vanish. The uppermost vertices have an associated supertrace structure str $\sigma^2 = 0$. In fact, we need never have drawn these diagrams. In the former case, the S vertex coefficient function is $S^{A\sigma}$; single A vertices vanish by both charge conjugation and Lorentz invariance (similarly in the latter case, but with $S \leftrightarrow \Sigma_g$). In anticipation of what is to come, though, we note that multiple supertrace terms can have separate str $A\sigma$ factors. This will play a key rôle in what follows, since str $A\sigma$ is none other than $2N\mathcal{A}^0$.

Thus, to recapitulate, only the first two diagrams survive. They come with the same relative factor, have exactly the same vertices and so can be combined. The result will be that the two vertices are now joined by the sum of $\dot{\Delta}^{AA}$ and $\dot{\Delta}^{AA}_{\sigma}$. It seems natural to define

$$\dot{\Delta}^{A^1A^1} \equiv \dot{\Delta}^{11} \equiv \dot{\Delta}^{AA} + \dot{\Delta}^{AA}_{\sigma} \,. \tag{52}$$

We can do an analogous analysis in the A^2 sector. The difference here is that the embedded σ of the analogue of diagram D.2 gives rise to a minus sign since, whilst str $A^1A^1\sigma =$ str A^1A^1, str $A^2A^2\sigma = -$str A^2A^2. In this case, we are led to the definition

$$\dot{\Delta}^{A^2A^2} \equiv \dot{\Delta}^{22} \equiv \dot{\Delta}^{AA} - \dot{\Delta}^{AA}_{\sigma} \,. \tag{53}$$

However, neither (52) nor (53) work quite as we would like: the kernels $\dot{\Delta}^{AA}$ and $\dot{\Delta}^{AA}_{\sigma}$ do not attach to just A^1 or A^2, as the labels of $\dot{\Delta}^{11}$ and $\dot{\Delta}^{22}$ seem to imply; we know that there is also attachment to $\mathcal{A}^0$.

Nonetheless, both the physics of the situation and the diagrammatics seem to be guiding us to a formalism where we work with A^1s and A^2s – the so-called $A^{1,2}$ basis. It turns out that the most efficient way to proceed is to follow this lead. Recalling (24), we now split up the first term into derivatives with respect to A^1 and A^2:

$$\frac{\delta}{\delta A_\mu} = 2\sigma_+\tau_1^a \frac{\delta}{\delta A^1_{\mu a}} - 2\sigma_-\tau_2^a \frac{\delta}{\delta A^2_{\mu a}} + \frac{\sigma}{2N}\frac{\delta}{\delta \mathcal{A}^0_\mu} \,. \tag{54}$$

We now exploit no-$\mathcal{A}^0$ symmetry and so use the prescription that, since all *complete* functionals are independent of $\mathcal{A}^0$, we can take $\delta/\delta\mathcal{A}^0$ not to act.

It is important to realise, though, that this does not mean that we can simply dispense with $\mathcal{A}^0$ altogether. Were we to attempt to do this, we could always regenerate it, via gauge transformations. Thus, the only way to ensure that various actions are invariant under no-$\mathcal{A}^0$ symmetry is to enforce constraints between various vertices: though $\mathcal{A}^0$ is thus removed in one sense, its effects are nonetheless present. We have seen an example of this already in Sect. 3. The vertices $S^{AA\sigma}$ and $S^{A\sigma,A\sigma}$ are both individually associated with $\mathcal{A}^0$ components. However, the set of relationships of which

$$S^{AA\sigma} + 2NS^{A\sigma,A\sigma} = 0 \tag{55}$$

is an example ensure that the action as a whole is independent of $\mathcal{A}^0$ [23].

Let us consider the effects of taking $\mathcal{A}^0$ not to act in more detail. First, we note that we can no longer use exact supersowing/supersplitting: there will be additional corrections, which we will compute in a moment. Temporarily neglecting this, let us see what we have gained.

In diagrams D.1 and D.2, the internal fields can now be taken to be A^1s. Upon combining the diagrams, and utilising (52), the internal fields now naturally label the kernel (similarly in the A^2 sector).

What of diagrams D.3 and D.2? We have already noted that they vanish anyway, but this is only an accidental feature of the particular vertex whose flow we chose to compute. The real point is that they both contain a str $\sigma A = 2N\mathcal{A}^0$, which is attached to a kernel. In our new picture, we simply never draw such diagrams: we are not interested in external $\mathcal{A}^0$s and need not consider internal ones because we do not allow $\delta/\delta\mathcal{A}^0$ to act.

Moreover, when working in the $A^{1,2}$ basis, all diagrams involving ◉ vanish. This is because the differentiated field is now restricted to being an A^1 or A^2. However,

$$\text{str}\,\sigma\frac{\delta}{\delta A} = \text{tr}\,\sigma_+\frac{\delta}{\delta A^1} - \text{tr}\sigma_-\frac{\delta}{\delta A^2} \equiv 0 \,.$$

Had we still been using exact supersowing and supersplitting, str $\sigma\delta/\delta A$ terms could have survived [23]. (If supersowing and supersplitting are exact, we can think of the

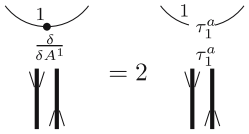

Fig. 10. Attachment of a kernel via $\delta/\delta A^1$

constrained superfield $\mathcal{A}$ behaving effectively like a 'full' superfield $\mathcal{A}^e$ [19]. Now str $\sigma\delta/\delta A^e \neq 0$.)

To compute the corrections arising from the abandonment of exact supersowing/supersplitting, consider attachment of a kernel via $\delta/\delta A^1$, as shown in

Note that, in the second diagram, we have retained the '1' which previously labelled the A^1, to remind us that the flavours of any fields which followed or preceded the A^1 are restricted.

Next, we use the completeness relation for SU(N),

$$2\,(\tau_1^a)^i{}_j\,(\tau_1^a)^k{}_l = \delta^i{}_l\delta^k{}_j - \frac{1}{N}\delta^i{}_j\delta^k{}_l\,, \tag{56}$$

to obtain Fig. 11, where attachments like those in the first column of diagram on the right-hand side will be henceforth referred to as direct.

There is a very similar expression for the A^2 sector. Now, however, σ_+s are replaced with σ_-s and the sign of the $1/N$ contribution flips [14]. We can also understand the sign flip heuristically because we are tying everything back into supertraces and not traces; we recall that the supertrace yields the trace of the bottom block-diagonal of a supermatrix but picks up a minus sign.

In the B, D and C sectors we do not get any $1/N$ attachment corrections. Derivatives with respect to the fields B and $\bar{B}$, can simply be written

$$\frac{\delta}{\delta B} = \sigma_- \frac{\delta}{\delta \mathcal{A}}\sigma_+\,, \tag{57}$$

$$\frac{\delta}{\delta \bar{B}} = \sigma_+ \frac{\delta}{\delta \mathcal{A}}\sigma_-\,, \tag{58}$$

and so derivatives with respect to these partial superfields just yield insertions of $\sigma_\pm$.

In the C-sector, $\mathcal{C}^0$ does not play a privileged rôle [14] and so has not been factored out of the definition of C^1 and C^2 (see (16)). Hence, derivatives with respect to the components of $\mathcal{C}$ simply yield insertions of $\sigma_\pm$.

Let us now reconsider the classical part of the flow of a vertex decorated by two fields. These fields can be any of A^1, A^2, C^1, C^2, F and $\bar{F}$ (though certain choices e.g. A^1A^2 correspond to a vanishing vertex). The diagrammatics is shown in Fig. 12, where we have neglected not only the quantum terms but also any diagrams in which the kernel is decorated.[10]

The differentiated fields now label the kernels, where we take $\dot{\Delta}^{C^1C^1} = \dot{\Delta}^{C^2C^2} = \dot{\Delta}^{CC}$ and $\dot{\Delta}^{\bar{F}F} = \dot{\Delta}^{F\bar{F}}$. The only subtlety comes in the $A^{1,2}$ sectors, where we know

[10] Such diagrams only exist in the C-sector, in this case, since this is the only sector for which one-point (seed action) vertices exist.

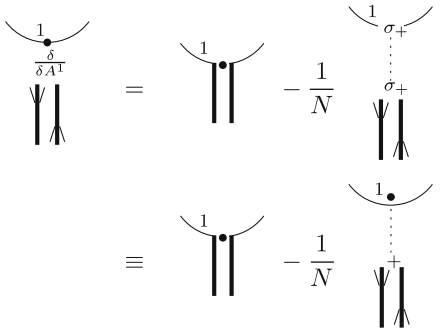

Fig. 11. A re-expression of Fig. 10

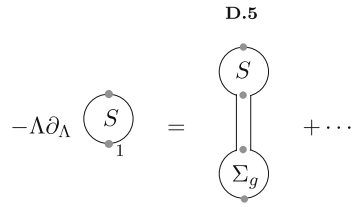

Fig. 12. Classical part of the flow of a two-point vertex decorated by the fields A^1, A^2, C^1, C^2, F and $\bar{F}$

that there are corrections, which have been implicitly absorbed into the Feynman rules. We will be more specific about the corrections in this case – i.e. where the kernel is undecorated.

From Fig. 11 we obtain the relation of Fig. 13.

The expression in Fig. 13 now simplifies. The loop in the middle of the final diagram is decorated only by σ_+^2 and so yields str $\sigma_+ = N$. This diagram then cancels either of those with factor $-1/N$. We now redraw the remaining diagram with factor $-1/N$, as shown in Fig. 14, together with a similar expression in the A^2 sector.

Then meaning of the double dotted lines and the associated field hiding behind the line of the supertrace should be clear: the double dotted lines stand for $\dot{\Delta}^{A^iA^i}$, and the sector of the associated fields tells us whether $i = 1$ or 2.

Returning now to diagram D.5 (Fig. 12) we should interpret the kernel when the internal fields are in the A^1 or A^2 sectors according to Fig. 14.

In our analysis of the terms spawned by the classical part of the flow equation, we have so far restricted ourselves to diagrams in which the kernel is undecorated and for which there are no insertions of the dynamical components of $\mathcal{C}$ via $\mathcal{P}$ (recall that such insertions occur as in Fig. 5).

Let us first relax just the former restriction and analyse the mapping into the A^1, A^2 basis [23]. The simplest case to deal with is where the decorations of the covariantised kernels $\{\dot{\Delta}^{\mathcal{A}\mathcal{A}}\}$ and $\{\dot{\Delta}^{\mathcal{A}\mathcal{A}}_\sigma\}$ are, on each side *independently*, net bosonic. In this scenario, we are just mapped into the A^1, A^2 basis, as before.

The next case to examine is where the decorations on one side of the kernel are net bosonic but those on the other side are net (anti) fermionic. This immediately tells us that one of the functional derivatives sitting at the end of the kernel must be (anti) fermionic. Now, as before, we would like to pair up diagrams with a $\{\dot{\Delta}^{\mathcal{A}\mathcal{A}}\}$ vertex with those

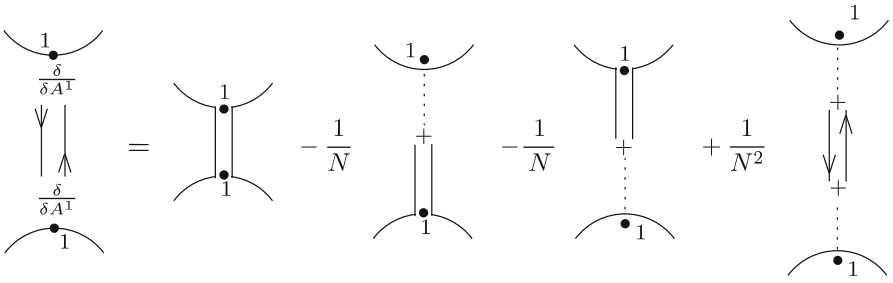

Fig. 13. The attachment corrections for $\dot{\Delta}^{11}$

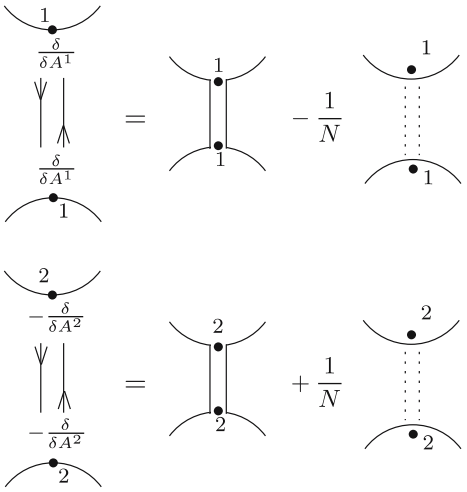

Fig. 14. The attachment corrections for $\dot{\Delta}^{11}$ and $\dot{\Delta}^{22}$

with a $\{\dot{\Delta}_\sigma^{\mathcal{A}\mathcal{A}}\}$ vertex. However, there is a subtlety: σ anti-commutes with net fermionic structures. Thus, of the four terms generated with a σ at the end of one side of the kernel attached to a separate str σ, two cancel. Hence, the vertex from $\{\dot{\Delta}_\sigma^{\mathcal{A}\mathcal{A}}\}$ has a factor of half relative to the vertex from $\{\dot{\Delta}^{\mathcal{A}\mathcal{A}}\}$.

We can still choose a prescription to map us into the A^1, A^2 basis by absorbing this factor into our definition of e.g. $\dot{\Delta}^{1B,F\cdots,\cdots}$, where both ellipses denote net bosonic decorations.[11]

The final case to examine is where the decorations on one side of the kernel are net fermionic whilst those on the other side are net anti-fermionic.[12] The functional derivatives must both be bosonic and in separate sub-sectors.[13] There are no surviving contributions involving $\{\dot{\Delta}_\sigma^{\mathcal{A}\mathcal{A}}\}$ vertices. Nonetheless, we can still define an object $\{\dot{\Delta}^{A^1A^2}\}$ though we note that it must have net fermionic decorations on both sides.

Let us now relax the second restriction above and so allow insertions of the dynamical components of $\mathcal{C}$ at the ends of kernels, via $\mathcal{P}$. Such diagrams occur only with $\dot{\Delta}_\sigma^{\mathcal{A}\mathcal{A}}$ kernels and there is no natural way of mapping such terms into the A^1, A^2 basis. There is, of course, nothing to stop us performing functional derivatives with respect to A^1 and A^2 only – indeed, this is what we will do. However, the differentiated fields do not now label the kernels in a natural way.

In fact, as we will see (see also [23, 52–54]), considerations such as this ultimately do not bother us: we will find that, in our calculation of β-function coefficients, all instances of these awkward terms cancel, amongst themselves. Hence, our strategy is to lump all the unpleasant terms into our diagrammatic rules, so that they essentially become hidden. We can, at any stage, unpack them if necessary but, generally speaking, we will find that we do not need to do so (see [23] for an explicit example of this).

This completes the analysis of the diagrammatics we have performed for the new flow equation. We have not explicitly looked at the quantum term, but there are no new considerations in this case. Thus, we can summarise the prescription that we use in the broken phase.

1. All decorative fields are instances of A^1, A^2, F, $\bar{F}$, C^1, C^2 and σ; $\mathcal{A}^0$ is excluded.
2. Differentiation is with respect to all dynamical fields, above, where:
   (a) differentiation with respect to A^1 or A^2 leads to attachment corrections of the type shown in Fig. 11;
   (b) differentiation with respect to all other fields just involves insertions of $\sigma_\pm$;
   (c) diagrams involving str $\sigma\delta/\delta A^{1,2}$ vanish, identically.
3. Full diagrams without any insertions of the components of ◎ at the ends of the kernels are naturally written in terms of the above fields and their corresponding kernels i.e. A^1s attach to a (decorated) $\dot{\Delta}^{11}$ etc.
4. Full diagrams with insertions of the components of ◎ are restricted to those for which at least one component is not a σ (in the case that both components are σs, these terms have already been used to map us into the $A^{1,2}$ basis). These diagrams involve the kernel $\dot{\Delta}_\sigma^{AA}$ but, for convenience, are packaged together with the decorated kernels of the previous item.

3.3 The new diagrammatics

3.3.1 Construction

The work of the previous section now guides us to a more compact and intuitive diagrammatics, which is considerably easier to deal with. By packaging up the remaining

[11] Note that the B denotes a functional derivative with respect to B; since this removes a fermion, the kernel decorations must be net fermionic.

[12] If the decorations on both sides are (anti) fermionic, then the vertex belongs to $\{\dot{\Delta}^{F\bar{F}}\}$.

[13] It is straightforward to check that one cannot construct a legal kernel of this type for which the functional derivatives are fermionic and anti-fermionic.

$\dot{\Delta}_\sigma^{AA}$ kernels with decorated instances of the other kernels, we have taken a step in the right direction. In anticipation that these compact, packaged objects cancel in their entirety when we perform actual calculations, it clearly makes sense to bundle together kernels of a different flavour. However, by doing this, we have started to combine diagrams with differing supertrace structures. In this section, we extend this to its natural conclusion.

The basic idea is that, rather than considering diagrams with a specific supertrace structure, we instead sum over all legal supertrace structures, consistent with the decorative fields. Thus, let us suppose that we wish to compute the flow of all vertices which can be decorated by the set of fields $\{f\}$. The new flow equation takes a very simple, intuitive form, as shown in Fig. 15.

Let us now analyse each of the elements of Fig. 15 in turn. On the left-hand side, we have the set of vertices whose flow we are computing. This set comprises all cyclically independent arrangements of the fields $\{f\}$, over all possible (legal) supertrace structures. When we specify the fields $\{f\}$, we use a different notation from before. As an example, consider $\{f\} = \{A^1_\mu, A^1_\nu, C^1\}$, shown in Fig. 16. Note that we have not drawn any vertices comprising a supertrace decorated only by an A^1, since these vanish.

It is apparent that we denote As by wiggly lines and Cs by dashed lines. A wildcard field will be denoted by a solid line.

Notice how, in the new style diagram, we explicitly indicate the sub-sector of all the fields. This is because there is no need for them to be on the same supertrace and so, for example, there is nothing to prevent an $A^1A^1C^2$ vertex. In the old notation, however, all fields on the same circle are on the same supertrace and so, once we know the sub-sector of one field, the sub-sectors of the remaining fields on the same circle follow, uniquely.

To symbolically represent the new vertices, we will somewhat loosely write e.g. $S^{11C^1}_{\mu\nu}$. If we need to emphasise that we are using the new style diagrammatics, as opposed to the old style diagrammatics, then we will write $S^{\{11C^1\}}_{\mu\nu}$, reminding us that the fields are arranged in all cyclically independent ways over all possible (legal) supertrace structures.

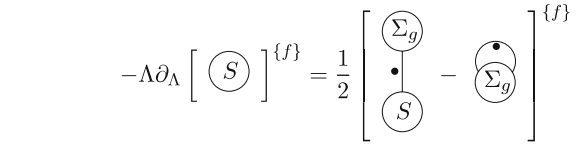

Fig. 15. The diagrammatic form of the flow equation, when we treat single and multiple supertrace terms together

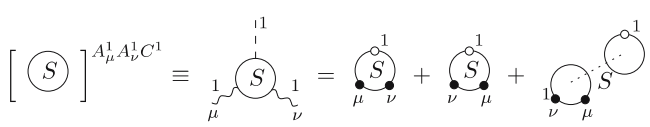

Fig. 16. A new style vertex decorated by two A^1s and a C^1

With these points in mind, let us return to Fig. 15. The diagrams on the right-hand side both involve the structure —•—. This is a dummy kernel which attaches, at either end, to dummy fields. The fields at the ends can be any of A^1, A^2, C^1, C^2, $\bar{F}$ or F, so long as the corresponding diagram actually exists. The dummy kernel can be decorated by any subset of the fields $\{f\}$ where, if a pair of decorative fields are both components of $\mathcal{C}$ (and one of them is dynamical), then we include the possibility that the kernel can be of the type $\dot{\Delta}_\sigma^{\mathcal{A}\mathcal{A}}$. In this case, we note that there are implicit factors of $1/16N$.

The relationship between the new diagrammatics for the kernels and the old diagrammatics is straightforward, and is illustrated in Fig. 17 for the case of a new-style kernel decorated by a single A^1.

Having described the new diagrammatics for vertices and kernels, we are nearly ready to complete our interpretation of Fig. 15. Before we do so, however, we use our new notation to hide one further detail: instances of σ. Instances of σ correspond either to insertions of $\pm\mathbb{1}$ in the relevant subspace or to factors of $2N$. Thus, instances of σ can be replaced by numerical factors accompanying kernels/vertices. We need only remember that the multiple supertrace decorations of kernels exist. Such terms require two instances of $\mathcal{C}$ (at least one of which we take to be dynamical). In the case that one of these fields is a σ, we must remember that it is now hidden.

With these implicit instance of σ in mind, the interpretation of the right-hand side of Fig. 15 is simple: the decorative fields $\{f\}$ are distributed around the two diagrams in all possible, independent ways.

Whilst we will generally use the new diagrammatics thus described, from now on, it is occasionally useful to flip back to the old style mentality of specifying the supertrace structure. It turns out that, in this paper, we only ever have recourse to do this for single supertrace terms and so introduce the notation 'Fields as Shown' or FAS. An example of this is illustrated in Fig. 18.

3.3.2 Constraints in the C-sector

We conclude our description of the new diagrammatics with an explicit illustration of their use. Recall from Sect. 2.1 that, in order to ensure quantum corrections do

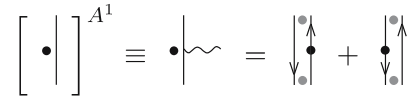

Fig. 17. A new style (dummy) kernel decorated by a single A^1

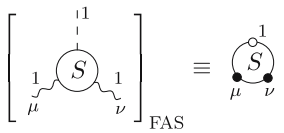

Fig. 18. An example of the meaning of FAS

not shift the minimum of the Higgs potential from the classical choice, σ, $\hat{S}$ is constrained. Assuming that these quantum corrections vanish means that all Wilsonian effective action one-point C vertices vanish. We can thus use the flow equation to give us a constraint equation, as shown in Fig. 19. Note that the external fields can be in either the 1 or 2 sub-sector.

To go from the first line to the second line, we have used (11) and have discarded all one-point, Wilsonian effective action vertices. To satisfy Fig. 19, we tune the one-point, seed action vertex in the first diagram, which is something we are free to do.

3.4 The weak coupling expansion

In preparation for the computation of perturbative β function coefficients, we examine the form the flow equation takes in the limit of weak coupling and investigate some of its properties.

3.4.1 The flow equation

Following [9, 19], the action has the weak coupling expansion

$$S=\sum_{i=0}^{\infty}\left(g^2\right)^{i-1}S_i=\frac{1}{g^2}S_0+S_1+\cdots\,, \tag{59}$$

where S_0 is the classical effective action and the $S_{i>0}$ the ith-loop corrections. The seed action has a similar expansion:

$$\hat{S}=\sum_{i=0}^{\infty}g^{2i}\hat{S}_i\,. \tag{60}$$

Note that these definitions are consistent with $\Sigma_g=g^2S-2\hat{S}$; identifying powers of g in the flow equation, it is clear that S_i and $\hat{S}_i$ will always appear together. With this in mind, we now define

$$\Sigma_i=S_i-2\hat{S}_i\,. \tag{61}$$

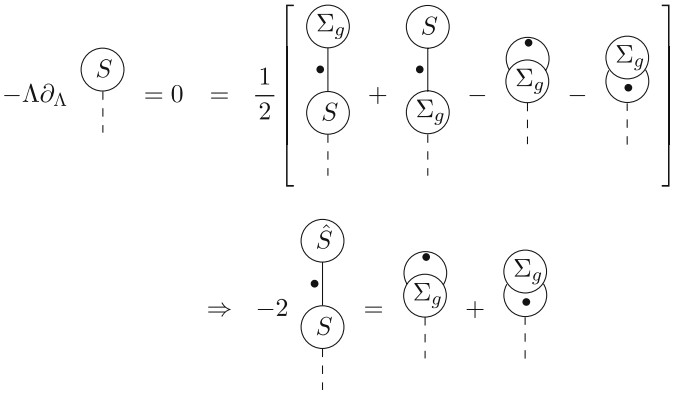

Fig. 19. The constraint arising from ensuring that the position of the minimum of the Higgs potential is unaffected by quantum corrections

The β functions for g and g_2 are

$$\Lambda\partial_\Lambda\frac{1}{g^2}=-2\sum_{i=1}^{\infty}\beta_i(\alpha)g^{2(i-1)} \tag{62}$$

$$\Lambda\partial_\Lambda\frac{1}{g_2^2}=-2\sum_{i=1}^{\infty}\tilde{\beta}_i(1/\alpha)g_2^{2(i-1)}\,, \tag{63}$$

where the $\beta_i(\alpha)$ are determined through the renormalisation condition (40) and the $\tilde{\beta}_i(1/\alpha)$ are determined through (42). The coefficient $\beta_1=-\tilde{\beta}_1$ is independent of α [19, 23]. For generic α, we expect the coefficient $\beta_2(\alpha)$ to disagree with the standard value; as we will explicitly confirm in [50], agreement is reached for $\beta_2(0)$.[14]

Utilising (62), (63) and (1), it is apparent that $\Lambda\partial_\Lambda\alpha$ has the following weak coupling expansion:

$$\Lambda\partial_\Lambda\alpha=\sum_{i=1}^{\infty}\gamma_i g^{2i}\,, \tag{64}$$

where

$$\gamma_i=-2\alpha\left(\beta_i(\alpha)-\alpha^i\tilde{\beta}_i(1/\alpha)\right)\,.$$

Writing[15]

$$\Lambda\partial_\Lambda S=\Lambda\partial_\Lambda|_\alpha S+\Lambda\partial_\Lambda\alpha\,\frac{\partial S}{\partial\alpha}\,,$$

the weak coupling flow equations are given by

$$\begin{aligned}\dot{S}_n=&\sum_{r=1}^{n}\left[2(n-r-1)\beta_r S_{n-r}+\gamma_r\frac{\partial S_{n-r}}{\partial\alpha}\right]\\&+\sum_{r=0}^{n}a_0\left[S_{n-r},\Sigma_r\right]-a_1\left[\Sigma_{n-1}\right]\,,\end{aligned} \tag{65}$$

where we have now changed notation slightly such that $\dot{X}$ is redefined to mean $-\Lambda\partial_\Lambda|_\alpha X$. Incidentally, we note that the kernels $\dot{\Delta}^{ff}$ appearing in the flow equation are defined according to this new definition of $\dot{X}$. This is a choice we are free to make about the flow equation and do so, since it makes life easier.

The diagrammatics for the new weak coupling flow equation follow, directly. However, we note that the classical term can be brought into a more symmetrical form. This follows from the invariance of $a_0[S_{n-r},\Sigma_r]+a_0[S_r,\Sigma_{n-r}]$ under $r\to n-r$. We exploit this by recasting the classical term as follows:

$$\begin{aligned}&a_0[\bar{S}_{n-r},\bar{S}_r]\\&\quad\equiv a_0[S_{n-r},S_r]-a_0[S_{n-r},\hat{S}_r]-a_0[\hat{S}_{n-r},S_r]\,.\\&\quad=\begin{cases}\frac{1}{2}\left(a_0[S_{n-r},\Sigma_r]+a_0[S_r,\Sigma_{n-r}]\right) & n-r\neq r\\ a_0[S_r,\Sigma_r] & n-r=r\,.\end{cases}\end{aligned} \tag{66}$$

[14] We note that whilst we expect $\beta_2(0)=\tilde{\beta}_2(0)$, there is no reason to generically expect $\tilde{\beta}_2(1/\alpha)=\beta_2(\alpha)$ since g and g_2 are not treated symmetrically in the flow equation.

[15] We avoid writing $\partial/\partial\alpha$ as ∂_α to avoid confusion later, when we will have momentum derivatives which are written e.g. ∂_α^k.

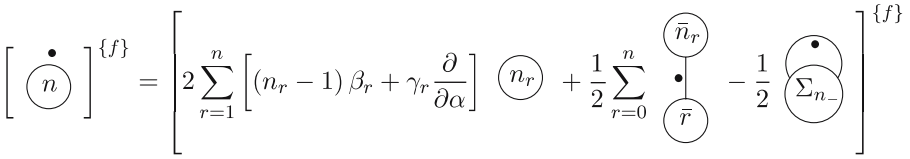

Fig. 20. The new diagrammatic form for the weak coupling flow equation

Hence, we can rewrite the flow equation in the following form:

$$\dot{S}_n = \sum_{r=1}^{n} \left[2(n-r-1)\beta_r S_{n-r} + \gamma_r \frac{\partial S_{n-r}}{\partial \alpha} \right] + \sum_{r=0}^{n} a_0 \left[\bar{S}_{n-r}, \bar{S}_r \right] - a_1 \left[\Sigma_{n-1} \right] . \tag{67}$$

The diagrammatic version is shown in Fig. 20. A vertex whose argument is a letter, say n, represents S_n. We define $n_r := n - r$ and $n_\pm := n \pm 1$.

Terms like the one on the left-hand side, in which the entire diagram is struck by $\Lambda\partial_\Lambda|_\alpha$, are referred to as Λ-derivative terms. On the right-hand side, in addition to the usual classical and quantum terms, we have what we call the β and α terms.

3.4.2 The effective propagator relation

The tree level flow equations are obtained by specialising equation (65) or (67) to $n = 0$:

$$\dot{S}_0 = a_0[S_0, \Sigma_0] . \tag{68}$$

We now further specialise, to consider the flow of all two-point vertices, as shown in Fig. 21. Recall that the solid lines represent dummy fields, which we choose to be instances of A^1, A^2, C^1, C^2, $\bar{F}$ and F.

Equation shown in Fig. 21 is analogous to (8), but there are a number of things to note. First, there is no possibility of embedding components of $\mathcal{C}$ at the ends of the kernels and so the $\dot{\Delta}_\sigma^{AA}$ kernel does not appear.[16] Secondly, diagrams containing one-point, tree level vertices have not been drawn, since these vertices do not exist in any sector, for either action.[17] Lastly, if we work in the C-sector, then each of the vertices can possess more than one supertrace. We can and do consistently set [23]

$$\hat{S}_0^{C^{1,2},C^{1,2}}(p) , \quad S_0^{C^{1,2},C^{1,2}}(p) = 0 .$$

As described in Sect. 2.1, our strategy is now to set the two-point, tree level, seed action vertices equal to their Wilsonian effective action counterparts and integrate up, choosing the integration constants appropriately [23]. Aided by the Ward identities, it is straightforward to obtain the effective propagator relation [19, 23]:

$$S_{0MS}^{XY}(p)\Delta_{SN}^{YZ}(p) = \delta_{MN} - p'_M p_N , \tag{69}$$

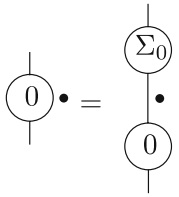

Fig. 21. Flow of all possible two-point, tree level vertices

Table 2. Prescription for interpreting (69)

	δ_{MN}	p'_M	p_N
$F, \bar{F}$	δ_{MN}	$(f_p p_\mu/\Lambda^2, g_p)$	$(p_\nu, 2)$
A^i	$\delta_{\mu\nu}$	p_μ/p^2	p_ν
C^i	$\mathbb{1}$	–	–

where the fields X, Z are any broken phase fields, the field Y is summed over and we identify the components of the right-hand side according to Table 2. (Note that the field Z must, in fact, be the same as Y, since 'mixed' effective propagators do not exist.)

The functions $f(k^2/\Lambda^2)$ and $g(k^2/\Lambda^2)$ need never be exactly determined (though for an explicit algebraic realisation for arbitrary α see [23]); rather, they must satisfy general constraints enforced by the requirements of proper UV regularisation of the physical SU(N) theory and gauge invariance. We will see the effect induced by the latter shortly.

The object $p'_M p_N$ is, of course, a gauge remainder, which we represent diagrammatically by ▶; the constituent components are furnished with the following diagrammatic representations:

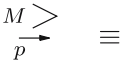

$$\equiv \quad p'_M , \tag{70}$$

$$\equiv \quad p_N , \tag{71}$$

3.4.3 Diagrammatic identities

We conclude this section with a set of diagrammatic identities. First, denoting the effective propagator by a long, solid line, we cast the effective propagator relation (69) in a particularly appealing diagrammatic form. Note that we have attached the effective propagator, which only ever appears as an internal line, to an arbitrary structure.

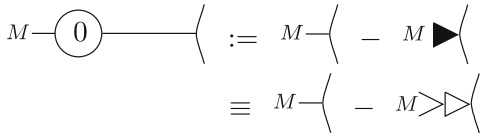

(72)

[16] Up to instances which have been used to map is into the $A^{1,2}$ basis, in the first place.

[17] Recall that one-point, seed action vertices exist only from the one-loop level.

It is important to note that we have defined the diagrammatics in (72) such that there are no $1/N$ corrections where the effective propagator attaches to the two-point, tree level vertex. We do this because, when the composite object on the left-hand side of (72) appears in actual calculations, it always occurs inside some larger diagram. It is straightforward to show that, in this case, the aforementioned attachment corrections always vanish [23].

The next diagrammatic identity follows from gauge invariance and the constraint placed on the vertices of the Wilsonian effective action by the requirement that the minimum of the Higgs potential is not shifted by quantum corrections:

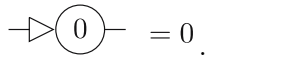

(73)

This follows directly in the A-sector, since one-point A-vertices do not exist. In the F-sector, though, we are left with one-point C^1 and C^2-vertices, but these are constrained to be zero.

From the effective propagator relation and (73), two further diagrammatic identities follow. First, consider attaching an effective propagator to the right-hand field in (73) and applying the effective propagator before $\triangleright$ has acted. Diagrammatically, this gives

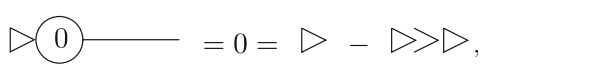

which implies the following diagrammatic identity:

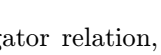

(74)

The effective propagator relation, together with (74) implies that

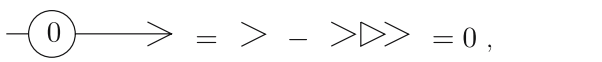

In other words, the (non-zero) structure $\longrightarrow$ kills a two-point, tree level vertex. But, by (73), this suggests that the structure $\longrightarrow$ must be equal, up to some factor, to $\triangleleft$. Indeed,

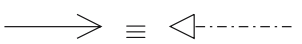

(75)

where the dot-dash line represents 'pseudo effective propagators'. The exact form of these is not required, though a particular algebraic representation is given in [23].

The final diagrammatic identity we require follows directly from the independence of $\triangleright$ on Λ (see Table 2):

(76)

4 Further diagrammatic techniques

The effective propagator relation allows us to replace a two-point vertex connected to an effective propagator with a Kronecker δ and a gauge remainder. In Sect. 4.1, we will see how we can deal with these remainders, diagrammatically. This will require that we broaden our understanding of both the Ward identities and no-$\mathcal{A}^0$ symmetry.

In Sect. 4.2, we utilise the insights gained from the treatment of the gauge remainders to develop a diagrammatic technique for Taylor expanding vertices and kernels in momenta.

4.1 Gauge remainders

Up until now, we have referred to the composite object $> \triangleright$ as a gauge remainder. Henceforth, we will often loosely refer to the individual components as gauge remainders. To make an unambiguous reference, we call $\triangleright$ an active gauge remainder, $>$ a processed gauge remainder and $> \triangleright$ a full gauge remainder.

4.1.1 Action vertices

We begin by considering an arbitrary action vertex, which is contracted with the momentum carried by one of its fields, X, as shown on the left-hand side of Fig. 22. All of the fields shown are wildcards, though the field X has no support in the C-sector. To proceed, we use the Ward identities (36) and (38), which tell us that we either push forward or pull back (with a minus sign) the momentum of X to the next field on the vertex. We recall from Sect. 3.2.1 that fields are read off a vertex in the counterclockwise sense; hence, we push forward counterclockwise and pull back clockwise.

Since the vertex contains all possible (cyclically independent) orderings of the fields, spread over all (legal) combinations of supertraces, any of the fields could precede or follow X. Hence, we must sum over all possible pushes forward and pulls back, as shown on the right-hand side of Fig. 22.

It is clear from the Ward identities (36) and (38) that the diagrams on the right-hand side of Fig. 22 have no explicit dependence on the field X. Nonetheless, to interpret the diagrams on the right-hand side unambiguously, without reference to the parent, we must retain information about X. This is achieved by keeping the line which used to represent X but which is now terminated by a half arrow, rather than entering the vertex. This line carries information about the flavour of X and its momentum, whilst indicating which field it is that has been pushed forward/pulled back onto. The half arrow can go on either side of the line.[18]

The new-style diagrammatics we have been using has been, up until now, completely blind to details concerning the ordering of fields and the supertrace structure. If we are to treat gauge remainders diagrammatically, we can no longer exactly preserve these features. Let us suppose that we have pushed forward the momentum of X onto the field

[18] This should be borne in mind when we encounter pseudo effective propagators, attached to $\triangleright$.

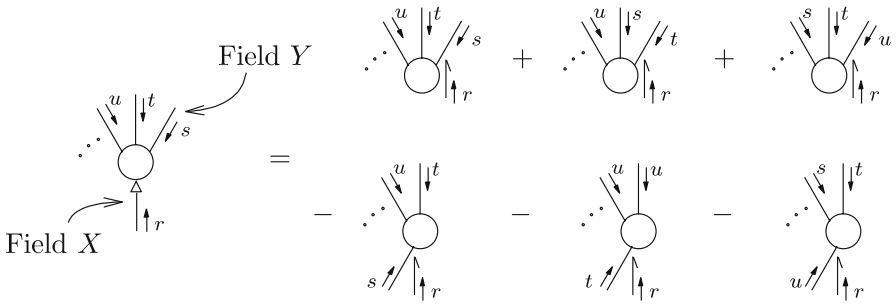

Fig. 22. The left-hand side shows the contraction of an arbitrary vertex with one of its momenta. On the right-hand side, the first row of diagrams shows all possible pushes forward onto the explicitly drawn fields and the second row shows all possible pulls back

Y, as depicted in the first diagram on the right-hand side of Fig. 22. Clearly, it must be the case that X and Y are on the same supertrace and that Y is immediately after X, in the counter-clockwise sense. The other fields on the vertex – which we will call spectator fields – can be in any order and distributed amongst any number of supertraces, up to the requirement that they do not come between the fields X and Y. To deduce the momentum flowing into the vertex along Y, we simply follow the indicated momentum routing. Hence, momentum $r+s$ enters the vertex along Y, in the case that it is the field Y that has been pushed forward (pulled back) on to. Similarly, if we push forward onto the field carrying momentum t, then momentum $r+t$ enters the vertex, along this field. The flavour changes induced in Y if X is fermionic, are given by Table 1.

However, we see that this has the capacity to reintroduce $\mathcal{A}^0$s, via the fields $\tilde{A}^i$. We now describe how we can use no-$\mathcal{A}^0$ symmetry to map us back into the $A^{1,2}$ basis.

Let us suppose that we have some vertex which is decorated by, for example, an F and a $\bar{B}$ and that these fields are on the same supertrace. Now consider contracting the vertex with the momentum of the F. There are two cases to analyse. The first is where there are other fields on the same supertrace as the F and $\bar{B}$. For argument's sake, we will take them to be such that the $\bar{B}$ follows the F (in the counterclockwise sense). Now the F can push forward onto the $\bar{B}$, generating an $\tilde{A}^1$. In this case, the vertex *coefficient function* is blind to whether its argument involves $\tilde{A}^1$ or A^1: starting with a vertex containing $\tilde{A}^1$, we can always remove the $\mathcal{A}^0$ part by no-$\mathcal{A}^0$ symmetry.

The second case to look at is where there are no other fields on the same supertrace as F and $\bar{B}$. Now the F can both push forward and pull back onto the $\bar{B}$ generating, respectively, $\tilde{A}^1$ and $\tilde{A}^2$. However, we cannot rewrite $\tilde{A}^{1,2}$ as $A^{1,2}$ since, whereas str $\tilde{A}^{1,2} \neq 0$, str $A^{1,2} = 0$. Our strategy is to rewrite vertices involving a separate str $\tilde{A}^{1,2}$ factor via no-$\mathcal{A}^0$ symmetry.

We have encountered a no-$\mathcal{A}^0$ relation already – see (55). Now we will generalise this relationship, which is most readily done by example. Consider the following part of the action, where we remember that all position arguments are integrated over:

$$\cdots + \frac{1}{3} S^{111}_{\alpha\beta\gamma}(x,y,z)\text{str}\ \tilde{A}^1_\alpha(x)\tilde{A}^1_\beta(y)\tilde{A}^1_\gamma(z) + \frac{1}{2} S^{11,A\sigma}_{\alpha\beta,\gamma}(x,y;z)\text{str}\ \tilde{A}^1_\alpha(x)\tilde{A}^1_\beta(y)\ \text{str}\ A_\gamma(z)\sigma + \cdots$$

We note that, in the second term, we have combined $S^{AA,A}$ with $S^{A,AA}$, thereby killing the factor of $1/2!$ associated with each of these vertices.

To determine the no-$\mathcal{A}^0$ relationship between these vertices, we shift A: $\delta A_\mu(x) = \lambda_\mu(x)\mathbb{1}$, and collect together terms with the same supertrace structure and the same dependence on λ_μ. By restricting ourselves to the portion of the action shown, we only find common terms which depend on a single power of λ_μ. By using a larger portion of the action we can, of course, obtain higher order relationships, although it can be shown that these all follow from the first order relations [18]. In the single supertrace vertex, this operation simply kills the factor of $1/3$; in the double supertrace term, we focus on shifting the lone A which yields:

$$\cdots + \lambda_\gamma(z) S^{111}_{\alpha\beta\gamma}(x,y,z)\text{str}\ \tilde{A}^1_\alpha(x)\tilde{A}^1_\beta(y) + \frac{1}{2}\lambda_\gamma(z) S^{11,A\sigma}_{\alpha\beta,\gamma}(x,y;z)\text{str}\ \tilde{A}^1_\alpha(x)\tilde{A}^1_\beta(y)\ \text{str}\ \sigma + \cdots$$

Taking into account invariance under the cylic permutation of the arguments of the supertrace in the first term, no-$\mathcal{A}^0$ symmetry requires:

$$S^{111}_{\alpha\beta\gamma}(x,y,z) + S^{111}_{\alpha\gamma\beta}(x,z,y) + 2N S^{11,A\sigma}_{\alpha\beta,\gamma}(x,y;z) = 0\,.$$

We now recast the final term, so that we work with $\tilde{A}^1$s and $\tilde{A}^2$s, rather than $A\sigma$. This is a little counterintuitive. At first, we recognise that $A\sigma = \tilde{A}^1 - \tilde{A}^2$. However, $\tilde{A}^1$ and $\tilde{A}^2$ are not independent. Specifically,

$$\text{str}\ \tilde{A}^1 = N\mathcal{A}^0 = -\text{str}\ \tilde{A}^2\,.$$

Consequently, we need to be careful what we mean by the vertex coefficient functions $S^{\cdots,\tilde{A}^{1,2}}$. If, as we will do, we treat the vertex coefficient functions $S^{\cdots,\tilde{A}^1}$ and $S^{\cdots,\tilde{A}^2}$ as independent then, by recognising that

$$S^{\cdots,\tilde{A}^1}(\text{str}\ \cdots)\text{str}\ \tilde{A}^1 + S^{\cdots,\tilde{A}^2}(\text{str}\ \cdots)\text{str}\ \tilde{A}^2$$

is equivalent to

$$S^{\cdots,A\sigma}(\text{str}\ \cdots)\text{str}\ A\sigma$$

and writing out the explicitly indicated supertraces in terms of $\mathcal{A}^0$ and N, we find that

$$S^{\cdots,\tilde{A}^1} - S^{\cdots,\tilde{A}^2} = 2S^{\cdots,A\sigma}\,.$$

The factor of two on the right-hand side is, perhaps, unexpected; we emphasise that it comes from splitting up the variable $\mathcal{A}^0$ between $\tilde{A}^1$ and $\tilde{A}^2$. In Fig. 23 we give a diagrammatic form for the subset of first order no-$\mathcal{A}^0$ relations which relate single supertrace vertices to two supertrace vertices.

A number of comments are in order. First, this relationship is trivially generalised to include terms with additional supertraces. Secondly, if we restrict the action to single supertrace terms, as in [18, 19], then the first two lines reproduce the no-$\mathcal{A}^0$ relations of [18]. Thirdly, the Feynman rules are such that some of the diagrams of Fig. 23 can be set to zero, for particular choices of the fields which decorate the vertex. For example, if all decorative fields are A^1s or C^1s, then the second row of diagrams effectively vanishes.

For the purposes of this paper, the only place we generate $\tilde{A}^1$s is as internal fields. Since internal fields are always attached to kernels (or effective propagators), we can absorb the factors of N appearing in Fig. 23 into our rules for attaching kernels/effective propagators to vertices. This is illustrated in Fig. 24, where the ellipsis denotes un-drawn pushes forward and pulls back, onto the remaining fields, $\{f\}$, which also decorate the vertex.

There are a number of things to note. First, the gauge remainder strikes the vertex and not the base of the kernel; this is ambiguous from the way in which we have drawn the diagrams though this ambiguity is, in fact, deliberate, as we will discuss shortly. Thus, whilst the vertex now possesses an $A^{1,2}$ field, the kernel is still labelled by $\bar{B}$. Secondly – and this is the whole point of our prescription – the field struck by the gauge remainder becomes an $A^{1,2}$, and not an $\tilde{A}^{1,2}$; the missing contributions to the vertex have been effectively absorbed into the kernel Feynman rule (cf. Fig. 11). Thirdly, we implicitly sum over all possible ways in which the un-drawn fields, $\{f\}$, decorate the vertex in all diagrams (including those with the old-style notation). This ensures that all diagrams in the no-$\mathcal{A}^0$ relationship shown in Fig. 23 are included. Lastly, we note once more that the Feynman rules are such that certain terms can be set to zero when we look at particular realisations of $\{f\}$.

We conclude our discussion of the effect of gauge remainders on vertices by considering diagrams generated by

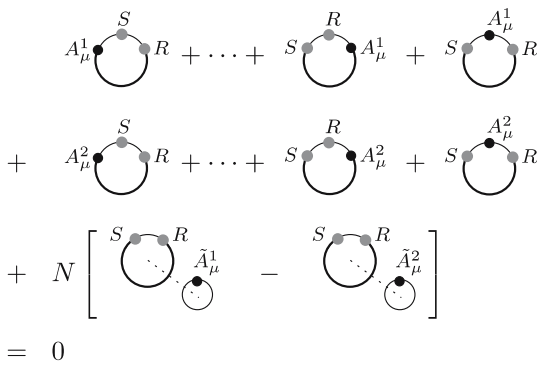

Fig. 23. Diagrammatic form of the first order no-$\mathcal{A}^0$ relations

the new terms in the flow equation in which a component of $\mathcal{A}$ decorating a vertex is replaced by a component of $\mathcal{C}$.[19] The situation is illustrated in Fig. 25 where, for reasons that will become apparent, we schematically indicate the type of vertex whose flow generates the terms we are interested in.

The effect of the gauge remainder requires a little thought. In diagram D.6, the gauge remainder can clearly strike the $\mathcal{C}$. However, in diagram D.7 the $\mathcal{C}$ is not part of the vertex coefficient function and so is blind to the effects of the gauge remainder.

Allowing the $\mathcal{C}$ of diagram D.7 to strike the $\mathcal{A}$, which labels the vertex coefficient function, the vertex coefficient function changes. Now we have a strange situation: looking just at the coefficient functions of the diagrams (i.e. ignoring the implied supertrace structure), diagrams D.6 and D.7 are consistent, after the action of the gauge remainder. However, the implied supertrace structures of the two diagrams seems to differ, because the $\mathcal{C}$ of diagram D.7 is blind to the gauge remainder.

The solution is simple: we allow the effect of the gauge remainder striking the $\mathcal{A}$ in diagram D.7 to induce a similar change in the $\mathcal{C}$. This amounts to a diagrammatic prescription which ensures that all our diagrams continue to represent both numerical coefficients and implied supertrace structure. The key point is that we are free to do this with the $\mathcal{C}$ since, not being part of a vertex it does not contribute to the numerical value of the diagram but serves only to keep track of the supertraces which have been implicitly stripped off from the vertex whose flow we are computing.

Finally, we should take account of attachment corrections, if we are to work in the A^1, A^2 basis. Attachment corrections effectively detach the embedded component of $\mathcal{C}$ from the vertex, causing it to become an isolated str $\mathcal{C}$. In diagram D.6, this field cannot now be struck by the gauge remainder. In diagram D.7, when the gauge remainder acts, it no longer induces a change in the embedded component of $\mathcal{C}$. In fact, such contributions must cancel against other terms formed by the action of the gauge remainder; this is discussed further in Sect. 4.1.3.

4.1.2 Kernels

Thus far, we have been considering the effects of gauge remainders on vertices of the actions. It is straightforward to generalise this analysis to the effect on vertices of the kernels; the generic case is shown in Fig. 26.

If the field whose momentum is contracted into the kernel is fermionic, then pushes forward and pulls back will involve flavour changes. Let us begin by supposing that one of the fields hit decorates the kernel (as opposed to being a derivative sitting at the end); in this case, the flavour changes are just given by Table 1. Note that instances of $\mathcal{C}$ embedded at the ends of the kernel behave like normal kernel decorations, as far as gauge remainders are concerned.

[19] Though not necessary for the following analysis, we recall from Sect. 3.2.5 that, in this case, in the A^1, A^2 basis, components of $\mathcal{A}$ must be replaced by *dynamical* components of $\mathcal{C}$.

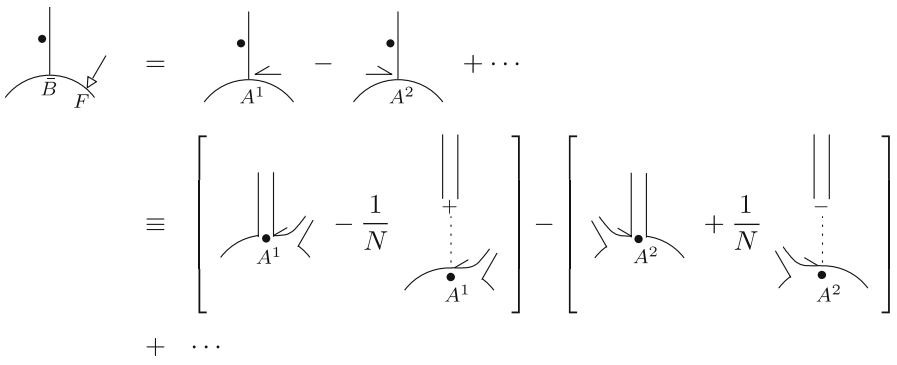

Fig. 24. Prescription adopted for internal fermionic fields decorating a vertex struck by a gauge remainder

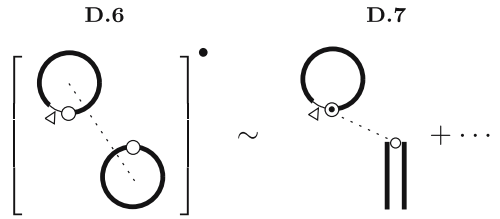

Fig. 25. A gauge remainder strikes a vertex in which a component of $\mathcal{A}$ has been replaced by a component of $\mathcal{C}$

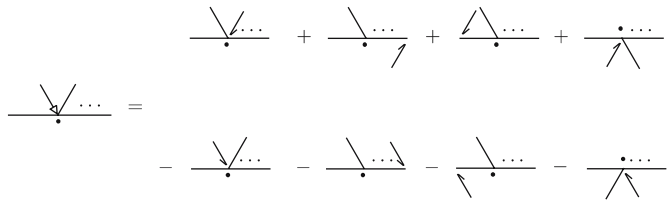

Fig. 26. Contraction of a vertex of an arbitrary kernel with one of its momenta. The sense in which we will take pushes forward and pulls back is as in Fig. 17

This follows from the gauge invariance of the flow equation and is natural if we view these embedded fields as behaving just like multi-supertrace components of the kernel. Of course, if the gauge remainder does strike a component of $\mathcal{C}$ which is really an embedded $\mathcal{C}$ then it must be that this component of $\mathcal{C}$ is forced to be on the same portion of supertrace as the rest of the kernel. This is just a manifestation of the statement that the action of gauge remainders necessitates partial specification of the supertrace structure (cf. our treatment of vertices).

When we generate internal $\tilde{A}^{1,2}$s, we would like to attach to them according to the prescription of Fig. 24 i.e. we wish to extend this prescription such that the structure to which the kernel attaches is generic, as opposed to being just a vertex of an action. We can and will do this, though note that whether or not the $1/N$ corrections actually survive depends on whether or not we endow our kernels with completely general supertrace structure. If we do allow completely general kernel decorations then the $1/N$ corrections arise – as they did before – by combining terms with a lone str $\tilde{A}^1$ (or str $\tilde{A}^2$) with those without. If, however, we take the only multi-supertrace terms of the kernel to be those involving embedded $\mathcal{C}$s, then the fact that the kernel satisifies no-$\mathcal{A}^0$ relations on its own causes the $1/N$ corrections to vanish. Since these corrections are to be hidden in our Feynman rules, it does not matter which scheme we employ.

The next task is to consider what happens when we push forward (pull back) onto the end of a kernel. This is done explicitly in [23]. However, we can deduce what the answer must be by gauge invariance considerations, as discussed in the next section.

4.1.3 Gauge invariance

We mentioned under Fig. 24 that the diagrams on the right-hand side of the figure are ambiguous: if we ignore the left-hand side, it is not clear whether we have pushed forward/pulled back around the bottom structure or pulled back/pushed forward down the kernel. In this section we will argue that the two must be equivalent, by gauge invariance. This is explicitly demonstrated to be true in [23].

Consider the flow of some vertex decorated by the fields $f_1 \cdots f_n$. Using the form of the flow equation given in Fig. 15, we explicitly decorate with f_1, but leave the other fields as unrealised decorations (see [23, 53, 54] for much more detail on this procedure). This yields the diagrams of Fig. 27.

Now consider contracting each of the diagrams of Fig. 27 with the momentum of f_1. On the left-hand side, this generates the flow of a set of vertices decorated by $m-1$ fields. Amongst the diagrams generated on the right-hand side are those for which we push forward/pull back onto fields to which the kernel attaches. For each of these diagrams, there is then a corresponding diagram (with opposite sign) where we have pulled back/pushed forward onto the end of the kernel. Such diagrams, in which we push forward/pull back onto an internal field cannot be generated by the left-hand side; thus as a consequence of gauge invariance, it must be that they cancel amongst themselves.

Proposition 1

Consider the set of diagrams generated by the flow equation, each of which necessarily possesses a single kernel that we will take to attach to the fields X_1 and X_2. Suppose that we contract each of these diagrams with the momentum of one of the (external) fields, Y.

Of the resultant diagrams, we collect together those for which the momentum of Y is pushed forward and/or pulled

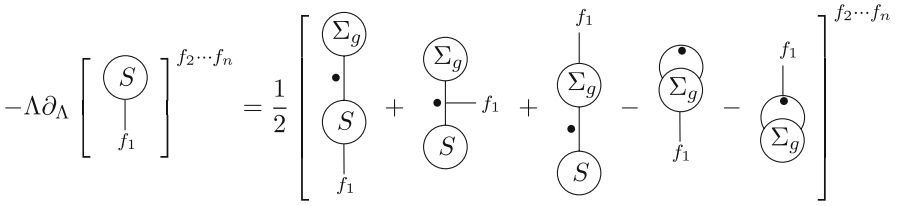

Fig. 27. Flow of a vertex decorated by the fields $f_1 \cdots f_n$

back round a vertex, onto X_1 (X_2). We add to this set of diagrams all those for which the momentum of Y is pushed forward and/or pulled back along the kernel onto the end attaching to X_1 (X_2).

We now split these sets into subsets, where the elements of each subset have exactly the same supertrace structure. The elements of each of these subsets cancel, amongst themselves.

In β function calculations, where active gauge remainders arise in a different context from that above, diagrams in which the ends of kernels are pushed forward and/or pulled back onto can survive. We can use the above relationship to always re-interpret such terms as diagrams in which the gauge remainder has instead pushed forward and/or pulled back onto the field on the vertex to which the appropriate end of the kernel attaches. The attachment corrections should be deduced according to the flavour of the field on the *vertex* to which the kernel attaches *after* any gauge remainders have acted.

4.1.4 Cancellations between pushes forward/pulls back

Referring back to Fig. 22, we now ask when it is possible for the pulls back of the second row to cancel the pushes forward of the first row (this argument can be repeated for kernels). It is clear that, if the field structure of corresponding terms is exactly the same, then they will cancel, due to the relative minus sign. For the purposes of this section, we wish to consider the case where any cancellations occur independently of the spectator fields. In other words, we will not consider cancellations which involve changing the ordering, flavour or indices of the spectator fields; this is delayed until the next section. Furthermore, whilst all the wildcard fields we are considering include all possible field choices, we do not sum over these choices, but consider each independently.

Let us temporarily suppose that X is in the A-sector and focus on the case where its momentum is pushed forward onto field Y. If both X and Y are bosonic, then the flavours of X and Y are independent of which field precedes the other. Moreover, for a given field arrangement, the flavours of the other fields will not change if the order of X and Y is swapped. In this case, the push forward onto Y will be exactly cancelled by the corresponding pull back.

However, if either X or Y is fermionic, then interchanging their order will necessarily change the field content of the vertex. This follows because a bosonic field in the 1-sector precedes an F and follows an $\bar{F}$, whereas a bosonic field in the 2-sector follows an F and precedes an $\bar{F}$. As an example, consider $p_\mu S^{1F\bar{F},\cdots}_{\mu RS\ldots}(p,r,s,\ldots)$. To cancel the push forward onto F_R would require us to change the flavour of X to A^2: $p_\mu S^{F2\bar{F}\cdots}_{R\mu S\ldots}(r,p,s,\ldots)$. Instead, we could try and cancel the push forward onto F_R by constructing the term $p_\mu S^{F\bar{F}1,\cdots}_{SR\mu\ldots}(s,r,p,\ldots)$, but now it is the $\bar{F}$ carrying the index R, rather than the F. As we will see in the next section such a term can, in general, either cancel or double the original push forward. However, for the purposes of this section, we note that the spectator field $\bar{F}_S$ has suffered a change and so we do not consider this further.

Similarly, if both X and Y are fermionic, then interchanging them will alter the field content of the vertex, if other fields are present on the same supertrace. Then, we have the choice of altering the spectators or letting $X, Y \to \bar{X}, \bar{Y}$. The former case will be dealt with in the next section. In the latter case, we note from Table 1 that pushing forward the momentum of F_R onto $\bar{F}_S$ yields $(A^1, C^1)_S$ whereas the pulling back the momentum of $\bar{F}_R$ into F_S yields $-(A^1, -C^1)_S$. These contribution do produce a cancellation over the first four indices, but the fifth index contributions add.

In conclusion, when dealing with a single vertex, a push forward can only completely cancel a pull back, independently of the spectator fields, when both fields involved are bosonic. When we generalise this analysis to full diagrams, rather than individual vertices, we might expect this constraint to be relaxed: all internal fields will be summed over and we have seen how, for example, pushing forward the momentum of an A^1 onto an F could be can be cancelled by pulling back the momentum of an A^2. Thus, if the A field is internal, then we will be including both cases, automatically. However, when dealing with full diagrams, we must be aware that interchanging fields can alter the supertrace structure of the diagram and so we will actually find that the conditions for cancellation between pushes forward and pulls back are even more stringent (see Sect. 4.1.6).

4.1.5 Charge conjugation

In the previous section we looked at whether pushes forward could cancel pulls back, independently of the spectator fields. If the properties of the spectator fields are allowed to change, then we find that every push forward is related to a pull back, by charge conjugation.

The diagrammatic recipe for charge conjugation is [8, 9, 19]:

1. reverse the sense in which we read fields off from the vertices/kernels,
2. pick up a minus sign for each field in the A-sector;
3. let $\bar{F} \leftrightarrow -F$;

where we must remember that fields pushed forward/pulled back onto may have changed flavour and that the

wildcard fields should be interpreted according to Table 1. Rather than having to specify the sense in which fields are to be read off, we can instead replace a given diagram with its mirror image, whilst obeying point two and three above.

Now let us return to Fig. 22 and consider taking the mirror image of the bottom row of diagrams. Since the location and order of the spectator fields is unspecified we see that, up to a possible sign, the first and second rows are actually identical! However, whether corresponding entries in the two rows add or cancel, depends on the whether the original vertex is even or odd under charge conjugation. In the former case, pushes forward and pulls back will add; in the latter case they will cancel.

4.1.6 Complete diagrams

So far, we have just been concerned with isolated vertices and so now turn to full diagrams. We still wish to combine pushes forward and pulls back using charge conjugation but, to do so, we must look at the charge conjugation properties of whole diagrams, rather than the properties of individual vertices.

We begin by looking at the example illustrated in Fig. 28. Each diagram has two external fields, which we will choose to be A^1s, carrying indices α and β and momenta p and $-p$. By Bose symmetry, the diagrams are symmetric under $p_\alpha \leftrightarrow -p_\beta$. We have abbreviated the vertex argument $\hat{0} \equiv \hat{S}_0$ to just the hat.

The first comment to make is that the diagrammatics is slightly different from the previous case. Rather than terminating the pushed forward/pulled back field-line with a half arrow, we just utilise the fact that the corresponding field line already ends in a $>$ and use this to indicate the field hit.

Returning to the diagrams of Fig. 28 we see that, not only can we collect pushes forward and pulls back, but we can also exploit any symmetries of the diagrams to collect terms. Looking at diagram D.8, it makes no difference whether the gauge remainder hits the field carrying α or the field carrying β. Since we can push forward or pull back onto either of these fields, this accounts for the factor of four multiplying diagram D.9.

Diagram D.10 is interesting. Having used charge conjugation to collect the push forward and pull back, let us now suppose that all fields leaving the three-point vertex are in the A-sector. We note that the field struck by the gauge remainder has an $\mathcal{A}^0$ component, but suppose that this has been absorbed into an attachment correction. In this picture, we cannot have an A^1 alone on a supertrace and so all three fields must be on the same supertrace. However, we are still free to interchange $A_\alpha(p)$ and $A_\beta(-p)$ and, summing over the two possible locations of these fields, we have:

$$\hat{S}^{111}_{\alpha\beta\rho}(p,-p,0) + \hat{S}^{111}_{\beta\alpha\rho}(-p,p,0)\,.$$

These two terms cancel, as a result of charge conjugation.

We might wonder if charge conjugation causes components of diagram D.9 to cancel. However, attachment corrections aside, the index structure $\beta\alpha R$ corresponds to a different supertrace structure from the index structure $\alpha\beta R$. In the former case, the two A^1s are on different supertraces whereas, in the latter case, they are on the same supertrace. This is illustrated in Fig. 29.

If we include attachment corrections (see Fig. 11), then the kernel of diagram D.9 can attach to the vertex via a false kernel. In this case, there is only one supertrace, and so all fields are necessarily on it. Such components of diagram D.9 do cancel amongst themselves. However, these cancellations are generally hidden by our notation and are of no practical importance anyway, until we come to extracting numerical contributions to β-function coefficients from Λ-derivative terms.

Returning to diagram D.10, for the diagram to survive, the field carrying momentum k must be in the F-sector. In this case, the gauge remainder can produce a C-sector field. Under interchange of α and β, such a vertex is even and so survives.

This serves to illustrate a general feature of these diagrammatics, alluded to at the end of Sect. 4.1.4. Suppose that we are pushing forward the momentum of a field X onto the field Y. If we can rearrange the diagram such that, leaving all other fields alone, we can place X on the other side of Y, then the resulting pull back onto Y will cancel the push forward, so long as no flavours or indices have changed in the rearrangement and the supertrace structure is still the same.

Here is how this applies to our examples. In the case of diagram D.9, to convert a pull back onto A^1_β into a push forward, we must change the location of A^1_α, to maintain the same supertrace structure (up to attachment corrections). The resulting term can then just be collected with the pull back, by charge conjugation. Hence the push forward onto A^1_β can never be completely cancelled by a pull back.

In the case of diagram D.10 we can convert a push forward into a pull back without changing the locations of the spectator fields and without having to change the supertrace structure. If the fields carrying momentum k are in the A-sector, then interchanging them does not result in any flavour changes, and so the push forward cancels the pull back. However, if the fields carrying momentum k are

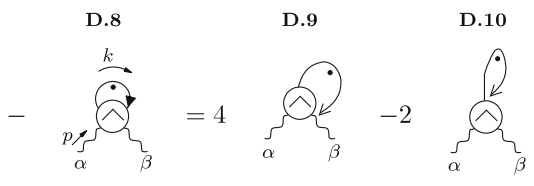

Fig. 28. Example of a gauge remainders in a complete diagram. The dummy index R is given by ρ, if restricted to the first four indices

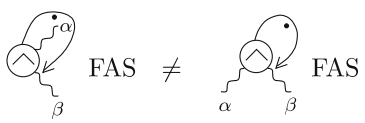

Fig. 29. Two components of diagram D.9which are not equal, due to their differing supertrace structure

fermionic, then interchanging them requires us to replace $\bar{F} \leftrightarrow F$. This constitutes a change of flavour and we find that the push forward does not completely cancel the pull-back, since we are left with a contribution arising from the C-sector.

We note that, just as we can use charge conjugation to redraw vertices struck by gauge remainders, so too can we use charge conjugation to redraw entire diagrams. Given some diagram, the diagrammatic effect of charge conjugation is to replace a diagram by its mirror image, letting $\bar{F} \leftrightarrow F$ (sic) and picking up a minus sign for each gauge remainder that has been performed.[20] Picking up a sign in this manner automatically keeps track of the signs associated with the rules of Sect. 4.1.5.

Let us now examine a second example of gauge remainders in complete diagrams, as shown in Fig. 30.

It is crucially important to recognise that, whilst diagram D.11 may superficially look like a diagram in which the kernel bites its own tail, it is very different. The difference arises due to the gauge remainder, and means that such diagrams cannot be discarded on account of (39). (We can view the gauge remainders as being some non-trivial kernel $K(x, y)$ sitting between the functional derivatives in (39) – which we take to carry position argument x – and $\{W\}$, which we take to carry position argument y. Only if the kernel reduces to $\delta(x-y)$, which it does not, can the constraint (39) contribute with non-zero measure.)

Comparing with Fig. 28, we see that diagram D.13 has exactly the same structure as diagram D.10. Although the former diagram involves a pull back along the kernel and the latter case involves a push forward around a vertex, we know from Sect. 4.1.3 that these two diagrams are identical. Taking into account the relative sign, it is clear that they cancel.

It is worth making some comments about the structure at the top of diagram D.12. The line segment which joins the top of the kernel to the $>$ – thereby forming a 'hook' – performs no rôle other than to make this join. In other words, it is neither a section of kernel nor an effective propagator. We could imagine deforming this line segment so that the hook becomes arbitrarily large. Despite appearances, we must always remember that this line segment simply performs the role of a Kronecker δ. When part of a complete diagram, this line segment can always be distinguished from an effective propagator, to which it can be made to look identical, by the context. This follows because hooks in which the line segment is a Kronecker δ only ever attach to effective propagators or kernels, whereas hook-like structures made out of an effective propagator only ever attach to vertices (see diagram D.13 for an example but note that, in this case, the effective propagator is differentiated). When viewed in isolation, we will always take the hook structure to comprise just a line segment and so will draw the hook as tightly as possible.

We conclude this section by discussing a particular scenario – which will crop up repeatedly in our computation

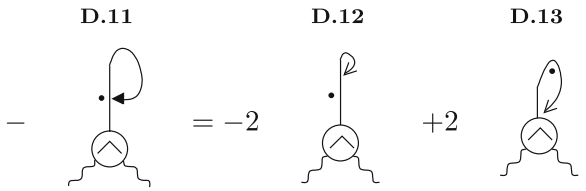

Fig. 30. Example of a gauge remainder on a kernel, in a full diagram

of β-function coefficients – in which it is possible to neglect attachment corrections.

Consider some complete diagram possessing a three-point vertex which is decorated by an external A^1 and is struck by a gauge remainder. The type of diagram we are considering is represented in Fig. 31, where the fields $\{f\}$ can attach anywhere except the bottom vertex, which must be three-point (hence the superscript three). If any of these fields are internal fields, then we take pairs of them to be connected by an effective propagator.

We now argue that we can forget about any attachment corrections. Let us start by supposing that the gauge remainder is in the F-sector. If the gauge remainder strikes the internal field, then it can generate an effective attachment correction. However this correction isolates the newly formed two-point vertex from the rest of the diagram, leaving us with $\mathrm{str}\, A^1 = 0$.

Next, suppose that the gauge remainder is in the A-sector. Since two of the three fields entering the vertex are now in the A-sector, the third must also be bosonic. Moreover, the final field must be in the A-sector also, else the action of the gauge remainder will produce an AC vertex, which does not exist. Now, any attachment corrections would mean that all fields on the vertex are guaranteed to be on the same portion of supertrace, with respect to the diagram as a whole, irrespective of location. Summing over the independent locations of the fields causes the diagram to vanish, by charge conjugation.

Henceforth, whenever we deal with a three-point vertex decorated by an external field and struck by a gauge remainder, we will automatically discard all attachment corrections. Let us now apply this to a specific case, illustrated in Fig. 32. Referring also to Fig. 28, diagram D.17 straightforwardly cancels diagram D.9.

4.1.7 Nested contributions

The basic methodology for nested gauge remainders is similar to the methodology just presented, but we must

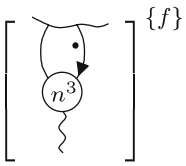

Fig. 31. A diagram for which attachment corrections are restricted

[20] So far, we have only encountered diagrams in which a single gauge remainder has acted, but we will come across more general cases later.

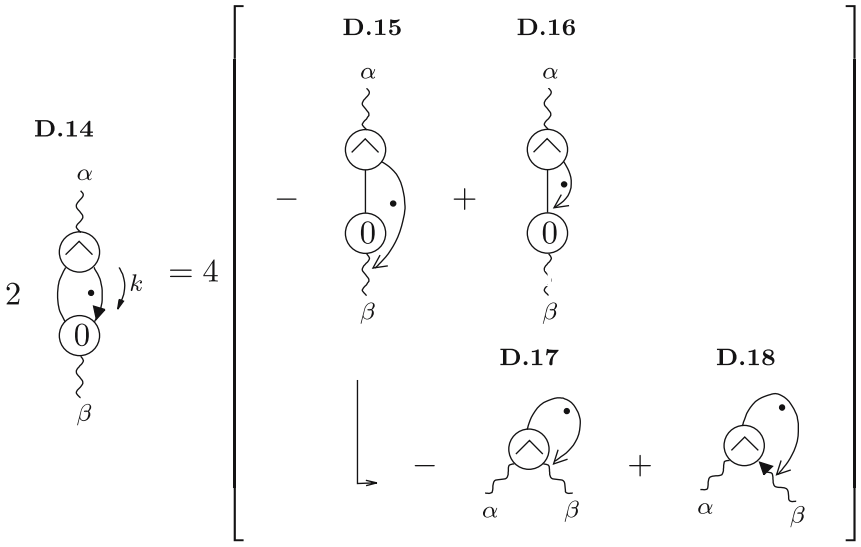

Fig. 32. Gauge remainder which produces a diagram in which the effective propagator relation can be applied

take account of the fact that the supertrace structure is now partially specified. In particular, this will generally mean that we cannot use charge conjugation to collect nested pushes forward and pulls back (the exception being if a gauge remainder produced in one factorisable sub-diagram hits a separate factorisable sub-diagram) and so must count them separately. Indeed, nested pushes forward and pulls back can have different supertrace structures as illustrated by considering the result of processing diagram D.18, as shown in Fig. 33.

We begin our analysis of the diagrams of Fig. 33 by noting that, from our discussion at the end of Sect. 4.1.6, there are no attachment corrections.

Diagrams D.19 and D.21 both have the supertrace structure $\pm N\mathrm{str}\ A^1_\alpha A^1_\beta$, with the plus or minus depending on the sector of the wildcard fields. On the other hand, diagrams D.20 and D.22 both have the supertrace structure $\mathrm{str}\ A^1_\alpha \mathrm{str}\ A^1_\beta = 0$. Note in the latter case that the particular supertrace structure puts constraints on the field content of the diagram. Specifically, the kernel in diagrams D.20 and D.22 cannot be fermionic. Let us suppose that it is. Then, the end which attaches to the vertex must be an F and so the end which attaches to the $\wedge$ must be an $\bar{F}$. However, referring to Table 1 we see that an $\bar{F}$ cannot pull back onto bosonic fields in the 1-sector. There is an inconsistency in such a diagram and so our original supposition that it exists must be wrong.

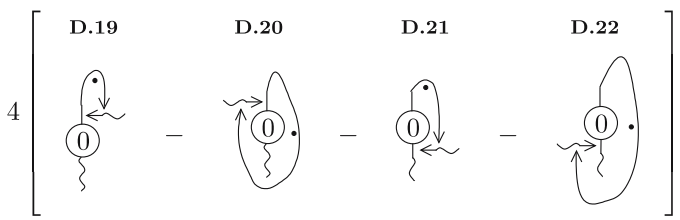

Fig. 33. Result of processing diagram D.18

4.2 Momentum expansions

The computation of β-function coefficients involves working at fixed order in external momentum. If a diagram contains a structure that is already manifestly of the desired order, then it is useful to Taylor expand at least some of the remaining structures in the external momentum. Vertices can always be expanded in momentum, as it is a requirement of the setup that such a step is possible [9, 10]. Whereas kernels, too, can always be Taylor expanded in momentum it is not necessarily possible to do so with effective propagators that form part of a diagram, as this step can introduce IR divergences, at intermediate stages. This will be discussed in detail in [50].

The key idea in what follows is that, if an A-field decorating a vertex decorated by n other fields carries zero momentum, then we can relate this vertex to the momentum derivative of a set of vertices decorated just by the n fields. This relation arises as a consequence of the Ward identity (36) and so it is no surprise that the diagrammatics of this section is very similar to those we employed for the gauge remainders.

4.2.1 Basics

Consider the general vertex, U, the decorations of which include an A^i-field carrying zero momentum. Let us begin by supposing that this A^i-field is sandwiched between the fields X and Y, both of which carry non-zero momentum. By the Ward Identity (36), we have:

$$\epsilon_\mu U^{\cdots XA^iY\cdots}_{\cdots R\mu\ S\cdots}(\dots,r,\epsilon,s-\epsilon,\dots) = U^{\cdots XY\cdots}_{\cdots RS\cdots}(\dots,r,s,\dots) - U^{\cdots XY\cdots}_{\cdots RS\cdots}(\dots,r+\epsilon,s-\epsilon,\dots)\,. \tag{77}$$

Taylor expanding both sides in ϵ and equating the $\mathcal{O}(\epsilon)$ terms yields:

$$U^{\cdots XA^iY\cdots}_{\cdots R\mu S\cdots}(\dots,r,0,s,\dots) = \left(\partial^{s'}_\mu - \partial^{r'}_\mu\right) U^{\cdots XY\cdots}_{\cdots RS\cdots}(\dots,r',s',\dots)\Big|_{r'=r,s'=s}\,. \tag{78}$$

Next, suppose that the fields X and Y sandwich not only the A^i carrying zero momentum, but also a second field, say Z, carrying zero momentum. In this case, it is straightforward to show, along the lines of (77) and (78), that:

$$U^{\cdots XA^iZY\cdots}_{\cdots R\mu TS\cdots}(\dots,r,0,0,s,\dots) + U^{\cdots XZA^iY\cdots}_{\cdots RT\mu\ S\cdots}(\dots,r,0,0,s,\dots) = \left(\partial^{s'}_{\mu}-\partial^{r'}_{\mu}\right)U^{\cdots XZY\cdots}_{\cdots RTS\cdots}(\dots,r',0,s',\dots)\Big|_{r'=r,s'=s}\ ; \tag{79}$$

in other words, the field Z is effectively transparent to the momentum derivative.

Equations (78) and (79), for the case that U is an action vertex, are represented diagrammatically in Fig. 34, which highlights the similarity between the momentum expansions and gauge remainders. The top row on the right-hand side correspond to 'push forward like' terms, whereas those on the second row correspond to 'pull back like' terms. (As with the gauge remainders, pushes forward are performed in the counterclockwise sense.) The ellipses round each of the vertices can include fields carrying zero momentum.

As with the gauge remainders, we must consider all possible independent locations of the A-field with respect to the other fields. Hence, terms between the first and second rows can cancel, if the field hit is bosonic.

We now want to convert derivatives with respect to the dummy momenta into derivatives with respect to the original momenta. There are two cases to deal with. The first – in which we shall say that the momenta are paired – is where there are a pair of fields, carrying equal and opposite momentum. The second – in which we shall say that the momenta are coupled – is where there are three fields carrying, say, $(r,s,-s-r)$.

Paired momenta. This is the simplest case to deal with. If the momentum r has been replaced with dummy momentum r' and $-r$ has been replaced with dummy momentum s' then

$$\left(\partial^{r'}_{\mu}-\partial^{s'}_{\mu}\right)\to\partial^{r}_{\mu}\,.$$

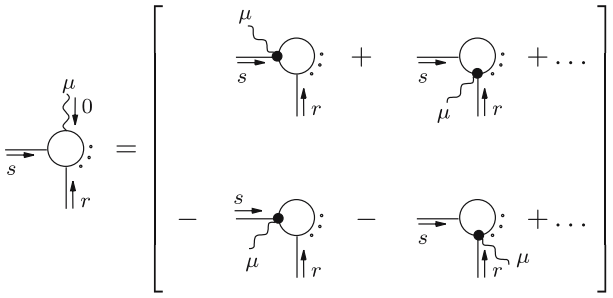

Fig. 34. Diagrammatics expression for a vertex decorated by an A-field carrying zero momentum. The *filled circle* attached to the A-field line tells us to first replace all momenta with dummy momenta; then to differentiate with respect to the dummy momenta of the field hit, holding all other momenta constant and finally to replace the dummy momenta with the original momenta

Hence, we can collect together a push forward like diagram with a pull back like diagram to give a derivative with respect to one of the original momenta. An example of this is shown in Fig. 35, for a field-ordered three-point vertex.

Coupled momenta. The structures in this section contain momentum arguments of the form $(r,s,-s-r)$. Referring back to (78), we will denote the dummy momenta by (r',s',t'). We can make progress by noting that:

$$\left(\partial^{r'}_{\mu}-\partial^{s'}_{\mu}\right)\to\left(\partial^{r}_{\mu}\big|_{s}-\partial^{s}_{\mu}\big|_{r}\right) \tag{80}$$

and likewise, for all other combinations of (r',s',t'). Thus, as with the previous case, we need to combine a pair of terms differentiated with respect to dummy momenta to obtain a structure which is differentiated with respect to its original momenta. The difference is that, whilst in the previous case the pair combined into one diagram, in this case they remain as a pair. An example is shown in Fig. 36.

The open circle attached to the A-field line represents a derivative with respect to the momentum entering the vertex along the field hit. However, this derivative is performed holding the momentum of the field hit in the partner di-

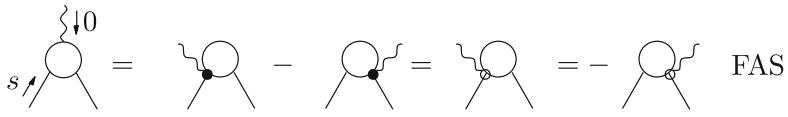

Fig. 35. A field ordered three-point vertex with zero momentum entering along an A-field can be expressed as the momentum derivative of a two-point vertex. The *open circle* attached to the A-field line represents a derivative with respect to the momentum entering the vertex along the field hit

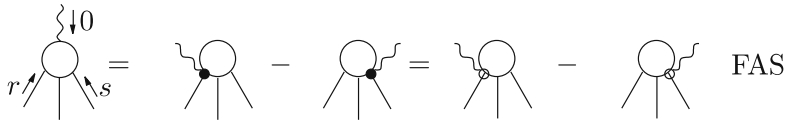

Fig. 36. A field ordered four-point vertex with zero momentum entering along an A-field can be expressed as the momentum derivative of two three-point vertices

agram constant. Hence, the final two diagrams of Fig. 36 must be interpreted as a pair. The difference between this and the paired momentum case highlights the care that must be taken interpreting the new diagrammatics.

4.2.2 Kernels

When we come to deal with kernels, we must adapt the diagrammatic notation slightly. If the momentum derivative strikes a field decorating a kernel, then we just use the current notation. However, it is desirable to change the notation when the momentum derivative strikes one of the ends a kernel. In complete diagrams, placing the diagrammatic object representing a momentum derivative at the end of the kernel becomes confusing; rather we place the object in middle and use an arrow to indicate which end of the kernel it acts on, as shown in Fig. 37.

Hence, the second diagram denotes a derivative with respect to $+k$, whereas the third diagram denotes a derivative with respect to $-k$.

4.2.3 Complete diagrams

We illustrate the application to complete diagrams by showing how to manipulate diagram D.16, as shown in Fig. 38.

Taking the external momentum of the parent diagram to be p, we note that the two-point vertex at the base of the diagram is $\mathcal{O}(p^2)$, which is the order in p to which we wish to work. We call this base structure an '$\mathcal{O}(p^2)$ stub'. The first step is to Taylor expand the three-point vertex to zeroth order in p, as shown in diagram D.23. There is now a discontinuity in momentum arguments, since although momentum l flows into and out of the differentiated two-point vertex, this vertex is attached to an effective propagator carrying momentum l and a kernel carrying momentum $l-p$. This discontinuity is indicated by the bar between the vertex and the kernel. We can Taylor expand the kernel to zeroth order in momentum, too, and this is done in diagram D.24. Since the discontinuity in momentum has now vanished, the bar is removed.

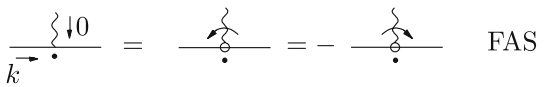

Fig. 37. A field ordered one-point kernel with zero momentum entering along a decorative A-field can be expressed as the momentum derivative of a zero-point kernel

In diagram D.25 we have introduced an arrow on the diagrammatic representation of the derivative. We have come across this arrow already the context of kernel but have not yet required it for vertices. Indeed, in the current example, it is effectively redundant notation. We note, though, that we can reverse the direction of the arrow, at the expense of a minus sign, as in diagram D.26. By reversing the direction of the arrow, we are now differentiating with respect to the momentum leaving the vertex along the struck field, rather than the momentum thus entering.

We conclude our discussion of momentum expansions by commenting on how we can redraw a diagram using charge conjugation. For any diagram, we use the following recipe:

1. take the mirror image (this includes reflecting any arrows accompanying derivative symbols);
2. pick up a minus sign for each performed gauge remainder;
3. pick up a minus sign for each derivative symbol.

5 One loop diagrammatics

In this section, we present the entire diagrammatics for the computation of β_1, arriving at a manifestly gauge invariant, diagrammatic expression, from which the universal value in $D=4$ can be immediately extracted. This computation of β_1 not only serves as an illustration of the diagrammatic techniques of Sects. 3 and 4, but is a necessary intermediate step in the computation of β_2. Much of the work presented in this chapter overlaps with the computation of β_1 presented in [19]. However, there are a number of important differences, which we now outline.

First, the computation here is done for an unrestricted Wilsonian effective action. Previously, the action was restricted to just single supertrace terms; a consequence of which is that the single supertrace terms $S_{0\mu\nu}^{AAC}(p,q,r)$ and $S_{0\mu\nu}^{AAC\sigma}(p,q,r)$ can be set to zero [19]. The second major difference is that the diagrammatics are no longer terminated after the use of the effective propagator relation: gauge remainders and $\mathcal{O}(p^2)$ manipulations are dealt with in an entirely diagrammatic fashion.

We also choose to use a completely general $\hat{S}$, thereby demonstrating complete scheme independence. In fact, the inclusion of $\hat{S}_1$ (higher loop vertices do not occur in the calculation) actually leads only to a trivial extension of the scheme independence. The instances of $\hat{S}$ beyond tree level

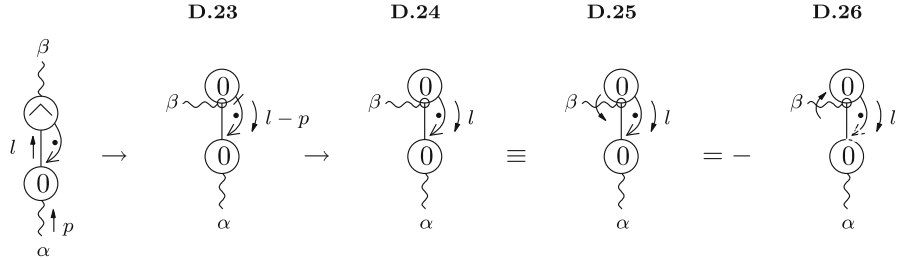

Fig. 38. Manipulation of a diagram at $\mathcal{O}(p^2)$. Discontinuities in momentum flow are indicated by a bar

are (at $\mathcal{O}(p^2)$) restricted to those of the form $\hat{S}_1^C$, and are only ever involved in cancellations via the weak coupling expansion of the constraint equation (shown in Fig. 19). Nonetheless, it is instructive to see this occurring and to confirm that β_1 is universal.

5.1 A diagrammatic expression for β_1

5.1.1 The starting point

The key to extracting β-function coefficients from the weak coupling flow equations (67) is to use the renormalisation condition (40), which places a constraint on the vertex $S^{11}_{\mu\nu}(p)$. From (41) and (59) we see that, apart from the required $\Box_{\mu\nu}(p)$, the $\mathcal{O}(p^2)$ part of $S^{1\,1}_{0\mu\nu}(p)$ is just a number (two) and that $S^{1\,1}_{n\geq 1\mu\nu}(p) = \mathcal{O}(p^4)$.

To utilise this information, we begin by specialising equation (67) to compute the flow of $S^{1\,1}_{1\mu\nu}(p)$:

$$\Lambda\partial_\Lambda S^{11}_{1\mu\nu}(p) = 2\beta_1 S^{11}_{0\mu\nu}(p) - \gamma_1 \frac{\partial S^{11}_{0\mu\nu}(p)}{\partial\alpha} - \sum_{r=0}^{1} a_0[\bar{S}_{1-r}, \bar{S}_r]^{11}_{\mu\nu}(p) + a_1[\Sigma_0]^{11}_{\mu\nu}(p)\,. \qquad (81)$$

The a_0 term can be simplified. Defining $\Pi^{XY}_{RS}(k) = S^{XY}_{RS}(k) - \hat{S}^{XY}_{RS}(k)$ and using the definition of the barred vertices, (66), we can write

$$-\sum_{r=0}^{1} a_0[\bar{S}_{1-r}, \bar{S}_r]^{11}_{\mu\nu}(p) = -2a_0[\Pi_0, S_1]^{11}_{\mu\nu}(p) + 2a_0[S_0, \hat{S}_1]^{11}_{\mu\nu}(p)\,.$$

All the a_0 terms generate two vertices, joined by a kernel. Unless one of these vertices is decorated by a single field, both vertices must be decorated by an internal field and one of the external fields. Now, one-point Π_0 vertices do not exist and two-point Π_0 vertices vanish, since we have identified the two-point, tree level Wilsonian effective action vertices with the corresponding seed action vertices. We choose to discard one-point S_1^C vertices at this stage of the calculation[21] and so $a_0[\Pi_0, S_1]^{11}_{\mu\nu}(p)$ does not contribute.

The next step is to focus on the $\mathcal{O}(p^2)$ part of (81). Noting that $S^{1\,1}_{1\mu\nu}(p)$ is at least $\mathcal{O}(p^4)$, and that the $\mathcal{O}(p^2)$ part of $S^{1\,1}_{0\mu\nu}(p)$ is independent of α, we arrive at an algebraic expression for β_1:

$$-4\beta_1\Box_{\mu\nu}(p) + \mathcal{O}(p^4) = a_1[\Sigma_0]^{11}_{\mu\nu}(p) + 2a_0[S_0, \hat{S}_1]^{11}_{\mu\nu}(p)\,, \qquad (82)$$

which is shown diagrammatically in Fig. 39. It is implicit in all that follows that, unless otherwise stated, the external indices are μ and ν and we are working at $\mathcal{O}(p^2)$.

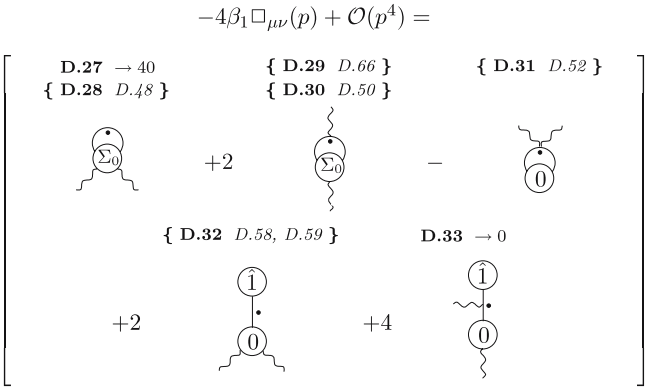

Fig. 39. A diagrammatic representation of the equation for β_1. On the right-hand side, we implicitly take the indices to be μ and ν and work at $\mathcal{O}(p^2)$

The diagrams are labelled in boldface as follows: any diagram containing Σ as a vertex argument has two labels: the first corresponds to the Wilsonian effective action part and the second corresponds to the seed action part. Diagrams with only a Wilsonian effective action vertex or a seed action vertex have a single label. If the reference number of a diagram is followed by an arrow, it can mean one of two things:

1. $\to 0$ denotes that the corresponding diagram can be set to zero, for some reason;
2. $\to$ followed by a number (other than zero) indicates the number of the figure in which the corresponding diagram is processed.

If a diagram is cancelled, then its reference number is enclosed in curly braces, together with the reference number of the diagram against which it cancels. A diagram will not be taken as cancelled until the diagram against which it cancels has been explicitly generated. Thus, at various stages of the calculation where we collate surviving terms, we include those diagrams whose cancelling partner does not yet exist.

Returning to Fig. 39, the first three diagrams are formed by the $a_1[\Sigma_0]$ term and the last two are formed by the $a_0[S_0, \hat{S}_1]$ term. We do not draw any diagrams possessing either a one-point, tree level vertex or a kernel which bites its own tail. In the third diagram, we have used the equality between Wilsonian effective action and seed action two-point, tree level vertices to replace $\Sigma^{XX}_{0RS}(k)$ with $-S^{XX}_{0RS}(k)$. The final diagram vanishes: the one-point vertex must be in the C-sector but, since an $\dot{\Delta}^{AC,A}$ kernel does not exist, it is not possible to form a legal diagram.

Note that we have not included the diagram which can be obtained from diagram D.33 by taking the field on the kernel and placing it on the top-most vertex, since such a term vanishes at $\mathcal{O}(p^2)$: the vertex $S^{1\,1}_{0\mu\alpha}(p)$ is, as we know already, at least $\mathcal{O}(p^2)$; the same too applies to $\hat{S}^{1\,1}_{1\mu\alpha}(p)$, as a consequence of the Ward identity (36).[22]

[21] We could instead process these terms, which would essentially amount to enforcing the constraint (shown in Fig. 19) on the fly [23].

[22] There is no argument that the $\mathcal{O}(p^2)$ part of $\hat{S}^{1\,1}_{n\geq 1\mu\nu}(p)$ vanishes, since the renormalisation condition does not apply to the seed action.

5.1.2 Diagrammatic manipulations

As it stands, we cannot directly extract a value for β_1 from (82). The right-hand side is phrased in terms of non-universal objects. Whilst one approach would be to choose particular schemes in which these objects are defined algebraically (up to a choice of cutoff functions) [10] we know from [19] that this is unnecessary: owing to the universality of β_1, all non-universalities must somehow cancel out. To proceed, we utilise the flow equations.

Our aim is to try and reduce the expression for β_1 to a set of Λ-derivative terms – terms where the entire diagram is hit by $\Lambda\partial_\Lambda|_\alpha$ – since, such terms either vanish directly or combine to give only universal contributions (in the limit that $D \to 4$) [19, 23, 50].

The approach we use is to start with the term containing the highest point Wilsonian effective action vertex. By focusing on the term with the highest point vertex, we guarantee that the kernel in the diagram is un-decorated. Now, we know that an un-decorated kernel is $-\Lambda\partial_\Lambda|_\alpha$ of an effective propagator. Hence, up to a term in which the entire diagram is hit by $-\Lambda\partial_\Lambda|_\alpha$, we can move the $-\Lambda\partial_\Lambda|_\alpha$ from the effective propagator to the vertex. This step is only useful if the vertex is a Wilsonian effective action vertex, for now it can be processed, using the flow equations.

From Fig. 39 it is clear that the highest point Wilsonian effective action vertex in our calculation of β_1 is the four-point, tree level vertex contained in diagram D.27. The manipulation of this diagram is shown in Fig. 40. For the time being, we will always take the Λ-derivative to act before we integrate over loop momenta (this is fully discussed in [23, 50]).

We can now use the tree-level flow equation (68) to process the Λ-derivative of the four-point vertex. The flow of a four-point vertex with two A^1 fields and two wildcards is shown in Fig. 55 (Appendix A). Throwing away all terms

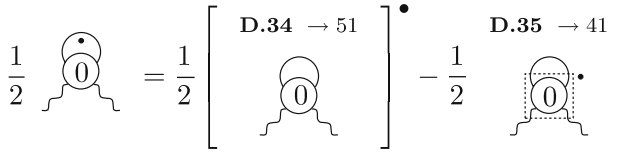

Fig. 40. The manipulation of diagram D.27. In the final diagram, the Λ-derivative operates on just the four-point vertex

which vanish at $\mathcal{O}(p^2)$ and joining the wildcards together with an effective propagator, we arrive at Fig. 41.

We now arrive at a key juncture in the diagrammatic procedure: Diagrams D.36–D.38, D.41 and D.42 can be further manipulated using the effective propagator relation. The results of this procedure are shown in Fig. 42. Diagrams in which a kernel bites its own tail have been discarded as have those in which a gauge remainder strikes a two-point vertex (see (73)). Henceforth, we will assume that such terms have always been discarded.

Three of the diagrams generated exactly cancel the contributions in the first row of Fig. 39 containing seed action vertices (or Wilsonian effective action two-point, tree level vertices).

Cancelation 1 *Diagram D.48 exactly cancels D.28.*

Cancelation 2 *Diagram D.50 exactly cancels D.30.*

Cancelation 3 *Diagram D.52 exactly cancels D.31.*

Other than the Λ-derivative term, diagram D.34, there are now only two diagrams left which contain four-point vertices. The first of these, diagram D.44, can be manipulated at $\mathcal{O}(p^2)$ since the bottom vertex is at least $\mathcal{O}(p^2)$ and so the rest of the diagram can be Taylor expanded to zeroth order in p. Note, in particular, that given the effective propagator $\Delta^{11}(p) \sim \mathrm{B}(p^2/\Lambda^2)/p^2$ [19, 23], the differentiated kernel which attaches to the two-point vertex

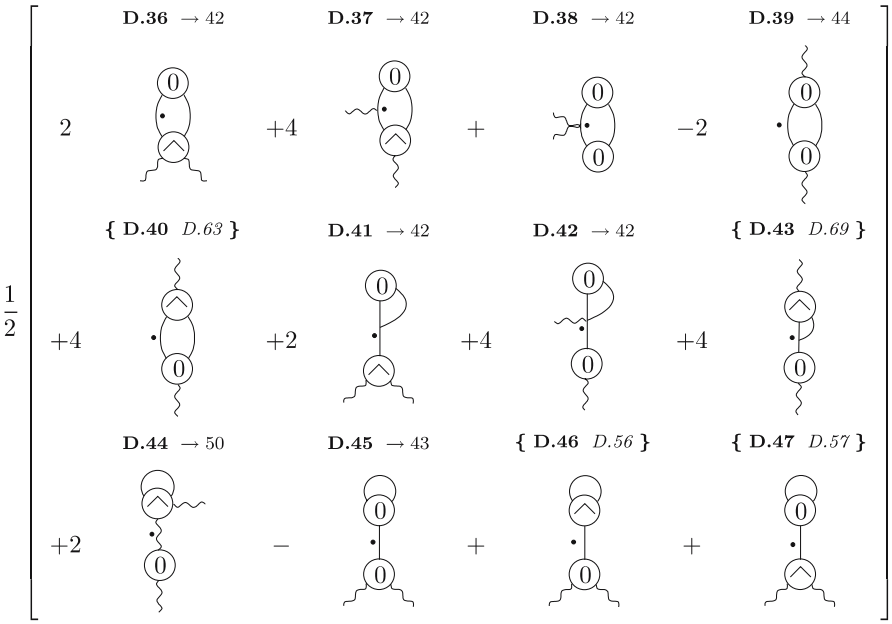

Fig. 41. The result of manipulating diagram D.35, using the tree-level flow equation

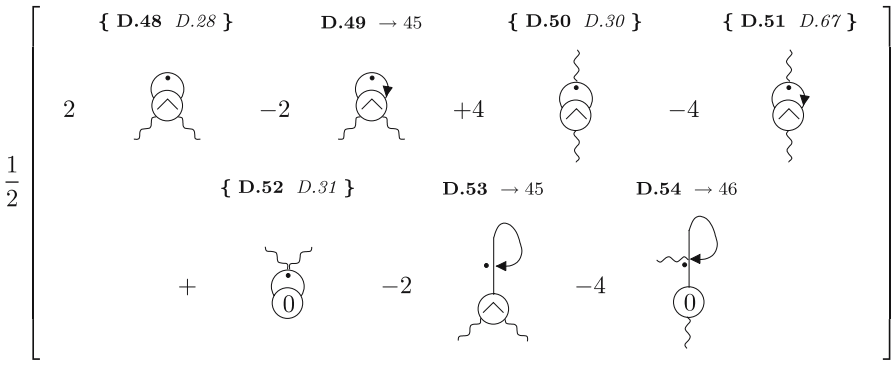

Fig. 42. Manipulation of diagrams D.36–D.38, D.41 and D.42

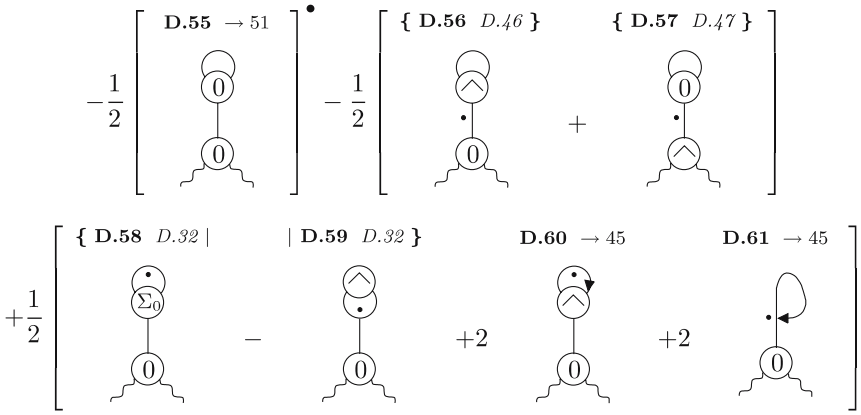

Fig. 43. Result of the manipulation of diagram D.45 using the tree level flow equation

contributes the non-universal factor $2\mathrm{B}'(0)/\Lambda^2$, where the prime denotes differentiation with respect to the argument. We henceforth call terms of this type $\mathrm{B}'(0)$ terms. If we were to explicitly perform this Taylor expansion, we would reduce the four-point vertex to the (double) momentum derivative of a two-point vertex [19].[23] In the second of the diagrams containing a four-point vertex, diagram D.49, the vertex is hit by a gauge remainder and so will automatically be reduced to a three-point vertex. Thus the effect of our manipulations is to ensure that all occurrences of the highest-point vertex in the calculation occur only in a Λ-derivative term.

Before moving on to the next stage of the calculation, we compare our current expression to that of reference [19]. Ignoring the multiple supertrace terms contained within each of our diagrams, the two expressions are superficially the same, up to diagrams D.41 and D.45–D.47. In each of these terms, the internal field joining the two three-point vertices must be in the C-sector. If it is in the F-sector, then each diagram vanishes because net fermionic vertices vanish. If it is in the A-sector, then charge conjugation invariance causes the diagrams to vanish when we sum over permutations of the bottom vertex. Looking a little harder, we see a related difference between the current expression and that of reference [19]: amongst the components of diagrams D.39 and D.40 are diagrams possessing AAC vertices.

[23] As we will see in Sect. 5.2 this manipulation is not necessary as there is a more elegant way to deal with the diagram.

Now, with the aim of removing all three-point vertices from the calculation (up to Λ-derivative terms), we iterate the procedure. Referring to Fig. 41, only diagrams D.45 and D.39 possess exclusively Wilsonian effective action vertices and an un-decorated kernel and so it is these which we manipulate.

Figure 43 shows the manipulation of diagram D.45 which proceeds along exactly the same lines as the manipulations of Fig. 40. This time, however, we utilise Fig. 53 for the flow of a three-point vertex with three wildcard fields and Fig. 54 for the flow of a three-point vertex containing two external A^1s (which carry moment p and $-p$). In this latter case, we discard all terms which vanish at $\mathcal{O}(p^2)$.

As with diagrams D.28, D.30 and D.31, we find that diagrams of the same structure as the parent but containing a seed action vertex are cancelled.

Cancelation 4 *Diagram D.56 exactly cancels D.46.*

Cancelation 5 *Diagram D.57 exactly cancels D.47.*

We also find, as promised, that the sole instance of a one-point, seed action vertex is cancelled.

Cancelation 6 *Diagram D.58 exactly cancels D.59 exactly cancel diagram D.32 by virtue of the weak coupling expansion of the constraint Fig. 19.*

In this context, the notation used in Fig. 43 to describe the cancellation of diagram D.32 has an obvious interpretation. Note that the only surviving terms from Fig. 43 both contain gauge remainders.

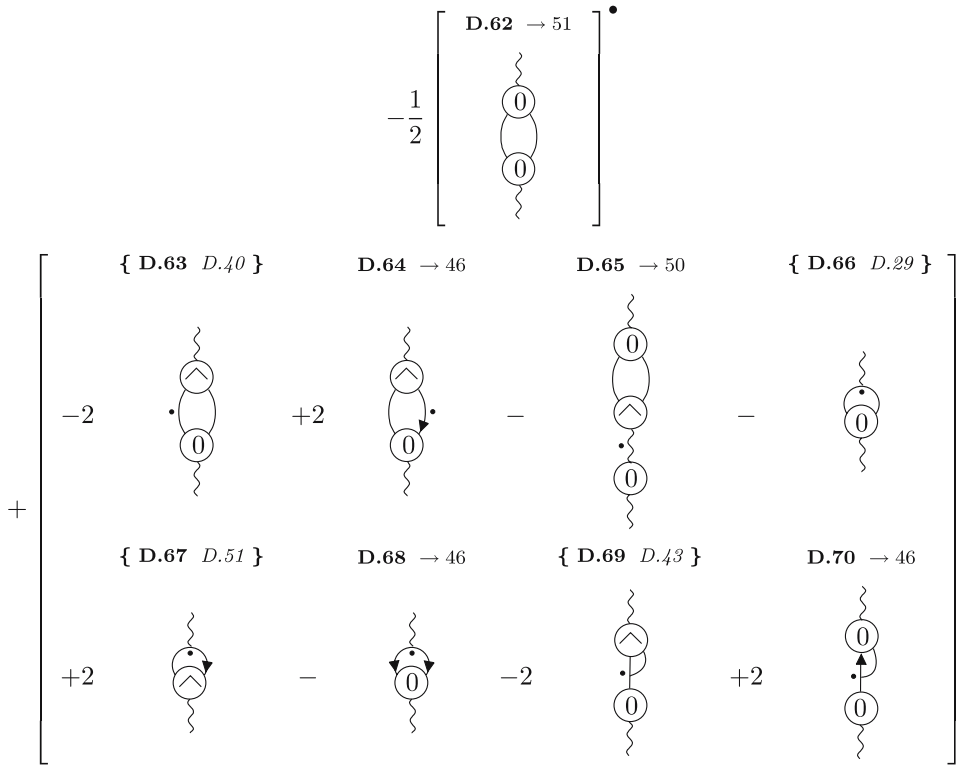

Fig. 44. Result of the manipulation of diagram D.39 using the tree level flow equation

Figure 44 shows the manipulation of diagram D.39, where the overall factor of $1/2$ arises from the symmetry of the Λ-derivative term D.62 under rotations by π (alternatively, the indistinguishability of the two internal fields). When we compute the flow of the vertices of diagram D.62, we can utilise this symmetry to remove the factor of $1/2$.

We find a number of cancellations. The first of these is the expected cancellation of the partner of the parent diagram, possessing a seed action vertex.

Cancelation 7 *Diagram D.63 exactly cancels D.40.*

The next cancellation completes the removal of all terms from Fig. 39 formed by the action of $a_0[\Sigma_0]$.

Cancelation 8 *Diagram D.66 exactly cancels D.29.*

Of the remaining cancellations, one involves two diagrams, each possessing active gauge remainders, which we notice can be cancelled without the need to perform the gauge remainders. The final cancellation occurs only at $\mathcal{O}(p^2)$.

Cancelation 9 *Diagram D.67 exactly cancels D.51. When a three-point tree level vertex is struck by a gauge remainder it is reduced to a two-point, tree level vertex. Since Wilsonian effective action two-point, tree level vertices are equal to the corresponding seed action vertices, it thus makes no difference whether the original three-point vertex is a Wilsonian effective action vertex or a seed action vertex.*

Cancelation 10 *Diagram D.69 cancels D,43 at $\mathcal{O}(p^2)$. In each case, we Taylor expand the three-point, tree level vertex to zeroth order in external momentum, reducing it to the momentum derivative of a two-point, tree level vertex. It is then of no consequence that one of the three-point, tree level vertices was a seed action vertex whereas the other was a Wilsonian effective action vertex.*

At this stage, up to diagrams in which the sole three-point vertex is hit by a gauge remainder, we have removed all three-point, tree level vertices from the calculation with the following exceptions:

1. the Λ-derivative terms, diagrams D.62 and D.55;
2. the B′(0) term, diagram D.65;
3. three diagrams D.53, D.60 and D.61, which are each left with a three-point, tree level vertex, even after the action of the gauge remainders.

The last three terms, which all possess an $S_{0\mu\nu}^{11C^{1,2}}$ vertex, have no analogue in the version of the calculation presented in [19]. To make further progress, we must process the gauge remainders. In Figs. 45 and 46, we utilise the techniques of Sect. 4.1 to manipulate the gauge remainders, stopping after the use of the effective propagator relation. We discard all terms which vanish due to their supertrace structure being str A_μ^1str A_ν^1 and neglect attachment corrections to three-point vertices which are decorated by an external field and struck by a gauge remainder (cf. Fig. 31).

Note that diagram D.85 is our first example of a diagram possessing a trapped gauge remainder. The full gauge remainder is prevented from killing the two-point, tree level vertex by the processed gauge remainder: the vertex and the full gauge remainder do not carry the same momentum. There is no corresponding diagram in which the gauge remainder instead bites the external field because then we are left with an active gauge remainder striking

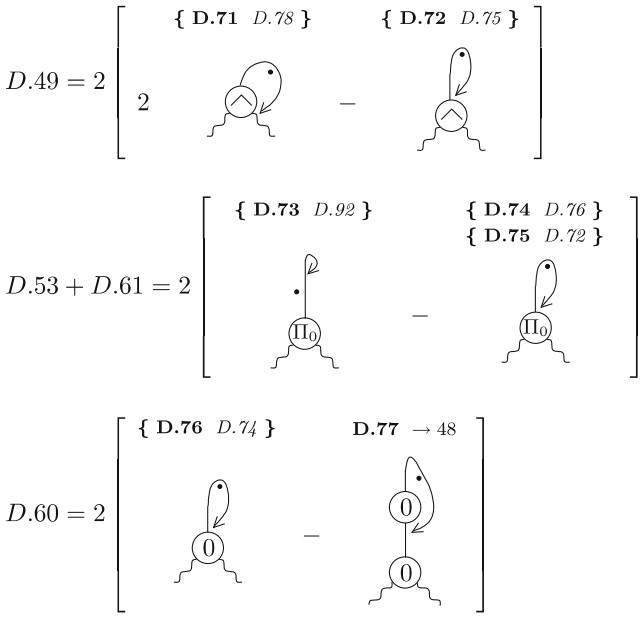

Fig. 45. Terms arising from processing the gauge remainders of the diagrams in Figs. 43 and 44 part I

a two-point, tree level vertex. Note also that all diagrams which either cannot be processed further or do not contain an $S_{0\mu\nu}^{11C^{1,2}}$ vertex cancel, amongst themselves.

Cancelation 11 *Diagram D.74 exactly cancels D.76.*

Cancelation 12 *Diagram D.75 exactly cancels D.72.*

Cancelation 13 *Diagram D.78 exactly cancels D.71.*

Cancelation 14 *Diagram D.82 exactly cancels D.85.*

Fig. 47. Diagrams arising from processing the nested gauge remainders of Fig. 46

Whilst these cancellations are very encouraging, it is not clear that we are any closer to solving the mystery of the diagrams containing $S_{0\mu\nu}^{11C^{1,2}}$ vertices. We will, however, persevere and process the nested gauge remainders arising from the previous procedure. The result of this is shown in Fig. 47.

Once again, we find a cancellation between a pair of the terms generated by this procedure.

Cancelation 15 *Diagram D.90 exactly cancels D.87.*

This exhausts the active gauge remainders and so is a good point to pause and collate the surviving terms. These fall into five sets:

1. The Λ-derivative terms, diagrams D.34, D.55 and D.62;
2. The B′(0) terms, diagrams D.44, D.65 and D.89. Notice that the last of these has been formed via the action of a nested gauge remainder;

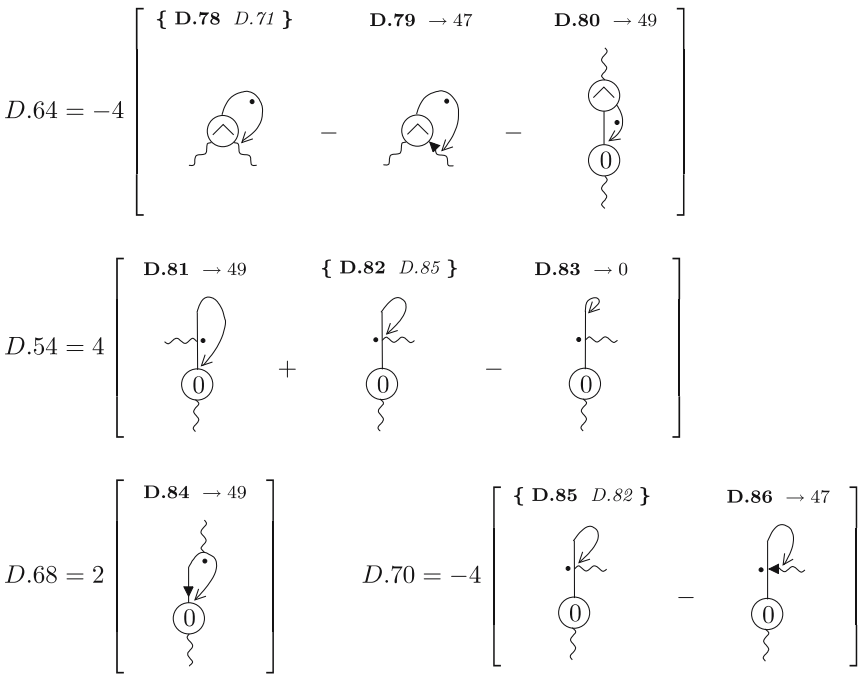

Fig. 46. Terms arising from processing the gauge remainders of the diagrams in Figs. 43 and 44 part II

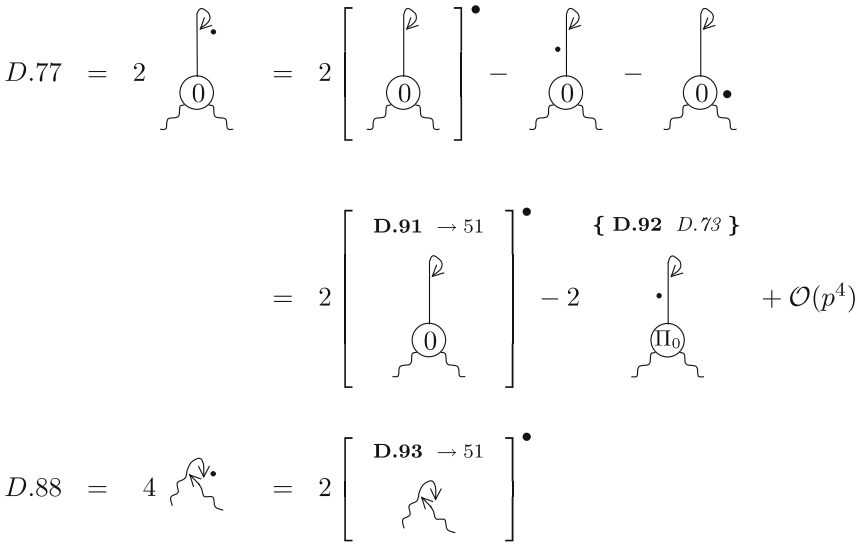

Fig. 48. Re-drawing of diagrams D.77 and D.88 using (83) and their subsequent conversion into Λ-derivative terms

3. Terms possessing an $\mathcal{O}(p^2)$ stub formed by the action of a gauge remainder, diagrams D.84, D.81 and D.80. Notice that the former of these has a trapped gauge remainder;
4. Terms possessing a $S^{11C^{1,2}}_{0\mu\nu}$ vertex, diagrams D. 73 and D.77;
5. Diagram D.88.

We will leave the first three sets of diagrams, for the time being, and focus on the final two. Remarkably, diagram D.77 from the fourth set and diagram D.88 share a common feature: a two-point, tree level vertex, attached to an undecorated kernel, which terminates in a processed gauge remainder. This two-point, tree level vertex cannot be directly removed by the effective propagator; however, we can use a combination of the diagrammatic identities (72)–(76) to make progress:

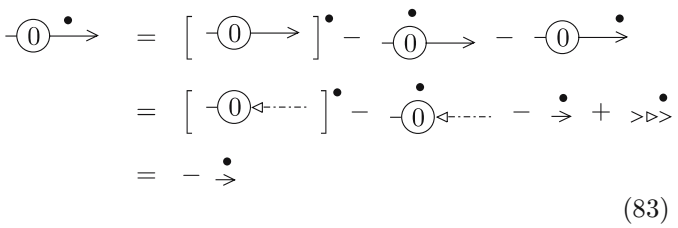

(83)

(Strictly, we should consider the above diagrams to occur in some larger diagrams, cf. (72).)

To go from the first line to the second, we have employed (75) and the effective propagator relation. On the second line, the first term vanishes, courtesy of (73); similarly the second term if we also employ (76). The final term on the second line vanishes courtesy of (74) and (76):

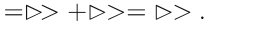

Redrawing diagrams D.77 and D.88 using (83), we find that they can be converted into Λ-derivative terms. The result of this procedure is shown in Fig. 48, where we have discarded any terms which vanish at $\mathcal{O}(p^2)$.

Note how diagram D.93 has a factor of 1/2, relative to the parent diagram. This recognises the indistinguishability of the two processed gauge remainders possessed by this diagram.

Finally, we find the cancellation of the remaining diagrams possessing a $S^{11C^{1,2}}_{0\mu\nu}$ vertex, up to those which are cast as Λ-derivative terms.

Cancelation 16 *Diagram D.92 exactly cancels D.73.*

Our next task is to analyse the surviving diagrams possessing an $\mathcal{O}(p^2)$ stub formed by the action of a gauge remainder. This is a two-step process. First, we Taylor expand each of the sub-diagrams attached to the stub to zeroth order in p.[24] We then re-draw them, if possible, using various diagrammatic identities. The results of the complete procedure are shown in Fig. 49.

To go from diagram D.80 to its daughters, we use the effective propagator relation and diagrammatic identities (73)–(76), having defined:

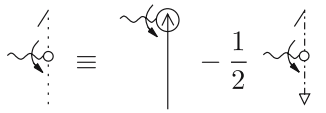

(84)

and

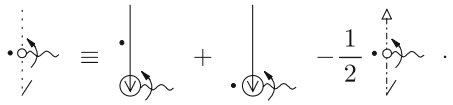

Cancelation 17 *Diagram D.94 exactly cancels D.96.*

Cancelation 18 *Diagram D.96 exactly cancels D.94.*

[24] In these cases, this process does not generate IR divergences and so can be safely performed.

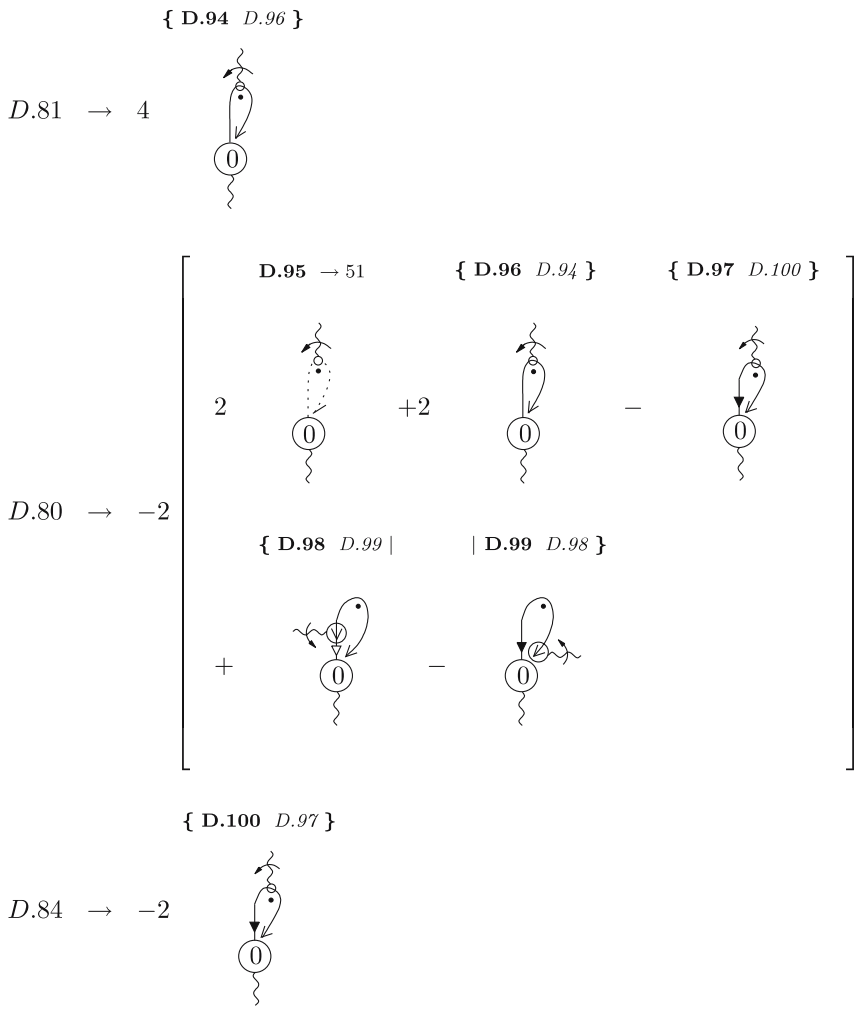

Fig. 49. Manipulations at $\mathcal{O}(p^2)$, followed by a re-expression of the resulting diagrams

Cancelation 19 *Diagram D.98 exactly cancels D.99. This follows since*

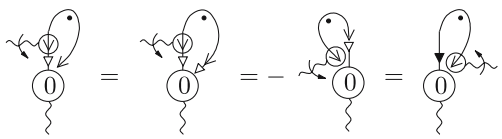

where the last step follows from first applying charge conjugation and secondly reversing the direction of the arrow on the derivative symbol, at the expense of a minus sign.

We now find that all terms, other than the Λ-derivatives, have cancelled, with the sole exception of the $\mathrm{B}'(0)$ terms – which have been collected together in Fig. 50.

In anticipation of the cancellation of the $\mathrm{B}'(0)$ terms, the Λ-derivative terms have been collected together in Fig. 51 to give an entirely diagrammatic expression for β_1, in terms of Λ-derivatives.

The diagrams in this expression will arise so many times in future that we will name them. The complete set of diagrams inside the square brackets will be referred to as $\mathcal{D}_1$. The first three of these are henceforth referred to as the standard set. The last diagram will be known as the little set.

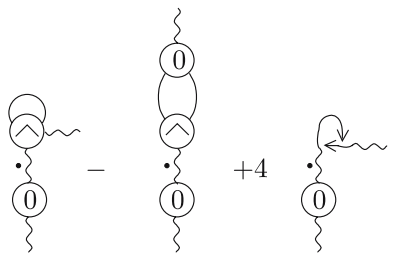

Fig. 50. The set of $\mathrm{B}'(0)$ terms (which do not manifestly vanish at $\mathcal{O}(p^2)$)

5.2 The B′(0) terms

The first thing to notice about the $\mathrm{B}'(0)$ terms is that they are very similar to the first three diagrams of Fig. 51. Indeed, the $\mathrm{B}'(0)$ terms are very nearly just the standard set joined to an $\mathcal{O}(p^2)$ stub, via an un-decorated kernel. The only difference is that the standard set contains exclusively Wilsonian effective action vertices, whereas the $\mathrm{B}'(0)$ terms do not. However, we know that the $\mathrm{B}'(0)$ terms can be manipulated, at $\mathcal{O}(p^2)$. Doing this, we can replace the four-point (three-point) seed action vertex with a double (single) momentum derivative of a two-point, tree level

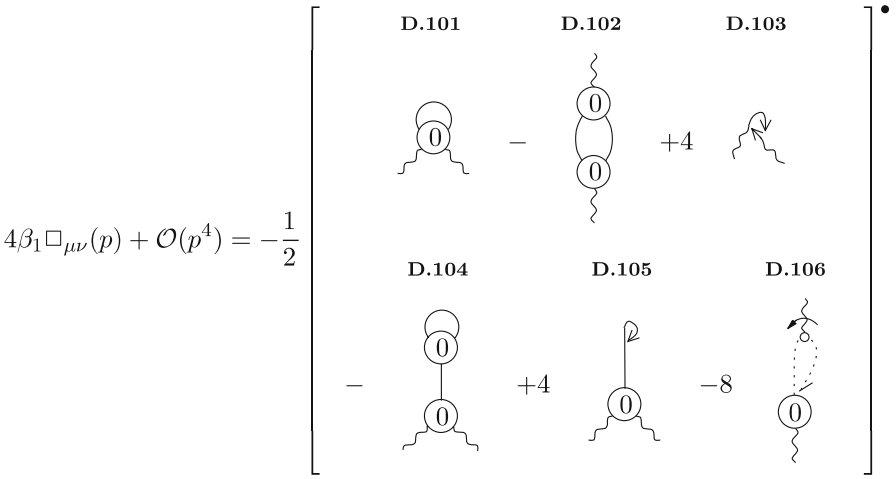

Fig. 51. Diagrammatic, gauge invariant expression for β_1, phrased entirely in terms of Λ-derivatives

vertex. Now, rather than making this replacement, we use the equality of the two-point, tree level Wilsonian effective action and seed action vertices to realise that, at $\mathcal{O}(p^2)$, we can trade the seed action vertices of the un-processed $\mathrm{B}'(0)$ terms for Wilsonian effective action vertices. Now the $\mathrm{B}'(0)$ terms take the form of the standard set attached to an $\mathcal{O}(p^2)$ stub, via an un-decorated kernel.

At this stage, we might wonder why the set of $\mathrm{B}'(0)$ terms does not contain diagrams like the fourth and fifth of Fig. 51. The answer is that we have discarded these terms already, on the basis that they vanish at $\mathcal{O}(p^2)$.[25]

There are several strategies to demonstrate that the $\mathrm{B}'(0)$ terms vanish. In reference [19], it was demonstrated algebraically that the $\mathrm{B}'(0)$ terms cancel, at $\mathcal{O}(p^2)$: Taylor expanding the standard set sub-diagrams to zeroth order in p, we can algebraically substitute for all constituent structures. There is, however, a much more elegant way to proceed which minimises the algebra and is more intuitive.

Let us assume for the moment that our calculation of β_1 is consistent (of course, part of the purpose of having performed this calculation is to demonstrate this). Then we know that the set of diagrams contributing to $\beta_1 \Box_{\mu\nu}(p)$ must be transverse in p. The $\mathrm{B}'(0)$ terms are automatically transverse and so the only diagrams not manifestly transverse are those constituting the standard set. For the calculation to be consistent, then, the standard set must be transverse in p and hence at least $\mathcal{O}(p^2)$. This immediately tells us that the $\mathrm{B}'(0)$ terms are at least $\mathcal{O}(p^4)$ and so can be discarded.

Hence, our task is to demonstrate the transversality of the standard set. Figure 52 shows the result of contracting one of the free indices of the standard set with its external momentum where, as usual, we have used the techniques of Sect. 4.1.

Now we analyse the diagrams on the right hand side. Algebraically, the first three terms go like:

$$A\text{-sector} = 4N \int_l \frac{l_\alpha}{l^2} \left(-1 + \frac{l\cdot(l+p)}{(l+p)^2} + \frac{p\cdot(l+p)}{(l+p)^2} \right)$$

[25] $\mathrm{B}'(0)$ terms corresponding to the little set do not occur at all.

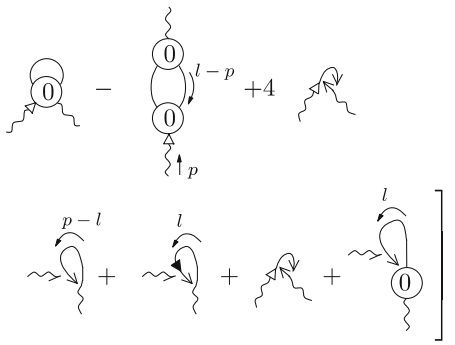

Fig. 52. The result of contracting the standard set with its external momentum. The first three diagrams on the right-hand side cancel and the fourth vanishes by Lorentz invariance

$$F\text{-sector} = 4(-N) \int_l \frac{f_l l_\alpha}{\Lambda^2} \left(-1 + \frac{l\cdot(l+p) f_{l+p}}{\Lambda^2} + 2g_{l+p} + \frac{p\cdot(l+p) f_{l+p}}{\Lambda^2} \right),$$

where the UV finite sum vanishes after using the relationship (74) and shifting momenta. The final term of Fig. 52 vanishes by Lorentz invariance: the l-integral contains a single index and the only momentum available to carry this index, after integration over l, is p. However, this index is contracted into a vertex transverse in p and so the diagram vanishes.

Therefore, contracting the standard set with its external momenta yields zero. Since the standard set carries two Lorentz indices we have proven that it must be transverse in external momenta, as predicted. This, then, guarantees that the $\mathrm{B}'(0)$ terms vanish, at $\mathcal{O}(p^2)$, and also confirms the consistency of the calculation.

6 Conclusions

The basis of this paper is the modification of the flow equation of [19], equation (20), via the redefinition (46), thereby

allowing straightforward renormalisation at one loop and beyond.

At the heart of these changes is the necessity to properly account for multiple supertrace terms, in particular lifting the restriction imposed in [19] that the Wilsonian effective action comprises only single supertrace terms. In turn, this guides us to the proper generalisation of the flow equation (46), where now multiple supertrace terms are effectively incorporated into the covariantisation of the kernels. Crucially, these generalisations must respect no-$\mathcal{A}^0$ symmetry, which plays a central rôle in properly understanding the broken phase diagrammatics.

The diagrammatic techniques of [19] were essentially developed for single supertrace calculations. With the rôle of $\mathcal{A}^0$ obscured, and $g(\Lambda) = g_2(\Lambda)$, it made sense to work with the field $A = \tilde{A}^1 + \tilde{A}^2$, which contains an $\mathcal{A}^0$ component. The benefit of keeping $\mathcal{A}^0$, despite the invariance of complete action functionals under no-$\mathcal{A}^0$ symmetry was that the diagrammatics became particularly simple, as both supersowing and supersplitting were effectively exact, in all sectors.

Having modified the flow equation, our first task was to suitably adapt the diagrammatic techniques. Initially, in Sect. 3.2, this was done along the lines of [19], retaining $\mathcal{A}^0$. However, it rapidly became apparent that the benefits of exact supersowing/supersplitting were really a red-herring. The generalisations of the covariantised kernels to multi-supertrace objects generates diagrams similar in structure to those we were able to remove by working in the exact supersowing/supersplitting picture. Thus, we were led to remove $\mathcal{A}^0$ from our picture, accepting the corrections that this now generates, but recognising that the overall diagrammatic structure is simplified.

Indeed, this inspired the new diagrammatic picture of Sect. 3.3, where we now package up the single and multi-supertrace terms. In retrospect, that such a simplification is possible is hardly surprising. Although all ingredients in the treatment of [19] were restricted to single supertrace terms, the structure of the diagrammatic cancellations strongly suggested that multi-supertrace terms, if included, would cancel in the same way. Indeed, since all non-universal contributions must cancel anyway, it is natural that sets of them can be packaged up together and thus removed in one go.

Moreover, our scheme now amounts to using standard Feynman diagrammatic expansions, except that the Feynman rules are novel and, embedded within the diagrams, there is a prescription for automatically evaluating the group theory factors.

An immediate consequence of these new diagrammatics is that the calculation of [19] can be essentially repeated, line for line. However, in the new way of doing things, multi-supertrace terms come along for the ride, without really adding any complication.[26]

Now, although much of the calculation of β_1 in [19] was done diagrammatically, these techniques were not pushed to their limit, since gauge remainders and $\mathcal{O}(p^2)$ terms were treated algebraically.

In Sect. 4 we showed how the gauge remainders and Taylor expansions can be performed diagrammatically, allowing us to reduce β_1 to a set of Λ-derivative terms, as demonstrated in Sect. 5. This represents a radical improvement over the approach in [19] and proves crucial for performing calculations beyond one-loop.

Utilising the iterative approach to the one-loop calculation, we have reduced β_2 to a set of Λ-derivative terms (and terms which vanish in the $\alpha \to 0$ limit).[27] Even so, it turns out that this iterative procedure generates far more diagrams at two loops than we had been expecting (of order 10 000), so of course it took a long time to complete the calculation. Nearly all of the diagrams cancel amongst themselves by the end of the manipulations. The few diagrams that remain have the property that explicit dependence on the seed action (part of the regularisation structure) and covariantisation has disappeared, reflecting the underlying universality of the answer.

Whilst this vast number of diagrams sounds extremely discouraging, one of us has since realised that the underlying structure of the calculation allows for some remarkable simplifications [23, 52–54]. Re-examining the β_1 diagrammatics, it becomes clear that the same steps are repeated numerous times. For example, cancellations 1–3 occur in parallel. Furthermore, the conversion of diagrams D.45 and D.39 into Λ-derivative terms mirror each other exactly (see Figs. 43 and 44). Both diagrams possess two three-point, tree level Wilsonian effective action vertices; upon their manipulation, the partner diagrams possessing seed action vertices are exactly cancelled. Indeed, thinking about this more carefully, if we take two three-point, tree level vertices, two effective propagators and two external fields, the only Λ-derivative terms we can construct are precisely diagrams D.55 and D.62. This suggests that the generation of these Λ-derivative terms can be done in parallel.

Indeed, this expectation is borne out [52] (see also [22]) and already represents a vast simplification of the calculational procedure. However, even more follows: pushing these methods to their limit, it appears that one can derive an expression for β_n, in terms of Λ-derivatives, *to all orders in perturbation theory* [23, 53, 54]. At a stroke, this removes the primary obstacle to extracting β function coefficients using this ERG.[28] We emphasise that the diagrammatic expression for β_1 (Fig. 51) can now be immediately written down without the need to explicitly perform any of the manipulations of Sect. 5 i.e. β_1 can be directly extracted from only six diagrams, three of which

[26] Effectively, the only additional terms arise from the existence of AAC vertices, which could be discarded in the original treatment, as a consequence of the action being restricted to single supertrace terms.

[27] The manipulation of a small number of the $\mathcal{O}(p^2)$ terms is most easily done using the subtraction techniques of [50].

[28] Of course, we have not actually evaluated the numerical value for β_2 in this paper – see [50]. This is itself a subtle procedure, but there are encouraging indications that, even here, we can expect similar simplifications to those involved in the reduction of β_n to Λ-derivative terms.

(D.101, D.104 and D.105) vanish in $D = 4$. While this is a great advance on the procedures we outline here, it also hints that there is a much simpler, more direct framework for performing computations without gauge fixing. This is an important direction for the future. Other important extensions which we believe are possible and are contemplating for the future, are the incorporation of quarks – so that the methods are applicable to QCD, developing the necessary techniques to compute correlators of general gauge invariant operators, and investigating non-perturbative approximations.

Acknowledgements. TRM and OJR acknowledge financial support from PPARC Rolling Grant PPA/G/O/2002/0468.

Appendix : Examples of classical flows

The first vertex whose flow we will need is a three-point, tree level vertex, decorated by three wildcard fields labelled R–T. This is shown in Fig. 53.

We now specialise the previous example to give the flow of a three-point, tree level vertex decorated by $A^1_\mu(p)$, $A^1_\nu(-p)$ and a wildcard field, which we note carries zero momentum. This is shown in Fig. 54 where we have suppressed all labels.

The third diagram vanishes. First, we note that the kernel must be bosonic. Now, it cannot be in the C-sector, because AC vertices do not exist. If the kernel is in the A-sector then, since the wildcard field carries zero momentum, this would require a two-point A-vertex carrying zero momentum, which is forbidden by gauge invariance.

The final diagram vanishes at $\mathcal{O}(p^2)$. The kernel must be in the A-sector and so each of the vertices contributes at least $\mathcal{O}(p^2)$, as a consequence of gauge invariance.

Note that, if the wildcard field is in the C-sector, then the second diagram also vanishes at $\mathcal{O}(p^2)$. The top vertex contributes at least $\mathcal{O}(p^2)$. The bottom vertex must also contribute $\mathcal{O}(p^2)$, by gauge invariance, since AC vertices do not exist.

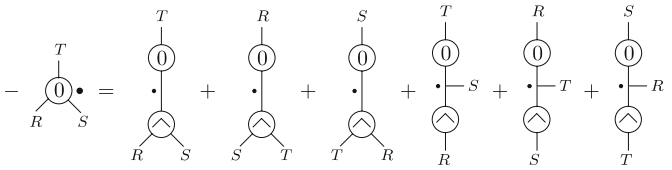

Fig. 53. The flow of a three-point, tree level vertex decorated by three wildcard fields

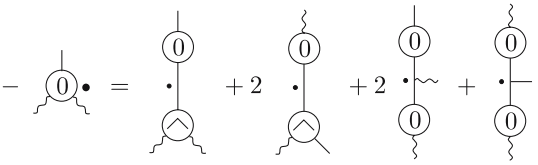

Fig. 54. Flow of a three-point, tree level vertex decorated by $A^1_\mu(p)$, $A^1_\nu(-p)$ and a dummy field. Lorentz indices, sub-sector labels and momentum arguments are suppressed

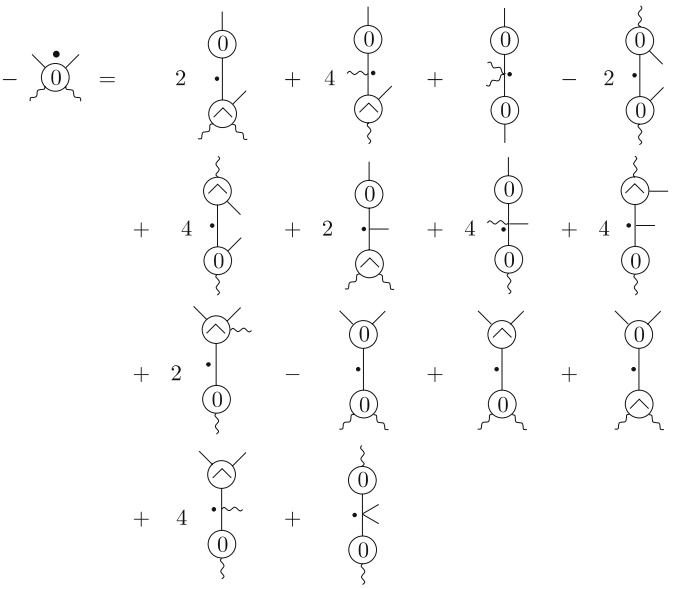

Fig. 55. Flow of a four-point, tree level vertex decorated by $A^1_\mu(p)$, $A^1_\nu(-p)$ and two dummy fields. Lorentz indices and momentum arguments are suppressed

The last example is of the flow of a four-point, tree level vertex decorated by $A^1_\mu(p)$, $A^1_\nu(-p)$ and two dummy fields, as shown in Fig. 55. Summing over the flavours of the dummy fields and noting that, in this current example, the dummy fields carry equal and opposite momenta, we can treat these fields as identical.

The penultimate diagram vanishes at $\mathcal{O}(p^2)$. The kernel must be in the A-sector, but then the diagram possesses an $\mathcal{O}(p^2)$ stub. However, the kernel, which carries three Lorentz indices, cannot have an $\mathcal{O}(p^0)$ contribution by Lorentz invariance. The final diagram, which possesses two $\mathcal{O}(p^2)$ stubs, clearly vanishes at $\mathcal{O}(p^2)$.

References

1. W. Pauli, W. Heisenberg, Zeitschr. Phys. **56**, 1 (1929)
2. R.P. Feynman, Acta Phys. Pol. **24**, 697 (1963)
3. C. Becchi, A. Rouet, R. Stora, Commun. Math. Phys. **42**, 127 (1975)
4. C. Becchi, A. Rouet, R. Stora, in: *Renormalisation Theory*, ed. by G. Velo, A.S. Wightman (Reidel, Dordrecht, 1976)
5. C. Becchi, A. Rouet, R. Stora, Ann. Phys. **98**, 287 (1976)
6. I.V. Tyutin, Lebedev Institute preprint N39 (1975)
7. T.R. Morris, Phys. Lett. B **357**, 225 (1995) [arXiv: hep-th/9503225]
8. T.R. Morris, in: The Exact Renormalization Group, ed. by Krasnitz et al. (World Sci., Singapore, 1999) p. 1 [arXiv: hep-th/9810104]
9. T.R. Morris, Nucl. Phys. B **573**, 97 (2000) [arXiv: hep-th/9910058]
10. T.R. Morris, JHEP **0012**, 012 (2000) arXiv: hep-th/0006064]

11. S. Arnone, Y.A. Kubyshin, T.R. Morris, J.F. Tighe, arXiv: hep-th/0102011
12. S. Arnone, Y.A. Kubyshin, T.R. Morris, J.F. Tighe, Int. J. Mod. Phys. A **16**, 1989 (2001) [arXiv: hep-th/0102054]
13. T.R. Morris, Int. J. Mod. Phys. A **16**, 1899 (2001) [arXiv: hep-th/0102120]
14. S. Arnone, Y.A. Kubyshin, T.R. Morris, J.F. Tighe, Int. J. Mod. Phys. A **17**, 2283 (2002) [arXiv: hep-th/0106258]
15. S. Arnone, A. Gatti, T.R. Morris, JHEP **0205**, 059 (2002) [arXiv: hep-th/0201237]
16. S. Arnone, A. Gatti, T.R. Morris, Acta Phys. Slovaca **52**, 615 (2002) [arXiv: hep-th/0205156]
17. S. Arnone, A. Gatti, T.R. Morris, Acta Phys. Slovaca **52**, 621 (2002) [arXiv: hep-th/0209130]
18. A. Gatti, A Gauge Invariant Flow Equation, Ph.D. Thesis (2002) [arXiv: hep-th/0301201]
19. S. Arnone, A. Gatti, T.R. Morris, Phys. Rev. D **67**, 085 003 (2003) [arXiv: hep-th/0209162]
20. S. Arnone, A. Gatti, T.R. Morris, O.J. Rosten, Phys. Rev. D **69**, 065 009 (2004) [arXiv: hep-th/0309242]
21. O.J. Rosten, T.R. Morris, S. Arnone, Proc. Quarks 2004, Pushkinskie Gory, Russia, 24–30 May 2004 [arXiv: hep-th/0409042], http://quarks.inr.ac.ru,
22. S. Arnone, T.R. Morris, O.J. Rosten, JHEP **0510**, 115 (2005) [arXiv: hep-th/0505169]
23. O.J. Rosten, The Manifestly Gauge Invariant Exact Renormalisation Group, Ph.D. Thesis (2005) [arXiv: hep-th/0506162]
24. M. Bonini, M. D'Attanasio, G. Marchesini, Nucl. Phys. B **418**, 81 (1994) [arXiv: hep-th/9307174]
25. M. Bonini, M. D'Attanasio, G. Marchesini, Nucl. Phys. B **421**, 429 (1994) [arXiv: hep-th/9312114]
26. M. Bonini, M. D'Attanasio, G. Marchesini, Nucl. Phys. B **437**, 163 (1995) [arXiv: hep-th/9410138]
27. M. Bonini, E. Tricarico, Nucl. Phys. B **606**, 231 (2001) [arXiv: hep-th/0104255]
28. C. Becchi, in Elementary Partilces, Field Theory and Statistical Mechanics (Parma, 1993) hep-th/9607188
29. M. Pernici et al., Nucl. Phys. B **520**, 469 (1998) [arXiv: hep-th/9710145]
30. M. Simionato, Int. J. Mod. Phys. A **15**, 2121 (2000) [arXiv: hep-th/9809004]
31. M. Simionato, Int. J. Mod. Phys. A **15**, 2153 (2000) [arXiv: hep-th/9810117]
32. M. Simionato, Int. J. Mod. Phys. A **15**, 4811 (2000) [arXiv: hep-th/0005083]
33. A. Panza, R. Soldati, Phys. Lett. B **493**, 197 (2000) [arXiv: hep-th/0006170]
34. M. Reuter, C. Wetterich, Nucl. Phys. B **427**, 291 (1994)
35. M. Reuter, C. Wetterich, Nucl. Phys. B **417**, 181 (1994)
36. F. Freire, D.F. Litim, J.M. Pawlowski, Phys. Lett. B **495**, 256 (2000) [arXiv: hep-th/0009110]
37. U. Ellwanger, Phys. Lett. B **335**, 364 (1994) [arXiv: hep-th/9402077]
38. M. D'Attanasio, T.R. Morris, Phys. Lett. B **378**, 213 (1996) [arXiv: hep-th/9602156]
39. D.F. Litim, J.M. Pawlowski, Phys. Lett. B **435**, 181 (1998) [arXiv: hep-th/9802064]
40. D.F. Litim, J.M. Pawlowski, hep-th/9901063
41. J.M. Pawlowski, Acta Phys. Slovaca **52**, 475 (2002)
42. D.F. Litim, J.M. Pawlowski, JHEP **0209**, 049 (2002) [arXiv: hep-th/0203005]
43. G.A. Vilkovisky, in: Quantum Theory of Gravity, ed. by S.M. Christensen (Adam Hilger, 1984), pp. 169–209
44. G.A. Vilkovisky, Nucl. Phys. B **234**, 125 (1984)
45. B. DeWitt, The Effective Action, in: Quantum Field Theory and Quantum Statistics, ed. by I.A. Batalin. C.J. Isham, G.A. Vilkovisky (Adam Hilger, Bristol, 1987)
46. V. Branchina, K.A. Meissner, G. Veneziano, Phys. Lett. B **574**, 319 (2003) [arXiv: hep-th/0309234]
47. J.M. Pawlowski, arXiv: hep-th/0310018
48. J.I. Latorre, T.R. Morris, JHEP **0011**, 004 (2000) [arXiv: hep-th/0008123]
49. J.I. Latorre, T.R. Morris, Int. J. Mod. Phys. A **16**, 2071 (2001) [arXiv: hep-th/0102037]
50. T.R. Morris, O.J. Rosten, Phys. Rev. D **73**, 065 003 (2006) [arXiv: hep-th/0508026]
51. G. 't Hooft, Nucl. Phys. B **72**, 461 (1974)
52. O.J. Rosten, J. Phys. A **39**, 8699 (2006) [arXiv: hep-th/0507166]
53. O.J. Rosten, J. Phys. A **39**, 8141 (2006) [arXiv: hep-th/0511107]
54. O.J. Rosten, Int. J. Mod. Phys. A **21**, 4627 (2006) [arXiv: hep-th/0602229]
55. J. Polchinski, Nucl. Phys. B **231**, 269 (1984)
56. K. Wilson, J. Kogut, Phys. Rep. C **12**, 75 (1974)
57. T.R. Morris, Nucl. Phys. B **495**, 477 (1997) [arXiv: hep-th/9612117]
58. C. Wetterich, Nucl. Phys. B **352**, 529 (1991)
59. T.R. Morris, Int. J. Mod. Phys. A **9**, 2411 (1994) [arXiv: hep-ph/9308265]
60. A.A. Slavnov, Theor. Math. Phys. **13**, 1064 (1972)
61. B.W. Lee, J. Zinn-Justin, Phys. Rev. D **5**, 3121 (1972)